Chapter 11

Injector Linac

11.1 Introduction

The electron–positron injector linac at KEK has delivered electrons and positrons for particle physics and photon science experiments since 1982. It was originally constructed for Photon Factory as a 2.5-GeV electron linac beginning in 1978 and was commissioned in 1982. A positron generator was added for the TRISTAN electron/positron collider project, and was operated until 1995. Then, the linac was upgraded for the KEKB asymmetric-energy collider project with energy enforcement up to 8 GeV [1, 2].

Since 2010, KEKB has been further rejuvenated for the SuperKEKB collider project. This project aims at a 40-fold increase in luminosity over the previous KEKB project, in order to increase our understanding beyond the standard model of elementary particle physics [3] after the KEKB project's decade of successful operation. The SuperKEKB asymmetric-energy electron–positron collider, with its extremely high luminosity, requires injection beams with high current and low emittance in the transverse and longitudinal directions [4]. It should also perform simultaneous top-up injections into four storage rings and a DR by pulse-to-pulse modulations (PPMs) to avoid interfere between three facilities: SuperKEKB, Photon Factory (PF), and PF Advanced Ring (PF-AR).

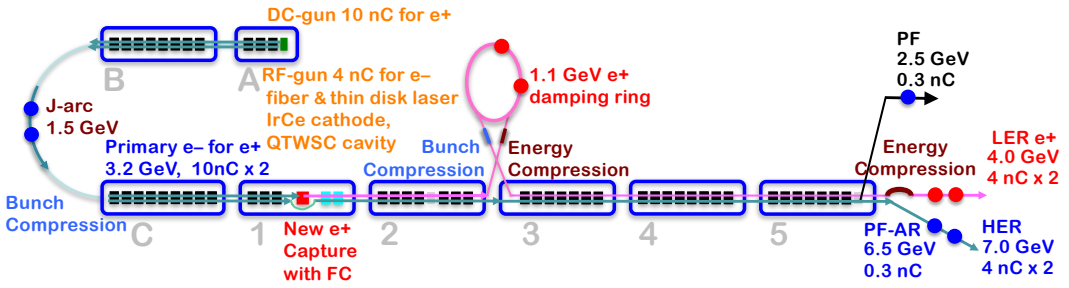

Figure 11.1: Overview of 600-m electron/positron injector linac with 60 accelerating units.

The 600-m injector linac is composed of 60 high-power accelerating units followed by a beam switch yard. The overview of the linac is shown in Fig. 11.1, and the photo of A and B sectors is shown in Fig. 11.2 as a typical injector section. The injector should meet the requirements of the SuperKEKB rings, with a small aperture at the interaction region, doubled stored beam currents, and short expected lifetimes. Low-emittance, high-current electrons are delivered by employing a photo-cathode RF gun. High-current primary electrons for positron production are generated by a thermionic gun, and then high-current positrons are produced using a flux concentrator (FC) and large-aperture accelerating structures (LASs), which are then damped to low emittance through a DR. Design parameters of the injection beams are listed in Table 11.1.

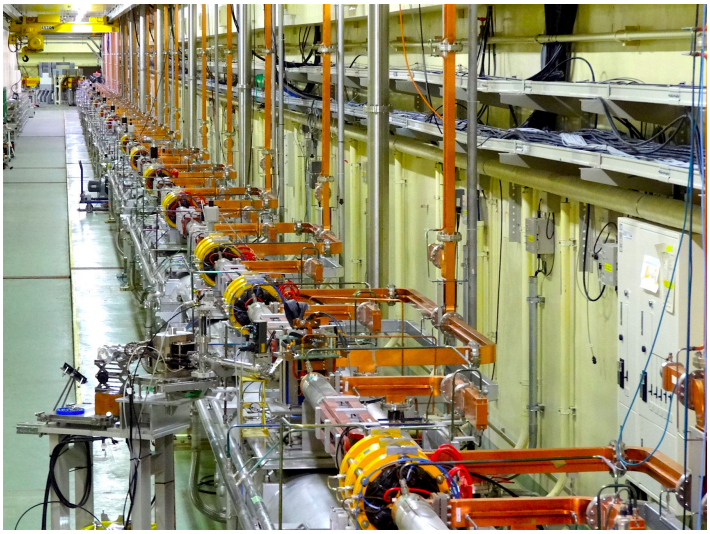

Figure 11.2: A typical part of the injector linac at the A and B sectors.

Beam	Positron	Electron	
Beam energy	4.0	7.007	GeV
Normalized emittance $\gamma\varepsilon_{x/y}$	100/15	40/20	μm
Energy spread	0.16	0.07	%
Bunch charge	4	4	nC
No. of bunches/pulse	2	2	
Repetition rate	50		Hz

Table 11.1: Injection beam parameters.

A low-emittance electron beam source and its transport are indispensable to realizing SuperKEKB's nano-beam scheme for higher collision rates. Although DR is employed to reduce positron emittance, cost and space restrictions make the same solution infeasible for electrons. Thus, we have developed a photo-cathode high-current RF gun. Generating a high-charge electron bunch (up to 4 nC) is a challenging target [5].

The positron beam should also be enhanced to a dual-bunch 4 nC beam in stages, because SuperKEKB has the doubled stored beam current and a much shorter beam lifetime of several minutes. A high-charge positron bunch is generated with a conventional 14-mm thick tungsten target, and is captured by employing an FC and LASs with velocity bunching, followed by a series of solenoid and focusing magnets [6]. As the generated beam emittance is large, it is damped by employing a DR at 1.1 GeV.

If a beam bunch accelerated in the structure is offset from the center, the generated

wakefield induces a transverse force to the tail, and the projected emittance can become very large. Suppressing this effect requires mechanical alignment of the quadrupole magnets and accelerating structures. The beam orbit should be stabilized by finding a low-emittance condition empirically [7]. A beam position read-out system of precision less than 10 μm is also needed to support the method [8].

Devices and monitors in the injector linac are operated via event-based, global, and synchronized controls to inject beams with different properties into four separate storage rings simultaneously [9]. A single injector linac would behave as four independent virtual accelerators (VAs) with hundreds of independent parameters modulated pulse-by-pulse at 50 Hz (Fig. 11.3) [10]. A new beam transport line for PF-AR direct injection prevents interference between the PF-AR and SuperKEKB HER, which shared the same beam transport line in the KEKB project [11].

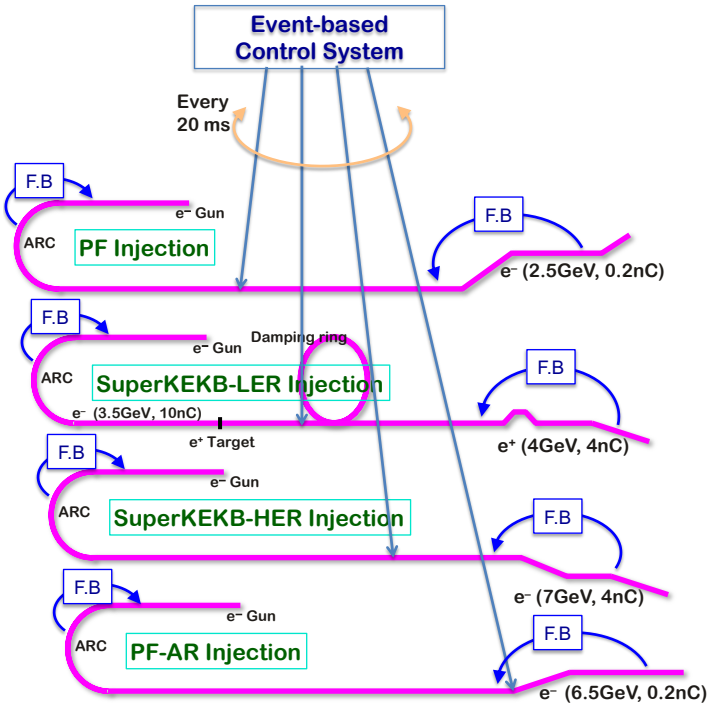

Figure 11.3: Single linac behaves as four virtual accelerators to inject their beams into four separate storage rings.

In the following sections the details of the injector design are described.

11.2 Electron Beam Injection

The electron beams with a charge of 4 nC and a normalized emittance of less than 10 mm mrad are expected to be generated in the photocathode RF gun for injector linac of SuperKEKB HER injection. To high-current, low-emittance beams generation, the laser source with mJ pulse energy, center wavelength of 260 nm and a pulse width of 20 ps are required at the A-1 unit (Fig. 11.4). Further its pulse shape should be reshaped to rectangle structure to obtain the required energy spread of 0.1 %.

The thermionic electron gun is rearranged to the upstairs for the 10 nC primary electron beam for the positron generation as shown in Fig. 11.5.

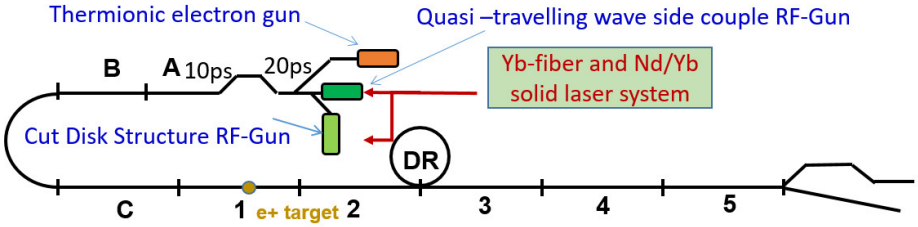

Figure 11.4: Layout of RF-gun and thermionic electron gun.

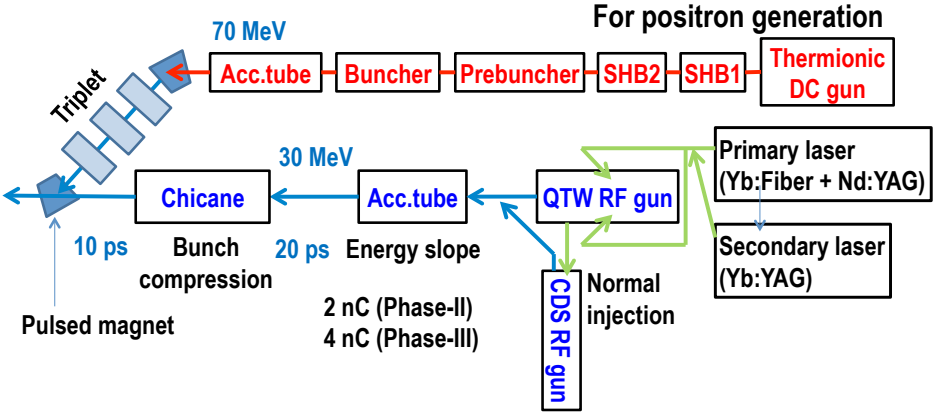

Figure 11.5: Layout of injector part.

11.2.1 High charge and low emittance electron beam

The acceptable normalized emittance for the SuperKEKB injection is 20 mm mrad. To achieve this emittance with the initial emittance of 10 mm mrad from RF-gun, the emittance dilution of 10 mm mrad is acceptable for the entire linac.

The advanced RF-Gun, which adopts the quasi-traveling wave annular coupled cavity, provides the high charge and low emittance beam for SuperKEKB. The optimum bunch length at RF-Gun for the low emittance electron beam is around 20 ps against the space charge effect. The longitudinal bunch shape was controlled by the laser system to obtain the required energy spread. After the RF-Gun, it is compressed to 10 ps using a chicane section.

The transverse wakefield becomes the main source of the emittance dilution for the high bunch charge of 4 nC after the beam orbit is well corrected in the LINAC beam optics. And the energy spread is determined by the longitudinal wakefield strength. The smaller alignment tolerance and the shorter bunch length can reduce the transverse wakefield strength. However, the shorter bunch length causes the stronger longitudinal wakefield.

Figure 11.6 shows the analytical calculation of the projected emittance in several cases of the bunch length and the alignment error. The bunch lengthes of 4 ps and 10 ps are required for the alignment error of 0.3 mm and 0.1 mm respectively from Fig. 11.6. Since our normal bunch length is 10 ps, we are working to reach the alignment error of 0.1 mm for each local section which consists of 8 units. However, it seems very hard to keep this small alignment error in our old support structure and the frequent earthquake. Thus we have to consider the 4 ps option for the alignment error of 0.3 mm.

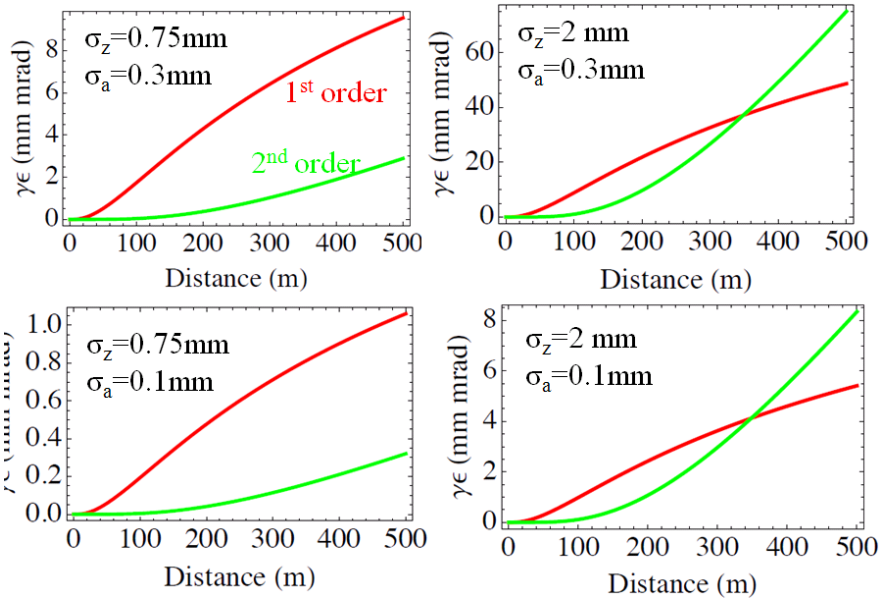

Figure 11.6: Analytical calculation of the projected emittance in several cases of the bunch length and the alignment error.

Further, the initial offset can compensate the transverse wakefield to recover the emittance dilution. The initial offset is taken as the two steering magnets with 90 degree phase difference of the beta function for each axis. Figure 11.7 shows the emittance optimization using the initial offset scan. It is realized using the RF deflector to observe the longitudinally sliced bunch shape.

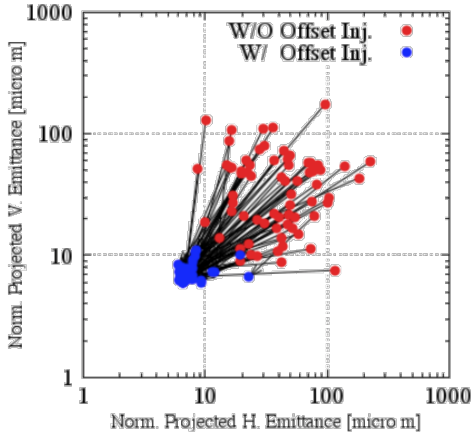

Figure 11.7: Initial offset to optimise the projected emittance.

The shorter bunch can suppress the emittance dilution due to the transverse wakefield. However, it causes a stronger longitudinal wakefield. The RF phase becomes deeper and deeper corresponding to the longitudinal wakefield strength to suppress the energy spread. Thus the bunch length was chosen by those balances.

The initial bunch length of 20 ps generated by the photocathode RF-Gun is compressed to 10 ps using the chicane at the low energy section. And the J-ARC section is placed at the energy of 1.5 GeV. This J-ARC optics was changed to the achromatic condition from the original isochronous design to obtain certain R56 to compress the bunch as shown in Fig. 11.8.

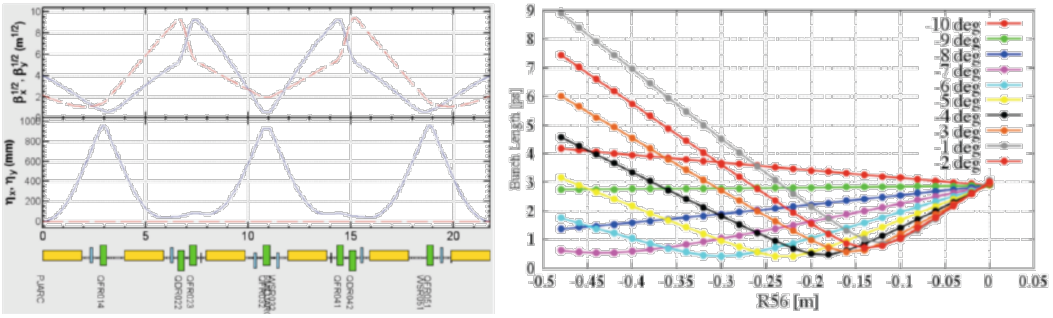

Figure 11.8: Achromatic design of J-ARC section.

We chose the positive R56 of 0.3, since negative R56 makes low energy tail and it consumes more RF slope to recover the energy spread against the longitudinal wake-field. Figure 11.9 shows the measured R56 of J-ARC using the RF phase variation of C-1 unit after J-ARC corresponding to the energy knob of B-5 and B-6 unit. This inclination leads the R56 of 0.23. It is slightly different from the designed value due to the fudge factor of the quadrupole magnets. However, the measured value is enough to determine the RF voltage for the designed bunch compression factor. One RF unit (B-7) with zero crossing RF phase is used to make the energy slope for the bunch compression. The bunch compression is performed only for the SuperKEKB HER injection since the timing of this RF unit for the energy slope is thrown away to the standby timing for the positron injection and PF injection. To compress the bunch length from 10 ps to 4 ps, the RF voltage becomes 60 MV from eq. 1. Thus the RF power of B-7 unit reduced to 8 MW.

$$\sigma_z - \sigma_z' = R_{56}\delta,$$

$$\delta = \frac{\Delta p}{p} = \frac{V_{1unit} \times 2\pi \times \dfrac{\sigma_z}{\lambda}}{p},$$

$$\frac{V_{1unit}}{p} = \frac{\lambda\left(1 - \dfrac{\sigma_z'}{\sigma_z}\right)}{2\pi R_{56}}.$$

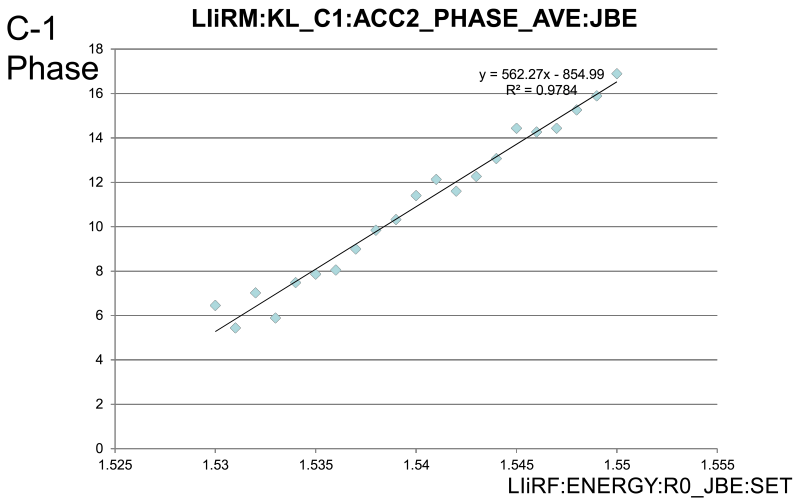

Figure 11.9: Measured R56 of J-ARC using the RF phase variation.

Figure 11.10 shows the beam tracking simulation of the transverse emittance growth with the alignment error of 0.3 mm with and without the bunch compression in the J-ARC [12]. The compressed bunch length of 4 ps leads to suppress the emittance growth.

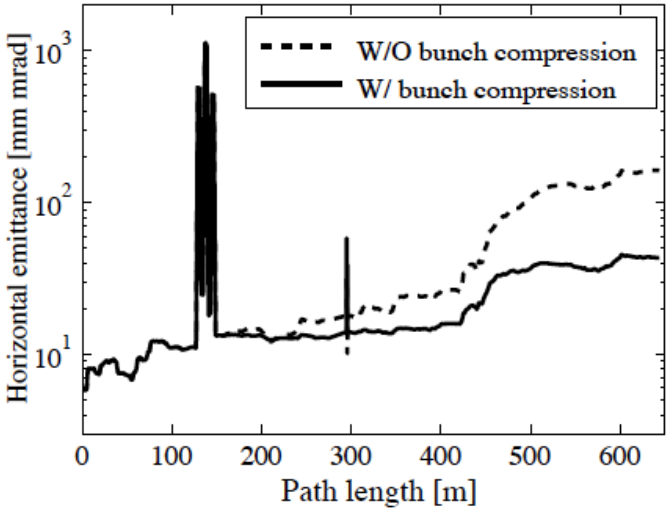

Figure 11.10: Beam tracking simulation with and without bunch compression in the J-ARC.

11.2.2 Longitudinal wakefield

The required energy spread of 0.1 % was achieved for the bunch charge of 1 nC at the previous KEKB operation. However, the required bunch charge becomes 4 nC for SuperKEKB and it induces the stronger wakefield. Further, the stronger longitudinal wakefield induced by the shorter bunch causes the larger energy spread [13]. Fortunately, the energy spread at the optimum RF phase dramatically decreases using the uniform charge density bunch as shown in Fig. 11.11.

As described before, the shorter bunch length suppresses the emittance dilution due to the transverse wakefield. However, it causes a larger energy spread due to the longitudinal wakefield. Also, the shorter bunch length requires the deeper RF phase to compensate the longitudinal wakefield and it causes a lower accelerating gradient.

Thus the uniform charge distribution must be required for any bunch length to reach the energy spread of 0.1 % at 4 nC operation. The longitudinal bunch shape is controlled by the laser system using the pulse stacking method or the chirped pulse amplification method.

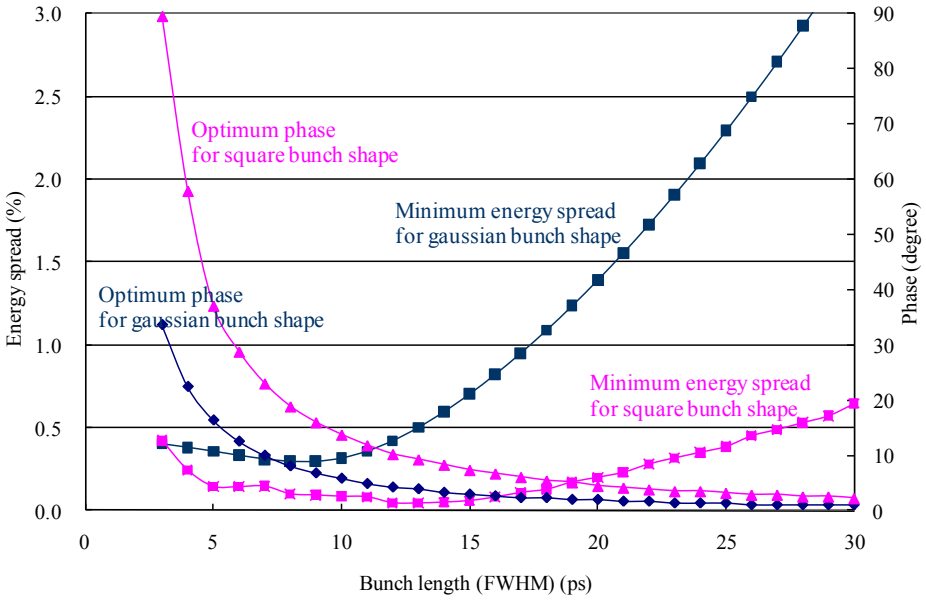

Figure 11.11: Minimum energy spread and optimum phase.

11.3 Accelerating Structure

One of the most basic missions of the accelerating structure is to accelerate the two bunches of electrons or positrons of 4-5 nC, being separated by 96 ns. The final electron energy for HER is 7 GeV, while the positron energy for DR is 1.1 GeV and that for LER 4 GeV. To meet this requirement, the accelerating structures are distributed as shown in Fig. 11.12 and listed in Table 11.2. The basic configuration of an accelerating unit is exactly the same as that of KEKB [14], having four accelerating structures being fed by a klystron with energy gain doubled by SLED.

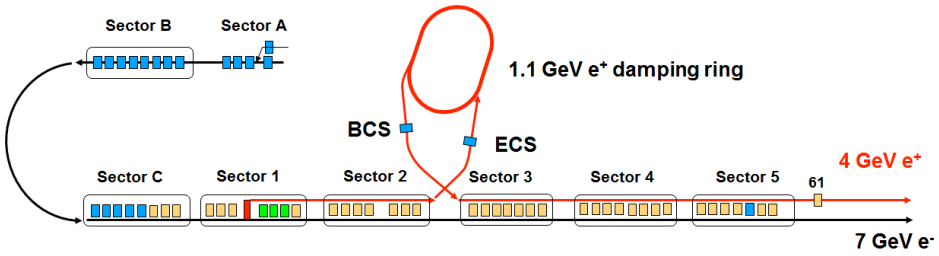

Figure 11.12: Linac schematic of acceleration unit configuration.

11.3.1 Electrical design

All the accelerator structures are the 2m-long, disk-loaded structures operated at $2\pi/3$-mode with pseudo-constant gradient in accelerating field by making the beam-hole aperture varying linearly from the fist disk to the last. These structures are categorized into three types: PF (photon factory) type [14], KEKB type [14] and LAS (Large-Aperture-S-band) type [15].

The primary mission of the PF and KEKB types is the beam acceleration, while the mission of the LAS type includes the capture and bunching of positrons. The relevant design parameters are listed in Table 11.3. The electrical design of the KEKB type is basically the same as that of the PF type, except for the structure of coupler. The length of the coupler gap of PF type is the same as the wave guide height of WR-284. On the other hand, the lengths of all the regular cells are 34.99 mm and the cells are composed of disks of 5 mm in thickness and cylinders of 29.99 mm in length.

Ten LAS-type structures have been introduced for the SuperKEKB. The basic design features are 1: large beam-hole aperture for large transverse acceptance, 2: shorter filling time, at least by half than the nominal accelerating structure of the PF and KEKB types, 3: smaller outer diameter than the inner diameter of the solenoid magnet for the LAS-type structure to be inserted, 4: the structure length is close

Sector	Unit(s)	No. of units	Structure type	SLED	No. of structures per unit
A	AT	1	KEKB	N	2
	GR_A1	1	KEKB	N	1
	A2 - A4	3	KEKB	Y	4
B	B1 - B8	8	KEKB	Y	4
C	C1 - C5	5	KEKB	Y	4
	C6 - C8	3	PF	Y	4
1	11 - 13	3	PF	Y	4
	15	1	LAS	Y [a)]	2
	16 - 17	2	LAS	Y	4
	18	1	PF	Y	4
2	21 - 23	3	PF	Y	4
	24	1	PF	Y	3+1 [b)]
	26 - 28	3	PF	Y	4
D	DN (ECS)	1	KEKB	N	2
	DS (BCS)	1	KEKB	N	1
3	32 - 38	7	PF	Y	4
4	41 - 48	8	PF	Y	4
5	51 - 54	4	PF	Y	4
	55	1	KEKB	Y	4
	56 - 57	2	PF	Y	4
6	61 (ECS)	1	PF	Y	2

a) System is with SLED, but it is operated without SLED as of 2018.
b) The fourth accelerating structure is 1 m long.

Table 11.2: Location of acceleration units.

to 2 m trying long to minimize the perturbation against solenoid-field uniformity by the wave-guide input and output but limited by the realistic handling size, and 5: as high acceleration efficiency as possible. The first feature is the natural demand for large acceptance. The second one stems from the operational experience of the 2m-long capture cavity used in the initial stage of KEKB, which suffered from frequent breakdowns and it was replaced by the shorter structures (1m long) [14]. This problem happens especially in the accelerating structures immersed in solenoidal field just after the target area. Since the configuration is the same for the LAS case, the short filling time is one of the most important requirement. The short filling time of LAS-type structure, 180 ns, less than a half of those of the PF/KEKB-type ones, is realized naturally from the large beam-hole aperture with associated high group velocity.

The minimum aperture diameter was set at 30 mm from positron beam dynamics. The disk thickness was chosen following that of PF/KEKB type. There remained a choice of taking the higher phase advance per cell to keep the reasonable gain with large aperture. We investigated the designs of 2 m accelerator structures with the $3\pi/4$ and $4\pi/5$ phase advances comparing to that of the $2\pi/3$ one. Even taking the small acceleration gain by 7% (20%) with the $3\pi/4$ ($4\pi/5$) phase advance design, the associated increase of filling time becomes as much as 30% (80%), and we finally chose the phase advance of $2\pi/3$ by giving priority to short filling time. We kept roughly the nominal length of 2 m for LAS but actually added 3 more cells with respect to the PF/KEK type to increase the effective acceleration length. In addition, the LAS input coupler has two irises opened symmetrically to the J-type waveguide as shown in Fig. 11.13 and canceling the dipole field component. In order to be inserted into the solenoid magnet with an inner diameter of 200 mm, the output coupler has two compact ports with the flanges mounted as close to the beam axis as possible, as shown in the same Fig. 11.13.

11.3.2 Mechanical design

There are five types of accelerating structures, being categorized mechanically as shown in Fig. 11.14. Firstly, there are two types of PF-type accelerating structures, both with the same electrical design but one, called "4-m structure" shown in Fig. 11.14a, which is 4 m long by mechanically connecting two electrically 2-m structures, and the other, the stand-alone 2-m long structure shown in Fig. 11.14b.

The beam pipe flanges of all the structures are EVAC NW40, except for the 4-m structure, where the upstream flange is MKH-type, while the downstream one EVAC NW40. The structures are evacuated from their beam pipes or the input and output waveguides.

Structure type	PF-type	KEKB-type	New structure	LAS-type
Number of cells N_C (regular+coupler)	54+2	←	←	57+2
Phase advance per cell	$2\pi/3$	←	←	←
Regular cell gap length D [mm]	29.99	←	←	←
Coupler cell gap length D_C [mm]	34	29.99	←	←
Maximum Ep / Eacc	2.1	←	1.9	2.4
Regular cell disk thickness t [mm]	5	←	←	←
Cell wall corner radius [mm]	0	0	13	0
Active structure length [mm] [a)]	1967.46	1959.44	←	2064.41
Beam hole flange-to-flange length [mm]	2066.447 [b)]	2072.43	2066.43	2191.01
Distance between wave guides [mm]	1928.447	1936.43	1928.49	2037.68
Tapering of beam hole aperture diameter ($2a$) [mm]	24.875 - 19.7 (0.075mm step) [c)]	←	23 - 19.73 (CG)	31.86 - 29.97 (0.033mm step)
Average intrinsic Q value Q_0	13700	←	15238	13600
Shunt impedance R_s $[M\Omega/m]$	57.3 - 58.3	←	61.5 - 68.3	46.07 - 48.44
Group velocity v_g/c [%]	1.37 - 1.13	←	1.17	3.86
Filling time T_f $[\mu s]$	0.462 - 0.558	←	0.563	0.179
Attenuation parameter τ	0.302 - 0.368	←	0.33	0.118
Energy gain without SLED $[MeV/structure/\sqrt{MW}]$	7.00 - 7.58	←	7.99	5.19
Energy gain ratio with SLED [d)]	2	←	←	2.4
Wave guide coupling aperture	Single	←	←	Dual
Wave guide iris lip	Sharp edge	←	Rounded ($r1$)	Rounded
Care against HOM	Linear taper in $2a$	←	$2a$ variation for CG	Linear taper in $2a$
Wave guide flange type	MKH	SLAC	MKH	SLAC

a) Active length is calculated as $(\lambda/3) * N_C + (D_C - D) * 2$, where λ is free space wave length and other parameters are given in the Table.

b) Details are given in the following section, "Mechanical design".

c) Linear tapering in beam-hole aperture is implemented. In addition, 5 types (A, B, C, D, E) of tapering are introduced to interleave among these types.

d) Klystron RF pulse is $4\mu s$ in width and its phase is flipped at $3\mu s$, making the compressed pulse of $1\mu s$ by using SLED.

Table 11.3: Accelerator structure parameters.

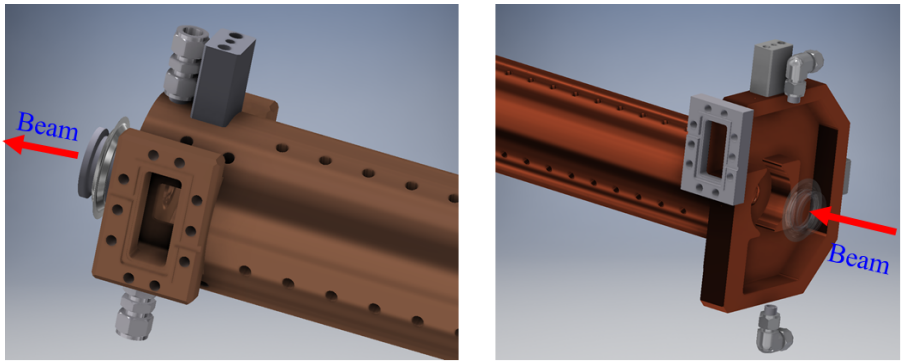

Figure 11.13: Input and output couplers of LAS.

The distance from the upstream flange to the downstream flange of the 4-m structure (a) is 4250.3mm, while those of others are listed in Table 11.3. Both of the structures, (a) and (b), are equipped with the diaphragms attached at both ends of the electrically 2-m structure, as shown in Fig. 11.15, where the distance between the two diaphragms is 2028.447 mm. The beam pipe flanges of 2-m structure (b) are NW40 type and the flange face is separated from the diaphragm by 19 mm. It is to be noted that the 4-m structure can be disassembled at the TiG joints of such diaphragms and can be converted to the 2-m structures (b) by adding the attachments converting from diaphragm to NW40.

11.3.3 Fabrication technology

The assembly technology applied for production of PF/KEK-type accelerating structures is based on the electroplating process over high-precision machined disks and cylinders. On the contrary, that of the LAS type is based on the high temperature brazing. These are different in surface qualities, such as out gassing feature, surface crystal appearance and mechanical hardness, etc. Accelerating structures which are being made from now on for the SuperKEKB will also be made by brazing technique, because because there is no company with a fabricating technique by electroplating in Japan.

The fabrication method of the PF/KEKB type is the following. The regular cells were made by the ultra-fine machined with diamond tool. These were then stacked and axially pressed by several tons of axial force while electroplating their outside by several millimeters. The coupler with a waveguide and a flange was fabricated by brazing and finally assembled to the electroplated regular cells with EBW (electron beam welding)

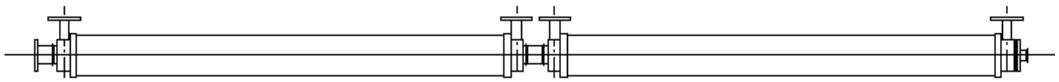

(a) PF-type 4-m accelerating structure.

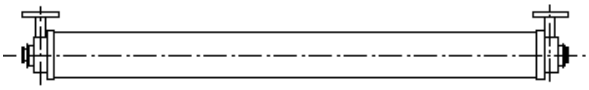

(b) PF-type 2-m accelerating structure.

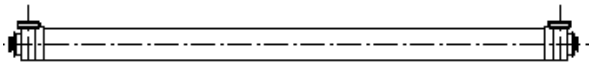

(c) KEKB-type 2-m accelerating structure.

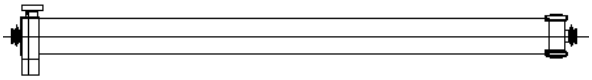

(d) LAS-type accelerating structure.

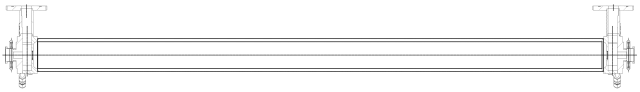

(e) 2-m accelerating structure under development.

Figure 11.14: Rough sketches of mechanically five types of accelerating structures for SuperKEKB.

method. It is to be noted that the regular-cell section is not high-temperature treated, resulting in keeping the surface hardness as of machining, though the coupler regions are high-temperature treated. The cooling water is introduced through two inlet ports mounted on input coupler body, flows around the regular section which is covered by stainless-steel jacket to make a water channel, and finally runs away through two outlet ports connected to output coupler body.

In contrast, the LAS-type structure was assembled by high-temperature vacuum brazing, meaning that the body was well annealed at higher than 800 degrees Celsius and the copper material becomes soft. Their couplers were machined by ultra-precision lathe, precision milled and then assembled with waveguide flanges using gold brazing. These are assembled with regular section by silver brazing. The cell frequencies were dimple-tuned after brazing. The water channels are integrated in each cell body and they are vacuum sealed from accelerating cell inside by brazing in the assembly stage.

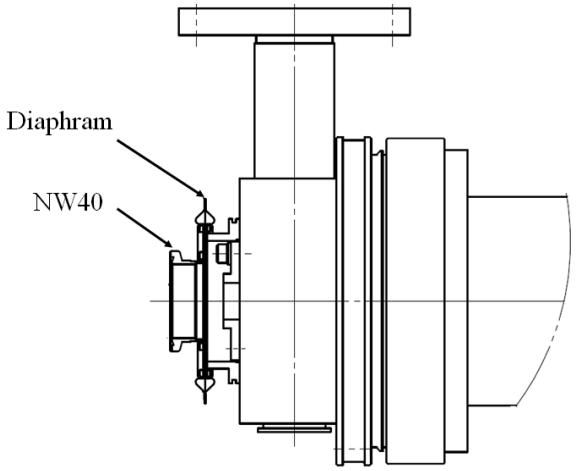

Figure 11.15: End part of the PF-type structures comprising of coupler, diaphragm and NW40 flange.

11.3.4 High power performance

PF/KEKB-type accelerating structures

The standard unit configuration is the same as that of KEKB and is shown in Fig. 11.16 [14]. Here, the 40 MW klystron output power is compressed by SLED and fed to four accelerating structures. This makes 20 MV/m acceleration.

From the KEKB operation period, many PF-type accelerator structures have been suffering from frequent breakdowns and heavy field emission so that such units have operated in reduced power, as shown in Fig. 11.17. The PF-type structures are mostly distributed downstream of the J-ARC (as shown in Fig. 11.12) so that we suspect that more electrons from the beam halo have been impinging into these structures.

At the beginning of KEKB, a few KEKB-type structures were tested up to 40 MV/m in order to prove the feasibility of the structures. They reached the nominal field of 20 MV/m in typically 100 - 200 hours at 50 Hz operation and the field emission is a few μA with decreasing feature as operation time [16]. However, the PF-type structures have been in operation for more than 30 years, comparing to the KEKB-type structures for 20 years, we speculate that the longer year operation and possible beam hitting might have caused the deterioration in many of the PF-type structures.

LAS-type accelerating structures

The three units, 15, 16 and 17, are comprised of the LAS-type structures. The unit 15, with two structures, are immersed in the solenoid field and driven by an RF unit

Figure 11.16: Schematic of unit accelerator.

with SLED. This unit is now being operated with rectangular pulses of 500 ns width. The unit 16 has four structures immersed in the solenoid field connecting to that of the unit 15. The four structures in the unit 17 are outside of the solenoid channel and in turn each structure is surrounded by three Q magnets.

All these LAS-type structures suffer from the huge gas burst especially when the magnet field ON and/or the SLED operation ON. The gas burst is sensitive to the magnitude of the magnetic fields. Also it frequently appears when SLED ON and was sensitive to the low power region before or even after the compressed output period. The effect of RF conditioning at a certain parameter works but does not continue long and the gas burst comes back easily. This means that the conditioning memory does not survive over days or weeks needed for stable operation. Moreover, the SLED operation

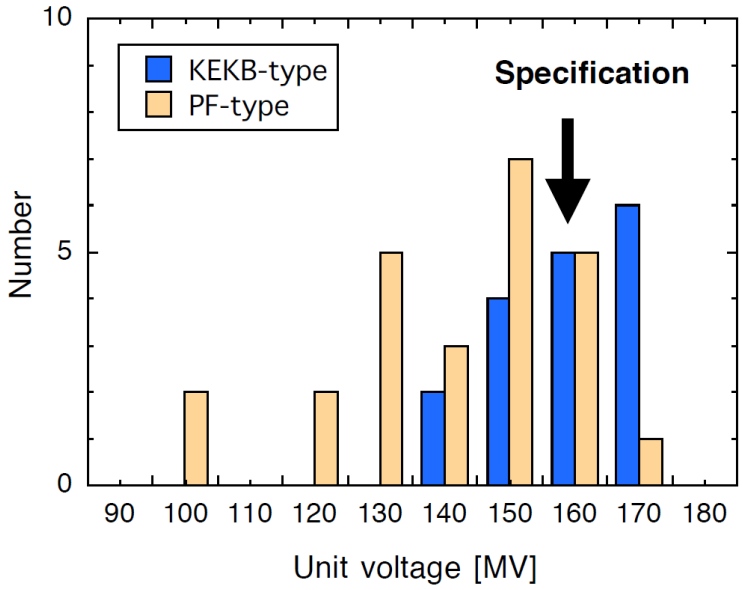

Figure 11.17: Operating voltage gain per RF unit as of spring 2018.

at even very small power causes the gas burst and sometimes including the vacuum breakdowns. One of the most annoying features against continuous linac operation is that once such gas burst happens, the operation of the unit should be stopped until the vacuum level around 10-6 Pa recovers and the RF power becomes back again, typically taking an hour or more.

There is the evidence of breakdown at the first LAS-type structure behind target in the unit 15, appeared only the upstream one. It shows the RF pulse shapes different than that of the usual vacuum breakdowns developed in a few tens of ns, which appear in many high gradient accelerating structures. The transmitted wave showed the linear decrease in RF voltage over 500 ns pulse, while the reflection was increased linearly over the same time. This feature is shown in Fig. 11.18.

The mechanisms of the gas burst and vacuum breakdown, should be identified and the problem must be cured for the stable operation. For the time being, the gradient of the LAS-type structures are limited and the recovery protocol from these problems is improved.

11.3.5 Water leakage issue

The water leakage from the couplers of PF-type structures has become more and more frequent in these years [17]. The schematic of the responsible area is shown in Fig. 11.19. The EBW was applied to connect the coupler to the main body composed of the

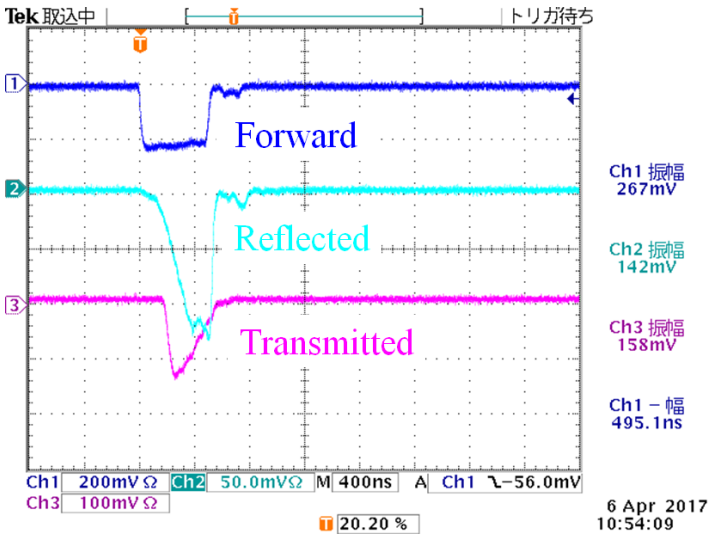

Figure 11.18: RF pulse shapes under vacuum breakdown at the first LAS structure in unit 15.

regular cells. This EBW is so tight that in some cases the cylinder next to the coupler suffered from the surface damage. Moreover, the cooling water runs with touching this welding line. If water leaks crossing this line and faces the vacuum, we should immediately drop the unit from the operation and the water channel is evacuated until the structure is lined off. The problem happened twice until now but we should note that more structures might actually suffer from it but not yet visible in vacuum gauge. Practically the more frequent water leakages happened toward outside at mostly the input coupler side. It is speculated that the route of the leak runs through brazing joint, touching the cooling water. This leakage is temporally cured from outside by a glue called "liquid seal". Since this problem comes from the intrinsic mechanical design of the coupler, the tight EBW/braze joint in the cylindrically non-symmetric structure, we should admit the rate of the leakage be accelerated. The only practical solution is to replace it with a new accelerating structure. It is to be noted that the EBW position is much far from the coupler in KEKB-type structure and it relaxes the problem. In addition, the KEKB-type structures are in operation for much shorter period than the PF-type period, so that the KEKB-type structures will be free from the problem during the SuperKEKB operation.

11.3.6 How to cope with the deterioration

The most robust way to cope with the above mentioned problems is to replace the badly behaved structures by new manufactured structures. They are mechanically designed

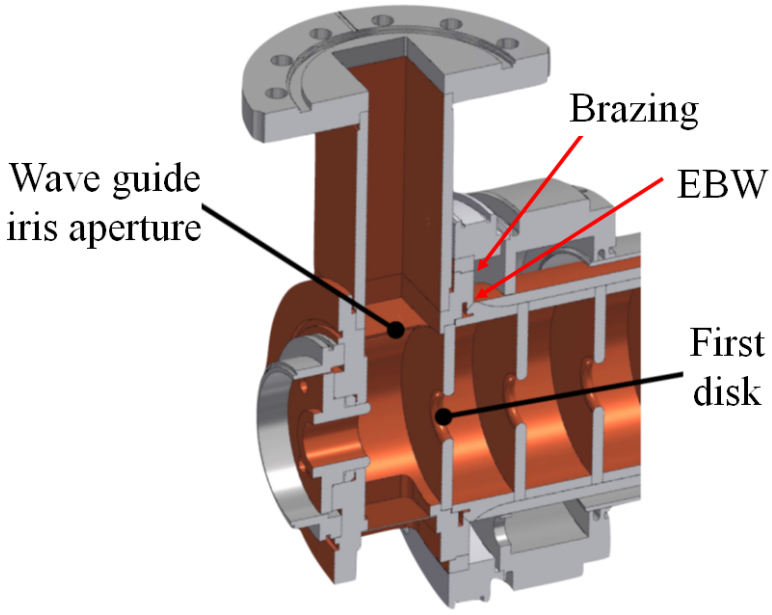

Figure 11.19: Cross section of coupler area of PF-type accelerating structure.

the same as that of PF-type 2-m structure and the detail is described in the following section.

Since the production takes years and needs non-negligible amount of budget, we should minimize the needed amounts of the new structures by rescuing some damaged structures. When the damage occurs in the 4-m PF type structure, the structure can be converted into two 2-m structures as described above. We can drop the bad one and rescue the well-behaved one in the 4-m structure. Since such converted 2-m structures are mechanically the same as the PF-type 2-m ones, Fig. 11.14b, they can be used as the independent 2-m structures.

11.3.7 Development for fabrication of new accelerating structure

The realistic and sure solution to obtain the stable acceleration of the linac free from the above-mentioned problems through the SuperKEKB period is to make the new accelerating structures and replace the deteriorated PF-type structures with them. We have started the development of the first prototype shown in Fig. 11.20 [18]. The relevant parameters are listed in Table 11.3.

The coupler cell and a half of the next cell is precision machined in a single body. The regular cells are rounded in their walls to increase their intrinsic Q values and the shunt impedance, resulting in a higher acceleration gain by 10% than that of

PF/KEKB-type one. The beam-hole apertures were designed to make the structure constant-gradient and make HOM (higher-order-mode) frequencies naturally spread so that the method for curing the multi-bunch (2 bunch) wake field instabilities by the HOMs is the same as that of PF/KEKB type. The iris connecting the coupler to the waveguide is precision milled to be all rounded, without any sharp edge. The cross sectional shape of the beam-hole iris was designed in the ellipsoidal shape to reduce the Ep/Eacc (the ratio of surface electric field to the accelerating field) as small as possible. Thus by avoiding the local high surface field in both electric and magnetic fields, the more stable performance under high gradient operation is expected. The structure is going to be assembled in vacuum brazing furnace and dimple-tuned finally.

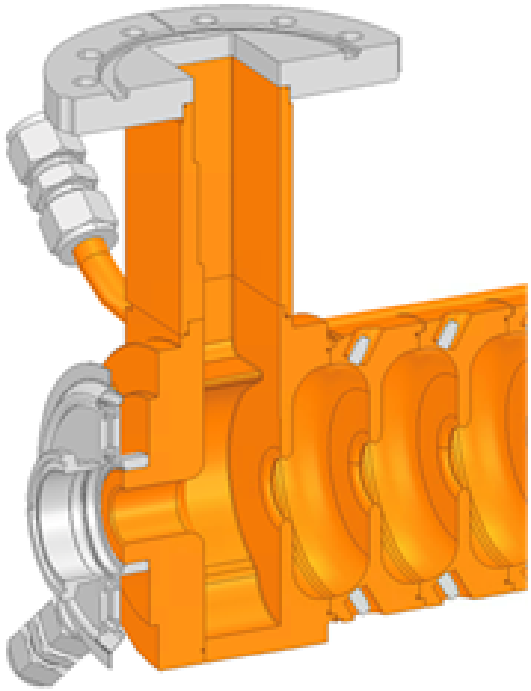

Figure 11.20: Accelerating structure under development.

11.4 RF source

After approximately 10 years of operation of the KEKB, the KEKB injector linac has been upgraded for use in the SuperKEKB. To archive 40-times higher luminosity by the nano-beam scheme compared with the KEKB, the electron/positron beam intensities and their emittances required for the linac must be upgraded. To satisfy these requirements at the linac, a photo-cathode RF gun is installed for the electron injection to the high energy ring (HER) and a damping ring (DR) is introduced for the positron injection to the low energy ring (LER).

Furthermore, the KEKB injector linac is used as a multi-purpose injector not only for the KEKB HER/LER, but also for the photon factory (PF), and the photon factory advanced ring for pulse X-rays (PF-AR). During the KEKB operation period, simultaneous top-up injection into the three storage rings with different energy (HER, LER, and PF) was established. In order to realize this operation, the beam injection parameters to each ring, such as the RF phase, must be switched pulse by pulse with a 50-Hz repetition rate of the linac using an event-based system.

To satisfy the requirements of the SuperKEKB and synchronize with the event-based system for top-up injection, various upgrades have been conducted from the RF system of the KEKB injector linac. These upgrades consists of the developments of compact klystron pulse modulator using a switching power supply and various low-level RF (LLRF) components, such as LLRF control unit and RF monitor unit, the installation of new RF sources (photo-cathode RF gun, energy compensation system at the DR, and bunch compensation system for the DR), and the reconfiguration of main drive line. Figure 11.21 shows the diagram of the upgraded RF system for the SuperKEKB injector linac. The entire rf system consists of a main drive system, eight sub-booster systems with two stand-alone rf drivers for the sub-harmonic buncher (SHB), and 60 high-power pulse klystrons with modulators.

11.4.1 Klystron pulse modulator

The rf system requires 60 high-power klystrons, each capable of 50 MW, 4.0 μs pulsed power at a repetition rate of 50 Hz [19]. The specification of the klystron pulse modulator is summarized in Table 11.4. Fourteen pulse modulators were replaced with a compact modulator to make space for new equipment in klystron gallery. The pulse modulator is a conventional line-type modulator with a charging power supply, a Pulse Forming Network (PFN), a thyratron switch tube, and a pulse transformer as shown in Fig. 11.22 [1]. In the conventional modulator, a LC resonant charging power supply was used to charge a PFN. The compact modulator was replaced it with a switching

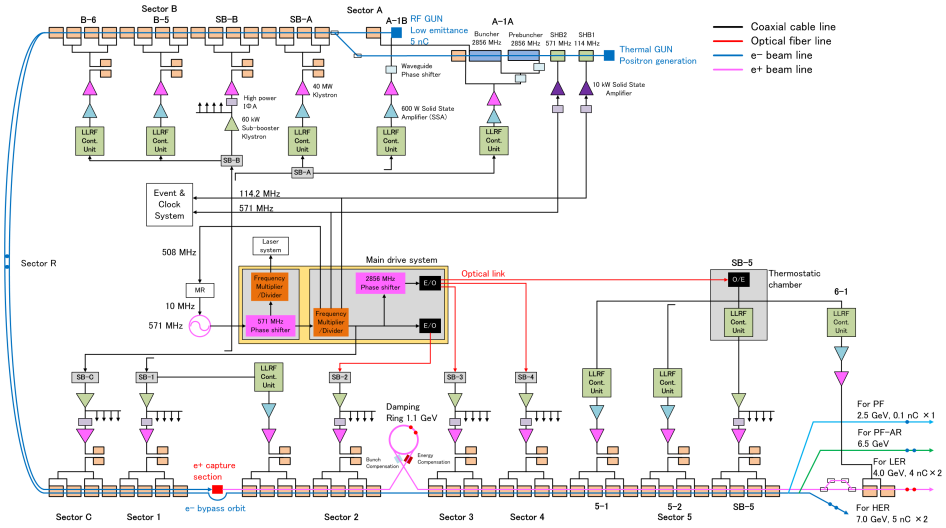

Figure 11.21: Diagram of the upgraded RF system for the SuperKEKB.

power supply, which reduces the modulator size by one-third of the conventional one. Figure 11.23 shows an overall view of the compact modulator with the klystron assembly and the SLED cavity. The switching power supply was developed by Nihon Koshuha Co., Ltd in collaboration with KEK [20]. The power supply is designed to be able to deliver 34 kJ/s with a maximum output voltage of 43 kV. The power supply is based on an IGBT-switched 20 KHz inverter. It has a voltage regulation of less than 0.3% peak-to-peak and is fed with a three-phase ac voltage of 420 V. Table 11.5 shows the specification of the switching power supply.

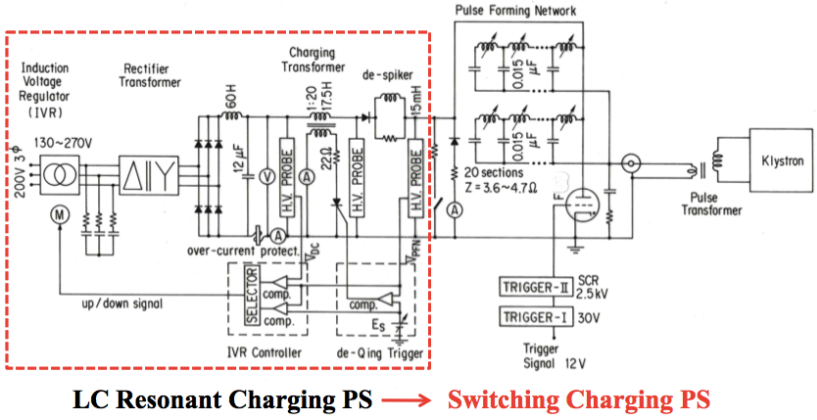

Figure 11.22: Simplified schematic diagram of the klystron modulator.

Parameter	Value
Klystron	
Output power	46 MW
rf pulse width	4.0 μs
Efficiency	45%
Perveance	2.1 $\mu A/V^{3/2}$
Beam voltage	298 kV
Repetition rate	50 pps
Pulse transfirmer	
Step-up ratio	1:13.5
Primary voltage	22.0 kV
Primary current	4.6 kA
PFN(2 par. PFN)	
Impedance	4.6 Ω
No. of cells	40
Cell inductance	1.31 μH
Cell capacitance	15.5 nF
Total capacitance	0.62 μF
Pulse width	5.7 μs
Thyratron	
Anode voltage	44 kV
Anode current	4.6 kA

Table 11.4: Specification of the klystron modulator.

Figure 11.23: Overall view of the compact modulator with the klystron assembly and the SLED cavity.

11.4.2 Drive system

The main drive system is equipped with a frequency multiplier/divider and newly installed two-frequency (571 MHz and 2856 MHz) phase shifters as shown in Fig. 11.21 [21]. The master frequency of the SuperKEKB injector linac is 571.2 MHz. The signal is generated with a signal generator (Keysight; E8663D-HY2), which is synchronized with the SuperKEKB master oscillator via a 10-MHz reference signal. In the main drive system, frequency multiplier/divider generates a 2856-MHz signal for the linac fundamental frequency, 571.2 MHz for SHB2, 114.24 MHz for SHB1 and clock signal for the event-based control system, 10.385 MHz for the beam trigger signal, and 508.8 MHz

Parameter	Value
Maximum output voltage	43 kV
Average capacitor charging power	34 kJ/s
Voltage regulation	$< 0.3\%$ peak-to-peak
Switching frequency	20 kHz
Input voltage	420 V, 3 Phase, 50 Hz AC
Cooling	Water, 5 L/min.
Size	480 mm(W), 760 mm(D), 680 mm(H)

Table 11.5: Specification of the switching power supply.

for the monitor signal to the SuperKEKB ring. The frequency multiplier/divider was manufactured to have a low noise performance to minimize any RF phase jitter. The block diagram of the frequency multiplier/divider is shown in Fig. 11.24 and the measured phase noise of each frequency is listed in Table 11.6. The phase drift of the signals (114.24 MHz/571.2 MHz/2856 MHz/508.9 MHz) output from the main drive system is measured with a sampling oscilloscope (Tektronix; TDS8000) and the measured data is recorded to the EPICS archiver.

Signal	Phase noise (jitter)
Signal	Phase noise (jitter)
114.24 MHz	3.2 mdeg. (78 fs)
571.2 MHz	10.4 mdeg. (51 fs)
2856 MHz	54.7 mdeg. (53 fs)
508.8 MHz	10.4 mdeg. (57 fs)

Table 11.6: Phase noise and jitter integrated from 10 Hz to 1 MHz of the outputs of the frequency multiplier/divider.

For laser oscillation of the RF gun, a supply of clock signals of 10.38 MHz, 114 MHz, and 2856 MHz are required from the main drive system. In the KEKB injector linac, the switching of the HER/LER beam mode and the injection phase adjusting was controlled with the phase shifter located in the KEKB ring, as shown in Fig. 11.24. However, the laser oscillation could not be maintained by the signal phase modulation caused by the fast (50 Hz) beam mode switching.

To establish the compatibility between the laser oscillation and the fast beam mode switching, the 571-MHz phase shifter was developed and the main drive system was reconfigured as shown in Fig. 11.24. The 571-MHz phase shifter consists of two I/Q modulators located in series and an event-receiver (EVR), and its phase modulation is controlled with the event-based system. The first I/Q modulator adjusts the HER injection phase with the phase modulation speed (1 degree/ms) that the laser oscillation is maintained. The second I/Q modulator is used for the injection phase switching between the HER and LER and for adjusting the LER injection phase.

The positron beam emitted from the DR is accelerated with RF sources located from sector 3 to sector 5, as shown in Fig. 11.21. However, the operating frequency of the DR and the HER/LER (508.9 MHz) is not an integer relation with the operating frequency of the linac (571.2 MHz). Owing to this relation, the positron injection to the LER is limited by a certain condition. To perform the positron injection to the LER

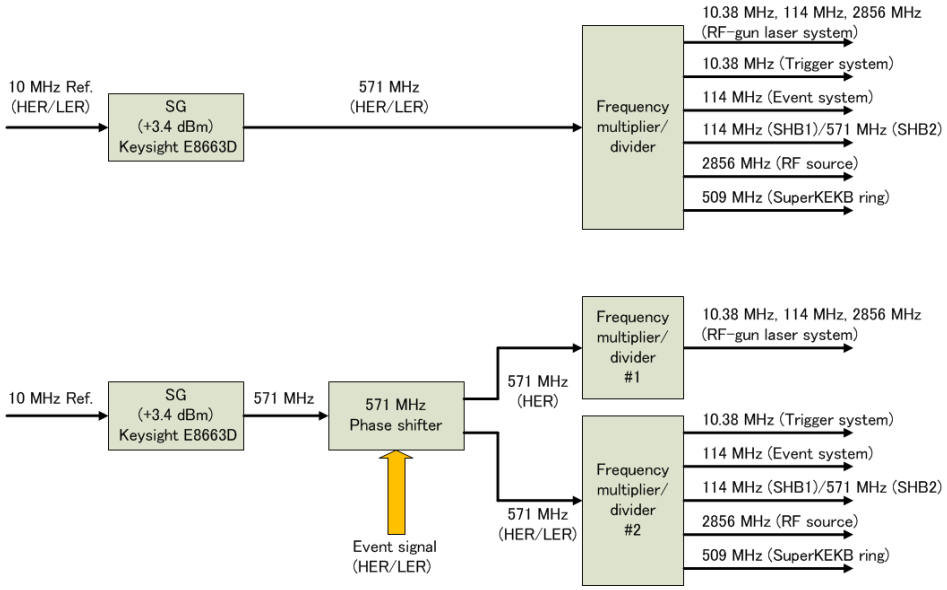

Figure 11.24: Configuration of the main drive system for the (a) KEKB injector linac, (b) SuperKEKB injector linac.

effectively, the 2856-MHz phase shifter was developed based on the LLRF control unit mentioned latter to change the phase during the positron injection mode. The output signal is converted into an optical signal with an E/O convertor and transmitted to sectors 3, 4, and 5.

These components of the main drive system are installed into a thermostatic chamber and placed under a temperature control of $28 \pm 0.03°C$. The thermostatic chamber is composed of two Peltier devices with an endothermic quantity of 250 W and a heater for precise temperature control. By adopting a Peltier component instead of a compressor, the RF components located inside the thermostatic chamber are not affected by mechanical vibrations and a long operational life can be expected.

As shown in Fig. 11.21, 2856 MHz signal is distributed into eight sectors (A-C and 1-5). In each sector, 60-kW sub-booster klystron supplies power to four or eight high-power klystrons as shown in Fig. 11.25 (left). However, for special purposes such as ones in the electron bunching section including electron gun, positron target and focusing section, and energy spread adjustment, one high-power klystron is directly driven with one 600-W solid-state amplifier as shown in Fig. 11.25 (right).

Owing to the recent technological advances and cost reduction in solid-state amplifiers, the cost of one 60-kW klystron and that of eight 600-W solid-state amplifiers necessary for constructing one sub-booster system is balanced. Therefore, 60-kW klystrons are expected to be obsoleted in the future and replaced with new sub-booster

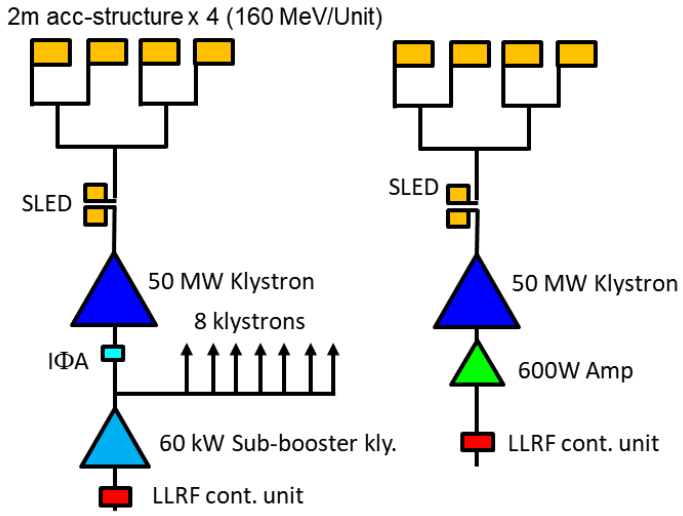

Figure 11.25: Klystron drive-line from a sub-booster klystron (left), and independent drive-line (right).

systems of 600-W solid-state amplifiers, as shown in Fig. 11.26.

11.4.3 LLRF control and RF monitor units

In simultaneous injection at the KEKB linac, the phases of RF pulse are controlled at 50 Hz repetition. To satisfy the requirement for the simultaneous injection, two type of the digital LLRF unit have been developed [22, 23]. One is LLRF control unit to control the phase of the RF pulse at 50 Hz repetition and the other is RF monitor unit to measure the amplitude and phase of RF pulse in each beam mode. These digital LLRF units consist of a FPGA board with an analog-to-digital converter (ADC) / digital-to-analog converter (DAC) board (six 14-bit ADC: AD9254, six 14-bit DAC: AD9744 for LLRF control unit and ten ADC, two DAC for RF monitor unit) connected via FMC connector, I/Q modulator/demodulator, and Armadillo CPU board with an LCD touch panel as shown in Fig. 11.27. The sampling clock of the FPGA, ADC and DAC is 114.24 MHz, which is the same frequency synchronized with the event-based system to cancel the sampling jitter. The RF pulse timing and phase inversion timing for SLED are supplied from the external signal generated with the event system and the recognition of a beam mode and the setting value of RF phase for LLRF control unit are received directly with the event receiver (EVR) implemented in the FPGA board via optical fibre link. The correction for the nonlinearity of I/Q modulator/demodulator is performed by calculation inside the FPGA using I/Q calibration table stored in the compact flash memory on the FPGA board. The specifications of the RF pulse

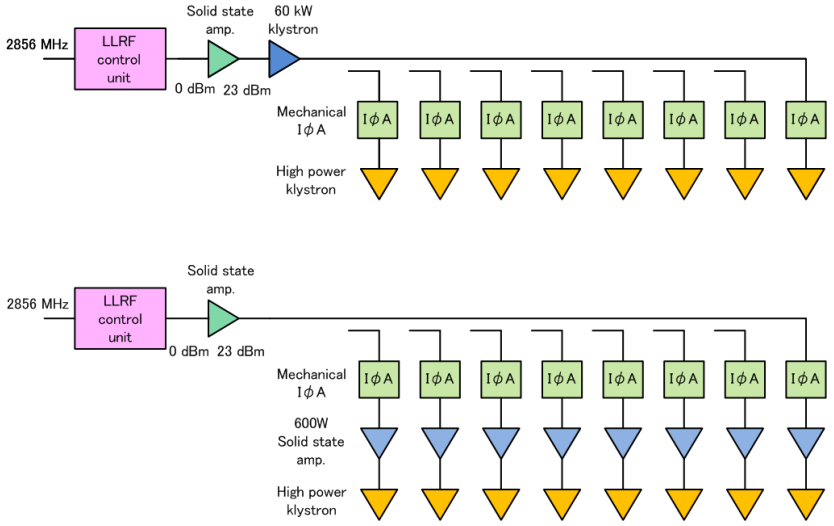

Figure 11.26: Diagram of the sub-booster system in the KEKB injector linac (up) and planned for Sthe SuperKEKB injector linac (down).

modulator are shown in Table 11.7. The typical result of the amplitude and phase accuracy of the RF output is shown in Fig. 11.28. The amplitude error is 0.02% rms and the phase error is 0.04deg rms in an amplitude setting of 100%.

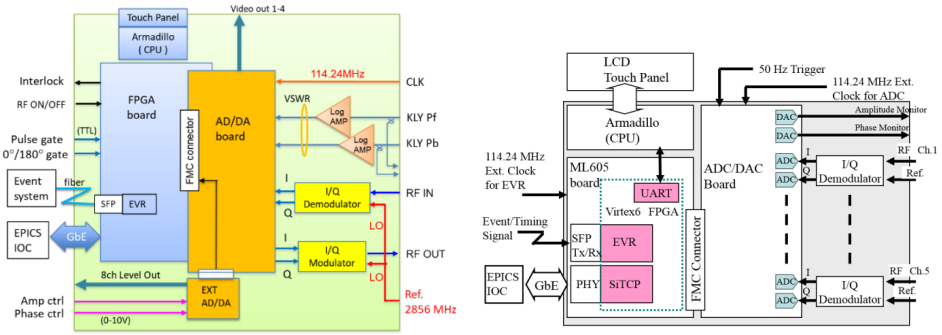

Figure 11.27: Block diagram of the LLRF control unit and RF monitor unit.

11.4.4 Application for stable operation

The I/Q component data of waveform measured in the digital LLRF unit are sent to the EPICS-IOC server at the 50Hz repetition rate through a Gigabit Ethernet implemented on the FPGA board. The EPICS-IOC server converts from the data of I/Q component to the data of amplitude and phase and sorts the amplitude and phase for every beam mode. The amplitude and phase waveform are monitored with waveform viewer in

Frequency	2856 MHz
RF output level	+10 dBm (100%)
Linearity of amplitude	0.3% rms and max $< \pm 0.5\%$
RF pulse rise time	< 35 ns (0 - 90%)
Phase setting-range	0 - 400°
Linearity of phase	0.3° rms and max $< \pm 0.5°$

Table 11.7: Specifications of RF Pulse Modulator.

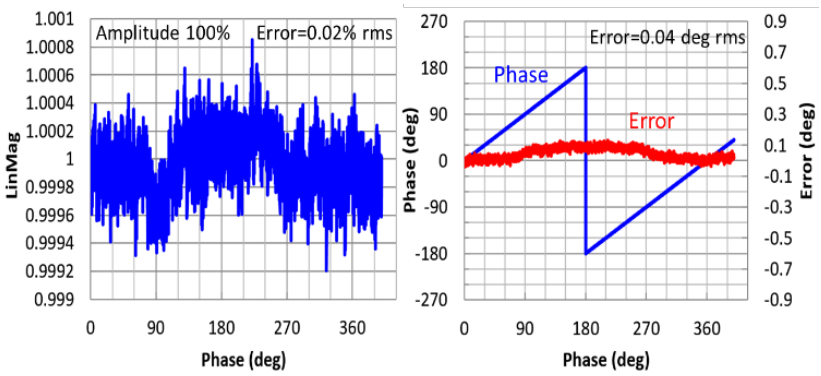

Figure 11.28: Amplitude error (left) and phase error (right) of RF output.

real time and the sampled data of amplitude and phase from waveform are stored in EPICS archiver.

Figure 11.29 (left) shows an SLED output signal with the waveform viewer. The upper waveform is the amplitude and the lower waveform is the phase. The user can choose the monitor signal and the beam mode by a pull-down menu. Figure 11.29 (right) shows the time trend of archived phase data and the chosen beam modes are KEKB e− (KBE) and KEKB e+ (KBE) and no-injection (NIM).

The waveform data is accumulated on the ring memory of the EPICS-IOC server. When the operation of high-power RF source is stopped by a safety interlock, the wave form data on the ring memory are archived to confirm the phenomenon and investigate the cause. Figure 11.30 displays the last and the next to the last event before a high power RF source suspends due to over VSWR limit. It is recognized that sudden increase in the backward power of the SLED (SLEDPB) occurred at the last event.

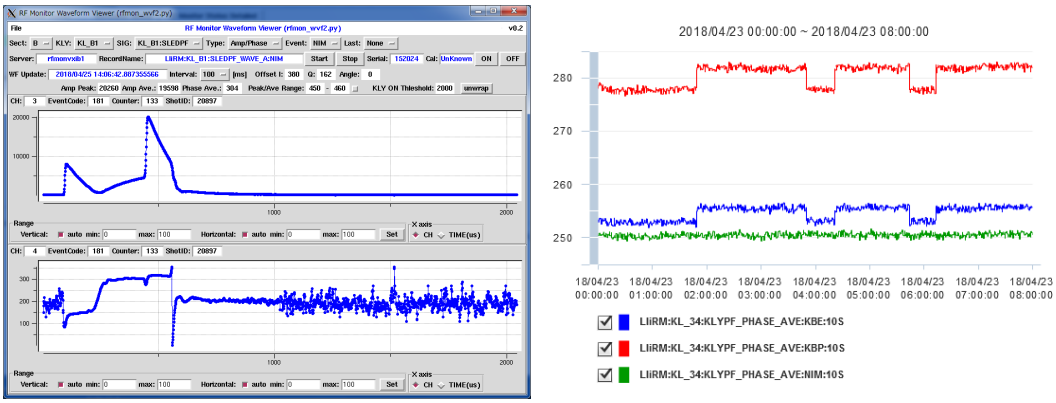

Figure 11.29: Display of waveform viewer (left) and archiver (right).

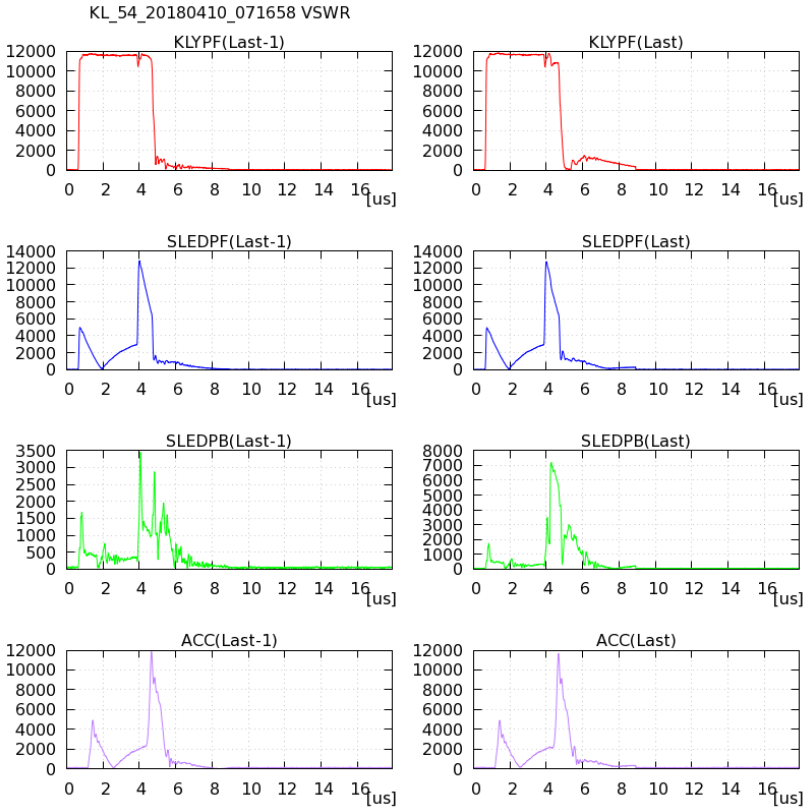

Figure 11.30: Archived waveform of the last and the next to the last event.

11.5 Magnet

In this section, the magnets introduced in the upgrade of the injector linac for SuperKEKB are described and the parameter tables are shown.

11.5.1 24 degree beam merger line

The two pre-injectors in double-deck layout as shown in Fig. 11.31 are used for SuperKEKB beam injection. The A1 pre-injector with a photo-cathode RF gun and a magnetic bunching section in the lower deck is used for an electron injection to HER. The AT pre-injector with a thermionic gun and an RF bunching section in the upper deck is used for an injection of the primary electron beam for positron production. It is used also for the injections to the Photon Factory ring and to the PF-AR rings. The beams from the AT pre-injector pass through the 24-degree beam merger line into the main beam line in the lower deck.

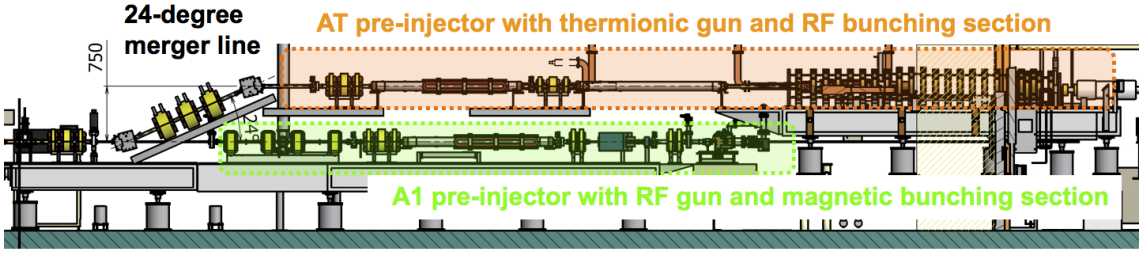

Figure 11.31: Double deck pre-injectors of SuperKEKB injector linac.

For the pulse-by-pluse switching of the beams from the AT and A1 pre-injectors, two pulsed bending magnets are used in the merger line as shown in Fig. 11.32. The beam line of a pair of the bending magnets and three quadrupole magnets interleaved between the them is designed to be achromatic and isochronous in the first order beam optics. For an independent beam optical matching and beam orbit tuning for the beams from the two pre-injectors, two pairs of the focusing and defocusing quadrupoles and the two pairs of the horizontal and vertical steering magnets were installed. A pair of the quadrupoles which is not shown in Fig. 11.32 was installed three meters downstream from the first pair.

The design parameters of the magnets are shown in the tables; the bending magnets are type_AT_J in Table 11.8, the quadrupole magnets are type_A1_M in Table 11.9 and the steering magnet are type_A1_M in Table 11.12. The pulsed current operation tests of the bending magnets were performed to investigate temperature rises in the stainless vacuum chamber and the coils of the magnet. It revealed that the temperature rise

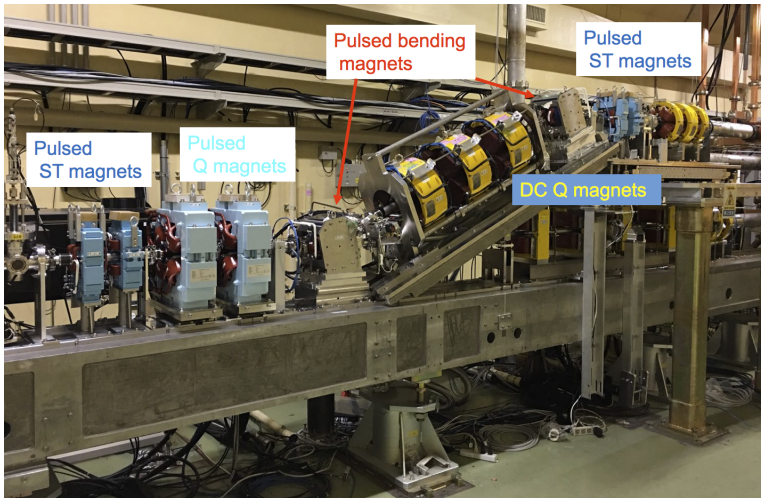

Figure 11.32: 24-degree beam merger line.

in the chamber was tolerable with a water cooling, however that in the air-cooled coil exceeded 70 degC at a condition of full pulse repetition of 50 Hz [24]. The bending magnets are planned to be replaced by those with sufficient cooling capacity.

11.5.2 Full pulse-magnet equipped beam line in Sector-3, 4, 5

In the upgrade for SuperKEKB, all the quadrupoles and the beam-steerings were replaced from DC magnets to pulsed magnets in the Sector-3, 4, 5 which is the region after the DR till the end of the linac. It is for the independent tuning of the beam optical matching and of the beam orbit for four beam-modes of different beam energies and beam parameters (7.0-GeV electron for HER, 4.0-GeV positron for LER, 2.5-GeV electron for PF and 6.5-GeV electron for PF-AR). The pulsed magnets were installed as a set of a focusing quadrupole, a horizontal steering, a vertical steering and a defocusing quadrupole magnets as shown in Fig. 11.33. This layout was determined to mitigate the required field gradient for the quads keeping the configuration as a periodic doublet focusing system. The parameters of the quads of type_32_4 used here are shown in Table 11.9 and those of the steerings of type_32_4 are in Table 11.12.

The 13 sets of the pulsed magnets were deployed in the Sector-3, 4, 5 in intervals of 19.2 m typically as shown in Fig. 11.34.

11.5.3 Positron focusing beam line in Sector-1, 2

In accordance with the upgrade of the positron captures section, the quadrupole focusing system was upgraded in the accelerator-units from #1-6 to #2-3 as shown in Fig. 11.35. In the unit #1-6 after the solenoidal focusing system of the positron capture

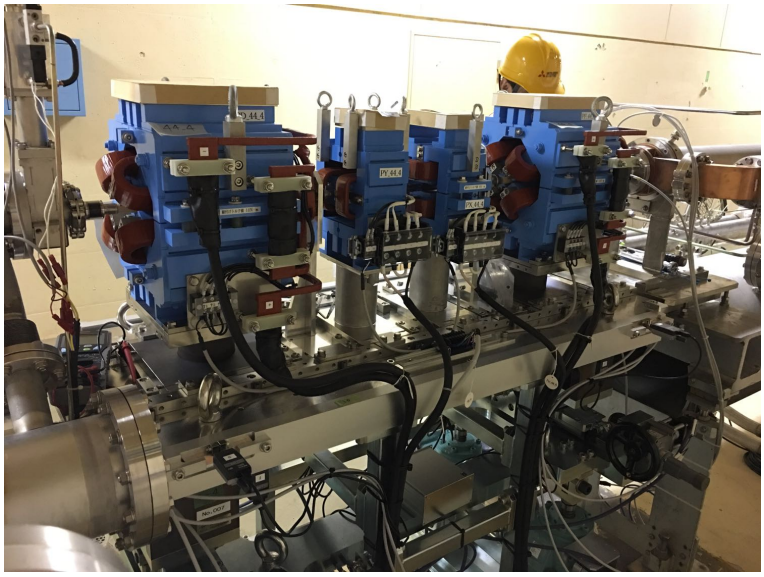

Figure 11.33: A set of pulsed quadrupole and steering magnets.

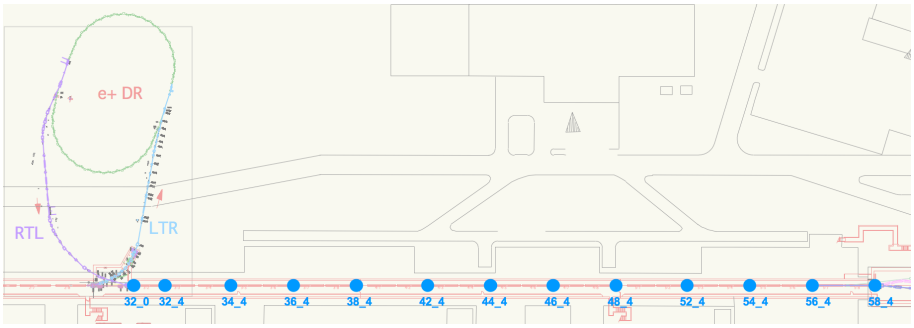

Figure 11.34: Layout of the pulsed magnet sets in Sector-3, 4, 5.

section, the 11 quads are used for a beam-optical matching to the subsequent FODO focusing system. The beam size of the positrons become large for the matching, the quads of type_16_41 in Table 11.10 and the steerings of type_16_5 in Table 11.12 were designed to have the beam-duct aperture diameter of 60 mm. In the units #1-7 and #1-8, most of the quads were installed outside of the accelerating structures, thus the quads of type_17_11 were design to have the bore diameter of 140 mm, sufficient for the LAS type structures. The quads of type_17_14 in Table 11.10 placed in between the accelerating structures have the bore diameter of 44 mm. The quads of type_21_11 have the bore diameter of 120 mm, sufficient for the ordinary S-band structures in the units #2-1, #2-2 and #2-3. While the quads in the Sector-3, 4, 5 are pulsed magnets, those in the Sector-1, 2 are DC magnets. Thus, the beam-optical settings are almost optimized for the positron beam, however it should be compatible with the high-energy injection electron beam in the common magnet fields. Though the quad settings are

common to the different beam modes, the beam orbits are independently tunable with the pulsed steering magnets. The steering magnets of type_16_5, type_17_2, type_12_2 and type_13_2 as shown in Tables 11.11 and 11.12 are used in Sector-1, 2.

Figure 11.35: Layout of the FODO magnets in Sector-1, 2.

Bending magnets	type_AT_J	type_16_C1
pole gap [mm] @center	20	76
pole width [mm]	40	230
pole length [mm]	154.9	180
yoke outer diameter [mm]	200 × 200	540 × 465
coil wire dimension	2 × 6 × 2pair	2 × 9
coil wire cross section [mm^2]	24	18
max. current [A]	300	60
max. field strength [T]	0.67	0.34
coil-wire turns/coil	18	175
coil length along beam line [mm]	250	239
current type (DC/pulsed)	pulse	DC
pole type (block/laminated)	laminated	block
coil resistance [Ω] (2coils)@50degC	0.016	0.371
coil inductance [mH] (2coils)	1.00	0.35
interlock (temper.) normal state		open
interlock (water) normal state	-	open
cooling (water/air)	air	water
cooling water flow rate [L/min]	-	2.8
effective field length [mm]	175.3	253.3

Table 11.8: Specifications of Bending magnets.

Quadrupole (pulsed)	type_A1_M	type_32_4
bore diameter [mm]	39	20
pole width [mm]	60	40
pole length [mm]	100	200
yoke outer diameter [mm]	360	260
coil wire dimension	$2 \times 9 \times$ 4pairs	$2 \times 14 \times$ 2pairs
coil wire cross section [mm^2]	72	56
max. current [A]	330	330
max. field gradient [T/m]	20*	60*
coil-wire turns/coil	10	8
coil length along beam line [mm]	190	303
current type (DC/pulsed)	pulsed	pulsed
pole type (block/laminated)	laminated	laminated
coil resistance [mΩ] (4coils)@50degC	5.4	8.0
coil inductance [mH] (4coils)	0.80	1.0
interlock (temper.) normal state	close	open
cooling (water/air)	air	air
effective field length [mm]	122.4	212.4

Table 11.9: Specifications of Pulsed Quadrupole magnets.

Quadrupole (DC)	type_16_41	type_17_11	type_17_14	type_21_11
bore diameter [mm]	68	140	44	120
pole width [mm]	80	80	80	80
pole length [mm]	160	300	160	300
yoke outer diameter [mm]	432	552	432	552
coil wire dimension	6.4×6.4 -ϕ4	6.4×6.4 -ϕ4	6.4×6.4 -ϕ4	6.4×6.4 -ϕ4
coil wire cross section [mm^2]	28.4	28.4	28.4	28.4
max. current [A]	80	100	80	80
max. field gradient [T/m]	9.0	7.3	17	8.1
coil-wire turns/coil	55	156	47	156
coil length along beam line [mm]	280	530	280	530
current type (DC/pulsed)	DC	DC	DC	DC
pole type (block/laminated)	laminated	laminated	laminated	laminated
coil resistance [mΩ] (4coils)@50degC	101	459	86	457
coil inductance [mH] (4coils)	35	272	32	316
interlock (temper.) normal state	open	open	open	open
interlock (water) normal state	open	open	open	open
cooling (water/air)	water	water	water	water
cooling water flow rate [L/min]	1.5	5.6	1.7	5.6
effective field length [mm]	180.8	334.4	173.7	327.8

Table 11.10: Specifications of DC Quadrupole magnets.

Steering (High inductance type)	type_R0_0	type_12_2	type_13_2
pole gap [mm] @center	44	35	35
pole width [mm]	70	80	150
pole length [mm]	100	150	150
yoke outer diameter [mm]	210	300 × 265	330 × 280
coil wire dimension	1 × 4	2 × 5	1 × 6
coil wire cross section [mm^2]	4	10	5.8
max. current [A]	10	10	10
max. field strength [mT]	70.1	77	71
coil-wire turns/coil	123	108	100
coil length along beam line [mm]	185	254	234
current type (DC/pulsed)	pulsed	pulsed	pulsed
pole type (block/laminated)	laminated	laminated	laminated
coil resistance [Ω] (2coils)	0.6 @45degC	0.25 @25degC	0.53 @25degC
coil inductance [mH] (2coils)	30.00	38	57
interlock (temper.) normal state	close	close	close
effective field length [mm]	141.5	190.7	192.3
comment		reuse	reuse

Table 11.11: Specifications of Steering magnets (High inductance type).

Steering (Low inductance type)	type_A1_M	type_16_5	type_17_2	type_32_4
pole gap [mm] @center	39	72	39	20
pole width [mm]	80	140	80	60
pole length [mm]	50	150	80	80
yoke outer diameter [mm]	220 × 219	340 × 312	220 × 219	180
coil wire dimension	1 × 5	2 × 5	1 × 5	1 × 5
coil wire cross section [mm^2]	5	10	5	5
max. current [A]	10	10	10	10
max. field strength [mT]	22.6	9.0	22.8	44.3
coil-wire turns/coil	36	26	36	36
coil length along beam line [mm]	120	228	148	148
current type (DC/pulsed)	pulsed	pulsed	pulsed	pulsed
pole type (block/laminated)	laminated	laminated	laminated	laminated
coil resistance [Ω] (2coils)@50degC	0.12	0.075 @35deg	0.133	0.12
coil inductance [mH] (2coils)	2.0	2.4	2.6	2.9
interlock (temper.) normal state	close	open	open	open
effective field length [mm]	91.8	211.5	120.4	107.4

Table 11.12: Specifications of Steering magnets (Low inductance type).

11.6 Pulsed Magnet

The KEK injector linac [2] has delivered electrons and positrons for particle physics and photon science experiments for more than 30 years. Figure 11.36 shows electron and positron accelerator complex in the KEK Tsukuba site. There are four storage rings, i.e. two rings for light source, PF and PF-AR, and two rings for electron positron collider, SuperKEKB [3] HER and LER. In addition to them, positron damping ring have been in operation since February 2018. All of the rings require full energy injection, 2.5 GeV for PF, 6.5 GeV for PF-AR, 4 GeV for SuperKEKB LER and 7 GeV for SuperKEKB HER as shown in the Fig. 11.36. To satisfy the requirement, 64 pulsed magnets were installed in 2017 and 32 more are planned to be installed in 2018. Using these magnets, magnetic field can be changed shot by shot in 20 ms and was optimized for each destination.

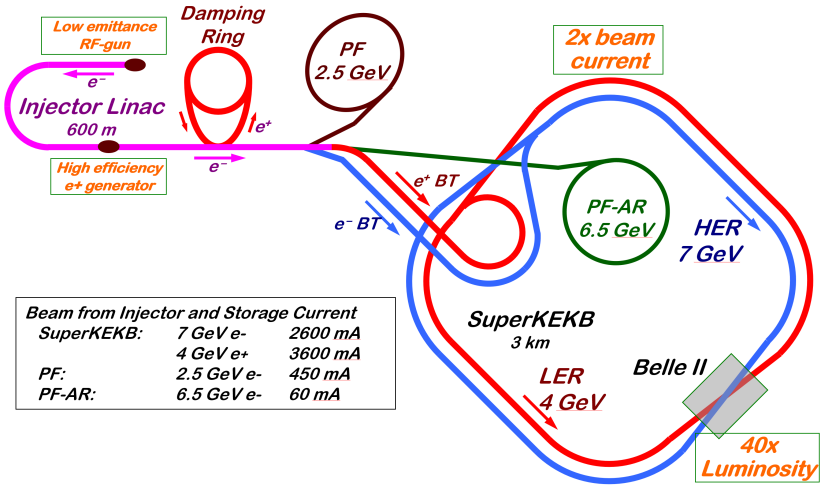

Figure 11.36: A schematic view of the electron and positron accelerator complex in the KEK.

There are 8 (A-C, 1-5) sectors in the linac. Each sector is about 80 m long and the total length of the linac is about 650 m. Figure 11.37 schematically shows beam energy along the beam line. To minimize the installation of the pulsed magnets, acceleration scheme is carefully adjusted to minimize the length of the beam line where the beam with different energy pass through.

The beam for the SuperKEKB HER, it is accelerated in all of the sectors. The beam for the PF, it is accelerated in sector A to 2 and decelerated in sector 3 to 5. The beam for the SuperKEKB LER, electrons are accelerated in sector A to 1 and generate positrons at the target located in the middle of the sector 1. Positrons, shown in dashed line, are accelerated rest of the sectors. Since the beam energy is the same

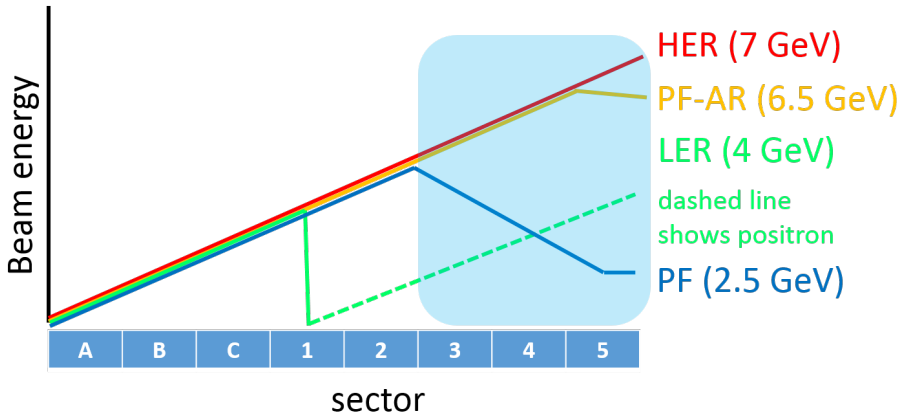

Figure 11.37: Beam energy along the beam line. Solid line shows electron beam dashed line shows positron beam respectively.

in the sector A to C and first half of the sector 1 regardless of the destination, it is not necessary to use pulsed magnets. On the other hand, in sector 3 to 5 shaded by light blue in the Fig. 11.37, beam with very different energy pass through, magnets in these sectors were completely replaced with pulsed magnets. In sector 2 and a part of sector 1, beam energy of the electron and positron is very different. Magnetic field optimized for the low energy positron beam affect the orbit of the high energy electron beam very little. In these section, DC magnets with compatible setting for both electron and positron beam are used except for several pulsed steering magnets at the moment.

11.6.1 Magnet and support

Several types of magnets were installed in the beam lines as summarized in the Table 11.13. Appearance of these magnets are shown in Fig. 11.38. In sector 3 to 5, a common unit shown in Fig. 11.39, which consists of two quad magnets (PM_32_4), a horizontal steering magnet (PX_32_4), a vertical steering magnet (PY_32_4) and a beam position monitor located on a motor controlled movable support, was installed at 13 points. Other types of steering magnets were installed in sector 1 and sector 2. Two quad magnets (PM_32_4) were installed in sector 1 just before the positron production target to focus the electron beam.

Type	L (1 kHz)	R	Max. current	Magnetic field	gap	Installed Number
PX_16_5	2.4 mH	71 mohm	40 A	1040 AT	72 mm	1
PY_16_5	2.4 mH	71 mohm	40 A	1040 AT	72 mm	1
PX_17_2	2.6 mH	127 mohm	40 A	1440 AT	39 mm	4
PY_17_2	2.6 mH	126 mohm	40 A	1440 AT	39 mm	4
PX_32_4	2.9 mH	115 mohm	40 A	1440 AT	20 mm	13
PX_32_4	2.9 mH	115 mohm	40 A	1440 AT	20 mm	13
PM_32_4	1.0 mH	8 mohm	330 A	60 T/m	ϕ 20 mm	28

Table 11.13: Several parameters of the installed pulsed magnets.

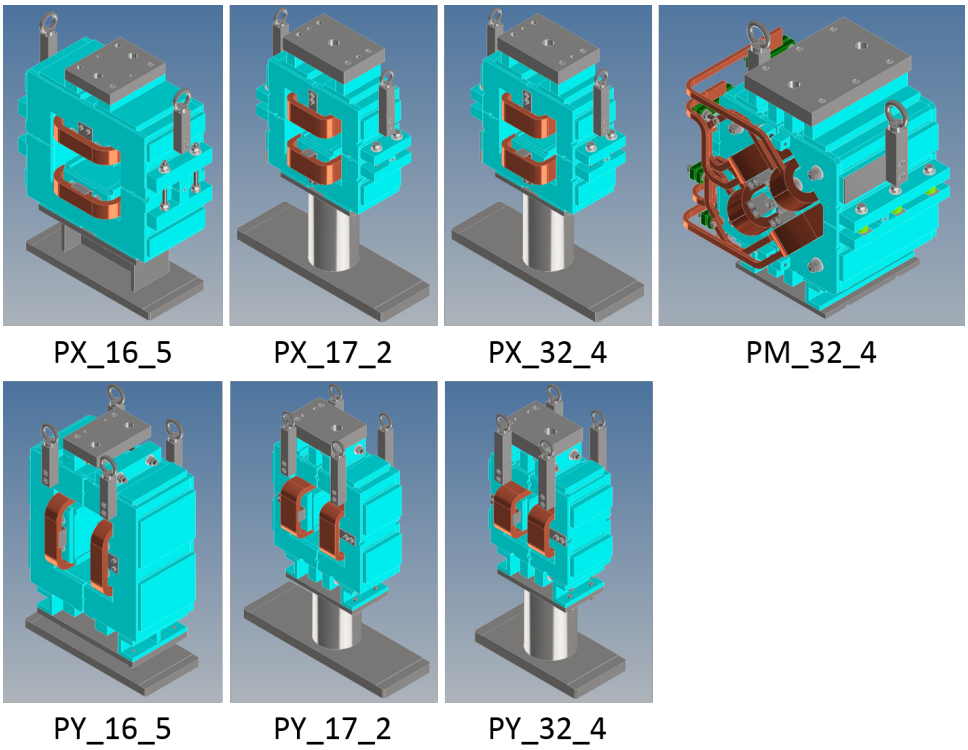

Figure 11.38: Appearance of installed pulsed magnets.

11.6.2 Pulsed power supply

Concept and overview

There are many requirements for the power supply to truly realize the required flexible operation. In addition, since the required number of the power supply is not a few, unit cost, installation space, energy efficiency are crucially important.

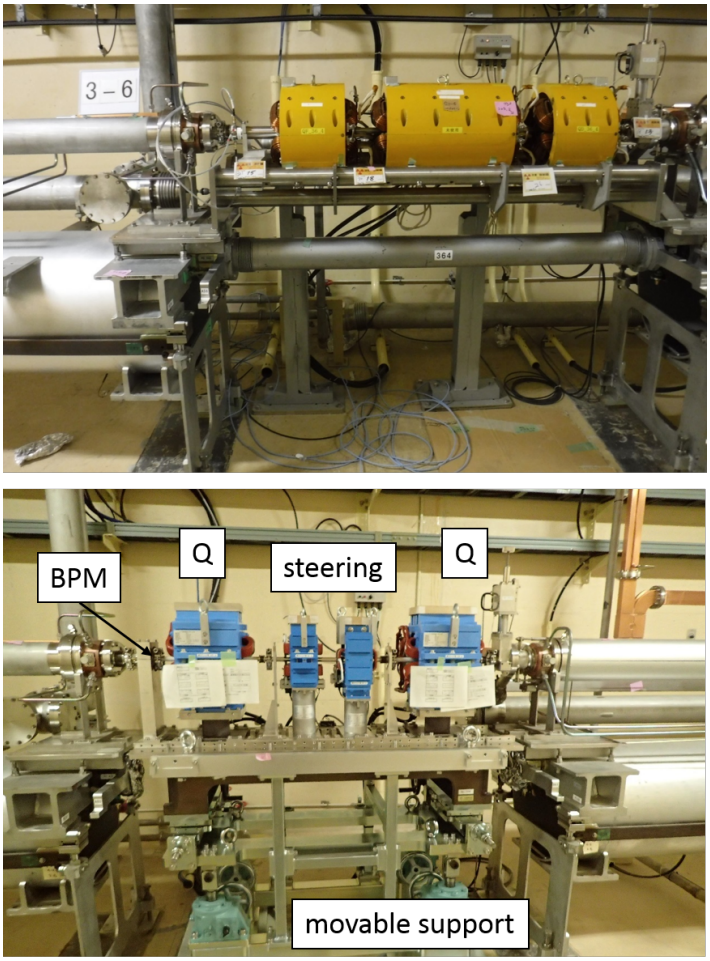

Figure 11.39: The upper photo shows old DC magnets before replacement. The lower photo shows newly installed unit.

Trigger rate of our linac is 50 Hz, but injection pattern is not fixed. The destination of the beam is delivered by the EVENT timing system via optical fiber just after the previous pulse. To interpret the information and change setting within 20 ms, fast and intelligent control system is necessary. To realize these requirements with minimum risks and cost, we decide to develop new power supplies by ourselves following the concepts bellows.

- realize high efficiency with energy recovery
- separate power circuit and control system
- use commercially available components as much as possible
- compatible with existent EVENT timing system
- compatible with existent EPICS control system [25]

Figure 11.40 shows a block diagram of the pulsed power supply system [26]. One standard unit which covers 4 quad and 4 steering magnets, shown in Fig. 11.41, consist

of a PXI express unit for fast control, DC power supplies, pulse drivers and NI cRIO unit for interlock and slow data acquisition.

There is one computer to control and monitor all of the 64 DC power supplies (DC power supply control server). A CSS archiver and A Network attached storage are used to log various data not only output current of the power supplies but temperature of the IGBT in the pulse driver, status of the DC power supplies and so on. EPCIS channel access protocol is mainly used for the communication among computers. LXI ver 1.3 protocol is used to control the DC power supplies and NI network shared variable is used to send fast waveform data.

As for the event timing system, dedicated optical fiber is directly connected to the module. Most of the software is written by LabVIEW 2016 (32 bit) with NI DSC module and running on Windows 8.1.

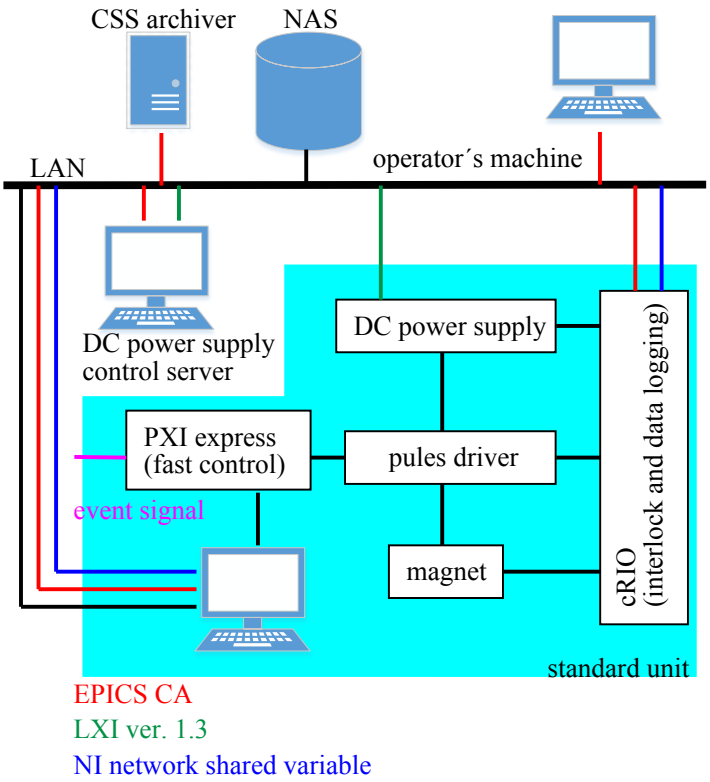

Figure 11.40: Block diagram of the power supply control and monitor system.

Pulse driver for quad magnet

Design parameters of the pulse driver for the quadrupole magnet is summarized in Table 11.14. To achieve these values, a novel switching power supply with energy recovery circuit was developed

Figure 11.41: A photo of the standard unit for 4 quad and 4 steering magnets.

parameter	**value**
max current	330 A
max voltage	230 V
stability	0.1%
cooling	water cooled
power consumption	1500 W
repetition	50 Hz

Table 11.14: Design parameters of the pulse driver for quad magnet.

Figures 11.42 and 11.43 show an appearance and a conceptual circuit diagram of the pulse driver respectively. The circuit consists of two IGBTs (IGBT 1 and IGBT 2), two capacitors (C_HV and C_LV), two DC power supply (VH and VL) and several diodes. After the trigger signal arrives, first, both of the IGBTs turn on and current provided from both of the capacitors pass the load through red lines shown in the upper figure in Fig. 11.43. When the current reach the set value, IGBT 1 turn off and the gate voltage of the IGBT 2 is controlled to keep constant output current. Finally, after the beam pass through the magnet, IGBT 2 turn off. Stored energy in the load (magnet) is recovered to the capacitor (C_HV) through the red line shown in the bottom figure

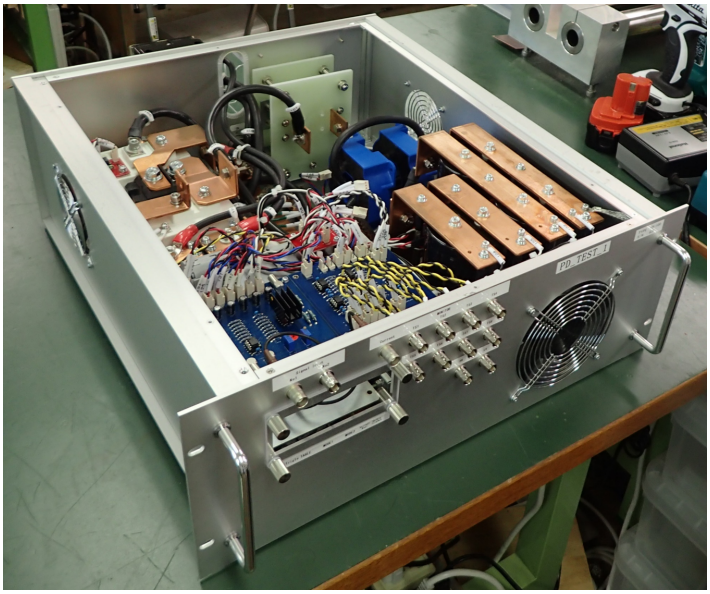

Figure 11.42: A photo of the pulse driver for quad magnet.

Fig. 11.43.

By combination of such energy recovery mechanism and water cooling system, the outsize dimension of the pulse driver is as small as EIA 3U in height. Output current is monitored and fed back by two independent DCCTs with hall sensor (LEM LF 1005-S) which are calibrated by a more precise external DCCT (Hioki 9709).

Pulse driver for steering magnet

Design parameters of the pulse driver for steering magnet is summarized in Table 11.15. Compared with the driver for quad magnet, output power is very small but bipolar output is required. To meet with this condition, power operational amplifier (Apex PA12 [27]) was used for the key device. Although such kind of amplifier is low efficiency compared to switching power supply, the output power is very small compared to the quad magnet above and the low efficiency affect the total power consumption very little.

Figure 11.44 shows an appearance of the pulse driver for the steering magnet. Air cooling was adopted for the simplicity and cost. Usually steering magnets are used in a pair of horizontal and vertical magnets, there are two circuit in one box of JIS 2U height (99 mm). Output current is monitored and fed back by two independent precision resister of 1 ohm which are calibrated by more precise external DCCT (Hioki 6862).

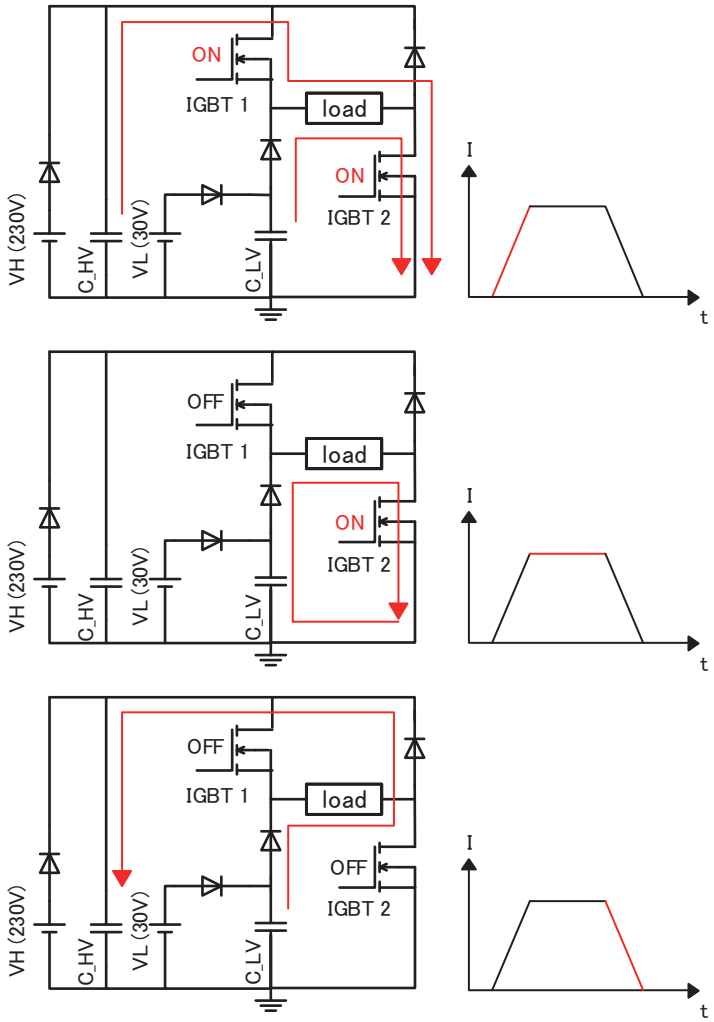

Figure 11.43: Conceptual circuit diagram of the pulse driver for quad magnet. Red allows shows the current path. Right side figures shows current profiles at corresponding states.

parameter	**value**
max current	± 10 A
max voltage	± 40 V
stability	0.01%
cooling	air cooled
power consumption	750 W
repetition	50 Hz

Table 11.15: Design parameters of the pulsed driver for steering magnet.

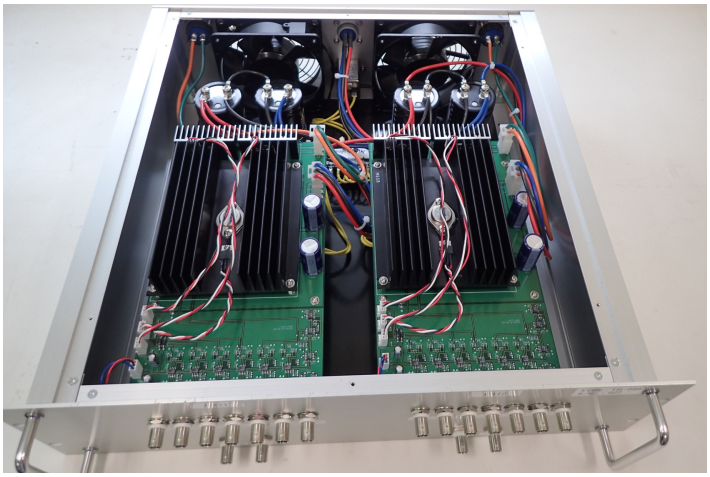

Figure 11.44: A photo of the pulse driver for steering magnet.

Control and monitor system

For the fast control, PXI express unit plays major role. The unit shown in Fig. 11.45 consists of a PC and a PXI express chassis (NI PXIe-1082) with four cards, a controller board (NI PXIe-8381) to connect to the PC, an event receiver board (EVR) (MRF PXI-EVR-230), a DAC board (NI PXI-6733), and a ADC board (NI PXIe-6356), which can set and monitor output current up to 8 pulsed power supply independently in 16 bit resolution with 1 MSa/s sampling or update rate. They are placed in the same rack and connected by a metal cable.

For the slow data acquisition and interlock system, NI compactRIO (NI cRIO-9063) unit is used. One unit consists of a 32 ch 250 kSa/s/ch ADC module (NI 9205), a 32 ch TTL digital I/O modules (NI 9403) and two 4 ch relay output modules (NI 9482). It covers 4ch of the pulsed power supply, namely for one PXI express unit (8 ch), two cRIO units are needed. To realize robust interlock system, cRIO is working not in a scan engine mode but in a FPGA mode. On the upper layer, EPICS CA server is running on the NI RT Linux. Not only the PVs for the ADC and DIO data, but the PVs for the high and low threshold, average number to control data acquisition are also prepared which can be set and read using EPICS CA protocol.

Trigger system

An EVR board in PXI form factor is used to integrate the timing system to the linac timing system. In our linac, event timing system by Micro-Research Finland Oy (MRF) is adopted. The EVR receive not only the timing information but also the mode number and shot ID. The mode number is used to determine the next output setting. The shot ID is used to tag the monitored information. The trigger timing is

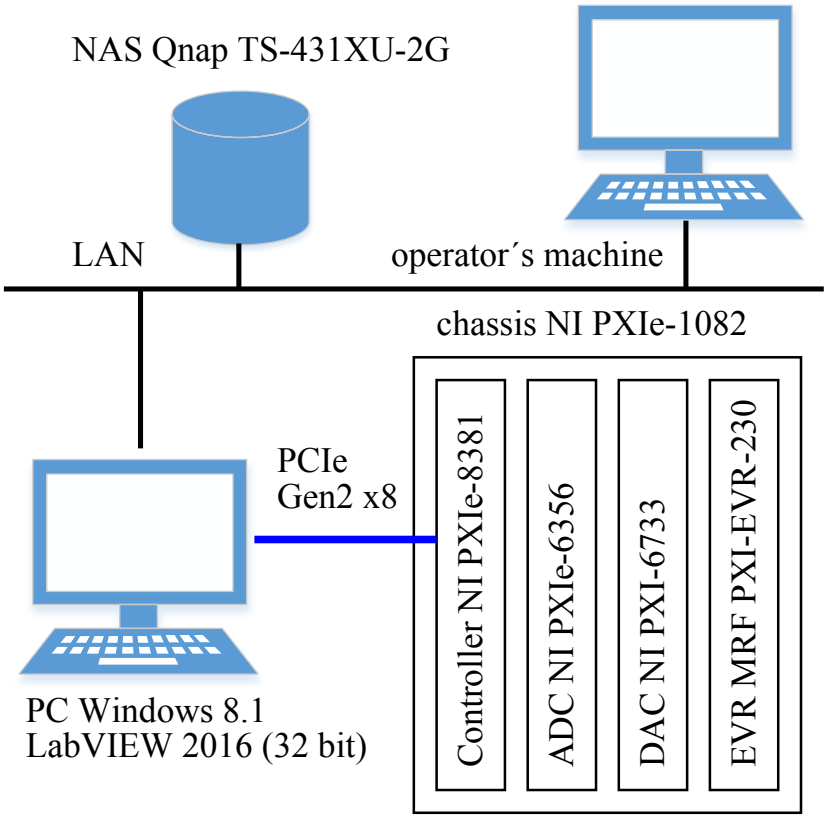

Figure 11.45: Components of the fast control system.

precisely (8.77 ns step) adjusted 3 ms before the beam arrival. Since the rising and falling time of the magnet current is in the order of ms, pules shape of the power supply does not important as long as the reproducibility is assured.

11.6.3 Performance evaluation

Efficiency

Power consumption of the pulsed power supply for quad magnet was calculated and measured by a power meter (Hioki, PW3335). Blue bars in Fig. 11.46 shows calculated power consumption from measured resistance and inductance of the magnet and cables when one magnet was operated at 300 A and 50 Hz without energy recovery. About 15% of energy is lost by ohmic heating of the coil and cable but 85% are stored in the inductance of the coil. It is in principle possible to recover the latter part of the energy to capacitors. Green bar in Fig. 11.46 shows measured power consumption in total including DC power supply. The red allow corresponds to recovered energy. The energy recovery efficiency compared with stored energy in inductance and total energy

are as high as 80.1% and 68.5% respectively.

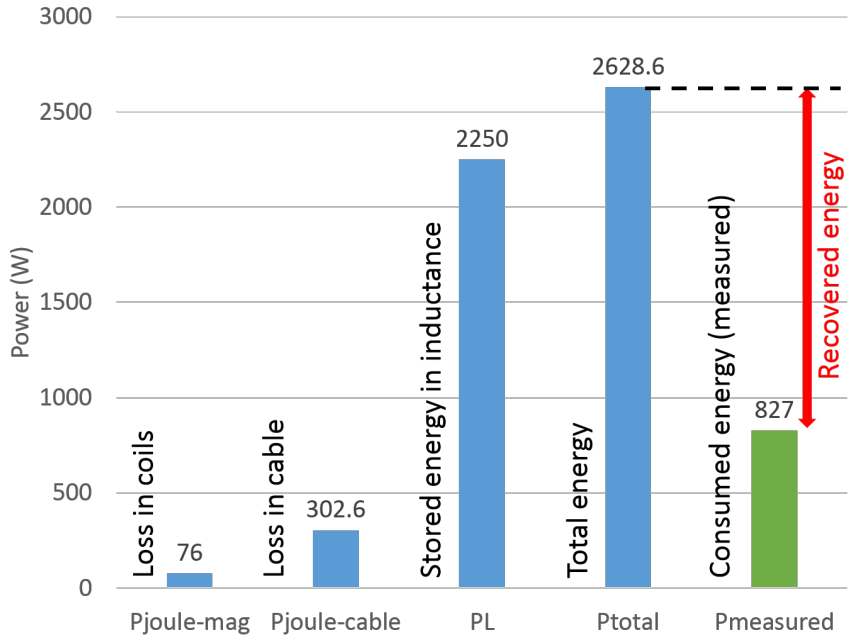

Figure 11.46: Energy balance of pulsed power supply for quadrupole magnet.

Stability

Figure 11.47 shows a stability measurement result of pulsed power supply of quad magnet for 24 hours. Horizontal axis shows the measured output current and vertical axis shows the number of entry. Bin width is 0.2 mA Output current was set to alternate between 0 A and 166 A at 50 Hz. Measured mean value and standard deviation of the output current were 165.946 A and 14.578 mA respectively which corresponds to 88 ppm (0.0088%) relative stability at this current. This is much smaller than design value (see Table 11.14).

11.6.4 Operation

After four months installation work from May, comprehensive test was done for a month in September in 2017. In November, simultaneous injection using the newly installed pulsed magnets were demonstrated successfully. Since the SuperKEKB phase two operation start from March in 2018 and light source rings restart in May, real simultaneous injection operation started in the middle of May and ended July in 2018 for summer shutdown. During entire period, there was no sever problem and the beam was delivered to all of the four rings stably.

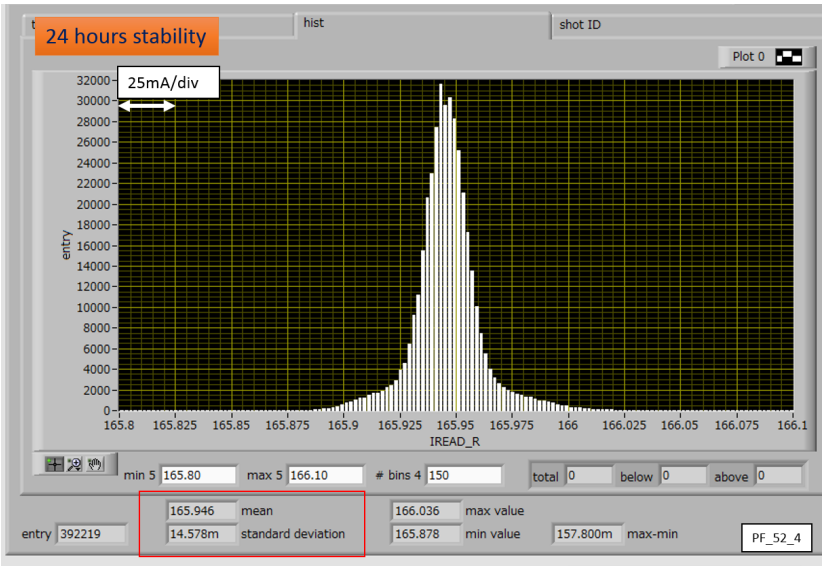

Figure 11.47: A histogram of the stability measurement of pulsed power supply for quad magnet.

Large number of DC magnets was replaced with new pulsed magnets in 2017 for the pulse-to-pulse beam modulation for 4 storage rings. Two kinds of pulsed power supplies for quad and steering magnet respectively were developed. Installation and commissioning of the system were successfull and they are now working in the KEK electron positron injector linac without any severe trouble for about 1 year.

11.7 Alignment

All of the hard wares in the beamline were re-aligned after the big earthquake in March 2011. This was done in the level needed for injecting into PF rings, but the requirement for the suppression of the emittance growth in injecting to the SuperKEKB main ring is tighter than KEKB so that the alignment should be improved to practically realize the regime of 0.1 mm in sigma.

11.7.1 Requirement for SuperKEKB

The linac is configured as J-shaped as shown in Fig. 11.48. Therefore, the alignment of the linac consists of those for the two straight lines and one 180-degree turnaround, starting from the gun and ending at the exit point at "E2".

The bunch charge injecting into the main rings has increased by 4-5 times compared to the KEKB with the emittance of an order of magnitude low. One of the most concerns to suppress the emittance growth of such a high-charge bunch in the linac is the single-bunch wakefield driven by the accelerator structures. From the emittance growth simulations assuming random misalignment of the accelerating structures, we found that the local alignment tolerance should be 0.1 mm in sigma and the global one 0.3mm [28]. The same tolerance is applied for the alignment of the quadrupoles and other hard wares unless specifically required by other reasons. Most of the BPM's are mounted in the quadrupole magnet bore. The tolerances for the horizontal and vertical misalignments are set the same because the tolerable emittance growth in both planes differs only by a factor 2.

In the above requirement, we should define the words "local" and "global" to specify the practical requirement. Since the emittance growth becomes large when the misalignment pattern along the beam direction coincides with the betatron wavelength, the tolerance requirement should be defined taking this feature into account. The typical betatron wavelength for electron beam is about 25m for sectors A to B, 50m from sectors 1 to 2, and 100 m from sectors 3 to 5. Those for positron vary from 7 m at the beginning just after target to 20m level at the transfer line to DR, while that from sector 3 to 5 is 50 m. We define the region of the local alignment tolerance to be within a fraction of the wavelength. On the other hand, it is natural that the global alignment tolerance is applied in the full span of each straight line.

11.7.2 Measurement tools

There are two key devices for linac alignment, a commercially available laser tracker and the laser QPD (quadrant-type Si photo-diode) system [29].

The introduction of the laser tracker, AT401 of Leica, is the most important change from the era of KEKB to SuperKEKB. It is used for the measurement over 10-20 m, covering one to a few girders. The measurement precision over 10 m is 0.1 mm, $15 + 6 \times L$ (microns) based on the specification of the device, where L is the distance in meter. Connecting multiple data sets can be used for the evaluation over the longer distance but not very long range because many-time connection integrates random and systematic errors. Rather than connection, the girder alignment over a medium range up to the betatron wavelength, such as 50 m in both directions giving 100 m in total, can be measured in one setting (without connection), though the bigger error in the long distance in mind, but it is to be noted that the linearly increasing error gives the same angle error even in a long distance.

Another important device is the Laser QPD system. The sensors and the vacuum chamber are the same as those of KEKB, but the laser passage was improved by properly shaping the beam with a big profile needed for passing over 500 m and feeding back the laser beam position at the endpoint by adjusting the laser pointing angle. This system gives the straight reference line rather straightforwardly, but we know that the QPD sensors suffer from the gain loss due to the irradiation by beam related radiation. Actually, 1/3 of the sensors used for KEKB were replaced by new ones. If the sensitivities of the four quadrants are the same, the calculated position is kept but we do not know confidently about the variation of radiation damage among four quadrants. Therefore, we use this system intensively for the initial alignment in the early stage. Note that we can measure the sensitivity as needed by tilting the laser beam so that this system can evaluate the relative motion precisely on-line and even after beam operation years. However, the actual center evaluation, not only the sensitivity, is needed for the alignment. Therefore, when we need any reference of a long-range straight line, we need to use this system with confirming the QPD sensor characteristics beforehand.

11.7.3 Reference frame

The coordinate system for the alignment of the linac is defined as Fig. 11.48. The nominal coordinate is defined as x-axis the right-ward direction seen sitting on the beam, y-axis upward and z-axis forming the right-handed Cartesian coordinate system. Note that the z-axis is in the negative beam direction. There are three regions to be

connected to make the J-shaped linac. These are the two straight lines, one 120 m line (AB line) from A1 gun to B sector end and another 500 m line (C5 line) from C sector to 5 sector connected at a turn-around called J-ARC. This configuration was formed for KEKB and we use it for the SuperKEKB.

We adopted the mutual relationship among these three regions as was to keep away from any large modification. The related measurement results and the adopted reference frame definition are listed in Table 11.16 and shown in Fig. 11.49. The start and endpoints of the longest straight line from sector C to 5 are the end of J-ARC (BM_06_D) and the reference point (E2) connecting the linac to the BT line for main rings. We tried to set the J-ARC plane to sit in the same plane with C5 line and AB line. However, the measured inclination angle of C5 line at J-ARC is 69 microrad from the horizontal surface, which is 19 microrad more than that of the AB line. Note that this 50 microrad is the comparable inclination angle to the geometrical one, 40 microrad, determined by the earth round surface between the horizontal surface at J-ARC and the 500-m straight line connecting the J-ARC and E2 point. As the practical value for the SuperKEKB design, we chose this inclination amount (50 microrad), taking the benefit that we do not need to change the level of the gun area. On the other hand, the C5 line was defined as the straight line connecting two points, BM_06_D and E2. It means that we accepted the difference in the inclination angle of C5 line between measured and design. However, the measurement error may be larger than this difference, because the measurement device is the laser tracker, which cannot accurately measure over a long distance and limited by several tens of microradians, and the measurement distance was over a limited length, only between C1 to C5 to represent the C5 line. The 500-m C5 line can only be evaluated using the laser QPD system but was not in full operation as of the reference frame definition in 2013. Now we can check the validity of the straightness by laser QPD system and the data measured in late 2017/early 2018 indicates that the line between C1 to C6 is only 2 microrad different w.r.t. the C5 whole line. However, even now, we cannot evaluate the mutual inclination difference between AB and C5 lines precisely with only a laser tracker so that it is not meaningful to discuss it further. We let the C5 line as is only if any need to adjust the absolute inclination angle comes up.

In summary, the inclination angle of the J-ARC was set the same as that of the AB line, while that of the C5 line is about 19 microrad downward toward E2 point. Even if this difference in the inclination at the J-ARC is real, it gives only 10 mm difference at the end of linac after passing 500 m so that this difference at the end is not the big issue.

The opening angle in the horizontal plane between AB and C5 lines was measured

as 114 microrad less than 180 degrees and we set the J-ARC rotation to symmetrically share the mismatch between the tangent of J-ARC and the straight lines, 57 microrad at each end, resulting in the rotation angle 180.007 degrees, as shown in Fig. 11.49.

The LTR and RTL lines are made referring to the G4' point near the down end of the unit #2–8 girder and the upstream points along the linac in the region over 20 meters or so. These reference points and angles were set by measuring the laser QPD in the C5 line mentioned above.

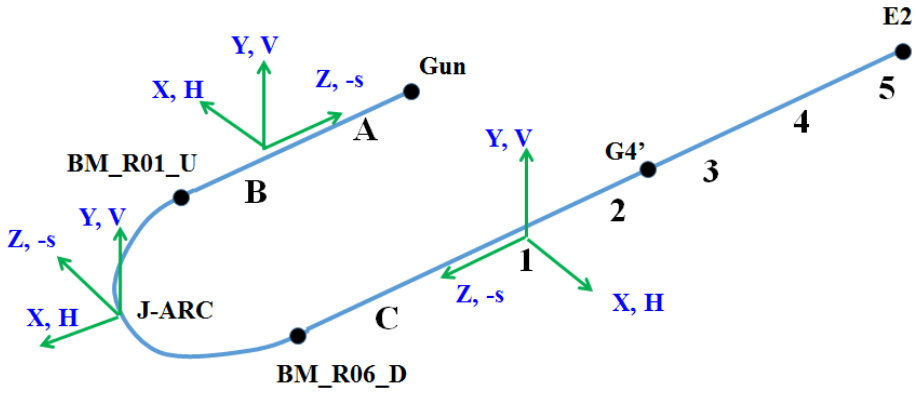

Figure 11.48: Linac configuration and the coordinate system for alignment presentation. It consists of the two straight lines, the first AB line and the second C5 line, and the 180 degree ARC, called J-ARC, connecting two straight lines. Typical coordinate system at each representative point in the linac is shown in the figure.

11.7.4 Nominal hardware setting mechanism and new features for SuperKEKB

The configuration of the accelerating structures sitting on a unit girder of 8.5 m is the same as KEKB and shown in Fig. 11.50. Sub-support planes (green plates in the figure) are precision set by the laser tracker with respect to the two reference points (red dots in the figure) at both ends of the girder shown. The introduction of these reference points is one of the new features for the SuperKEKB. These points are well aligned to the laser QPD system. The structures are mechanically set at 300 mm above the plate and at 120 mm from the reference bar precisely set on the plane.

Another new feature is the direct measurement of the accelerator structure position by the laser tracker w.r.t. the reference points of the girder. Typical pictures for the reflector setting are shown in Fig. 11.51 (left), where the reflector is precisely mounted on top of the coupler body of the accelerating structure. Many old quadrupole magnets,

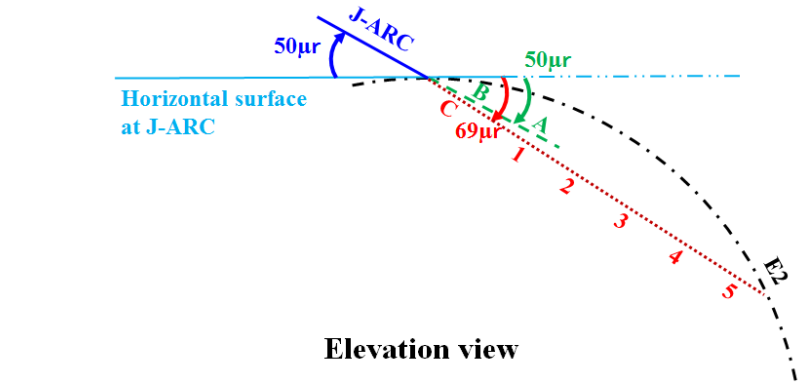

(a) Vertical inclination.

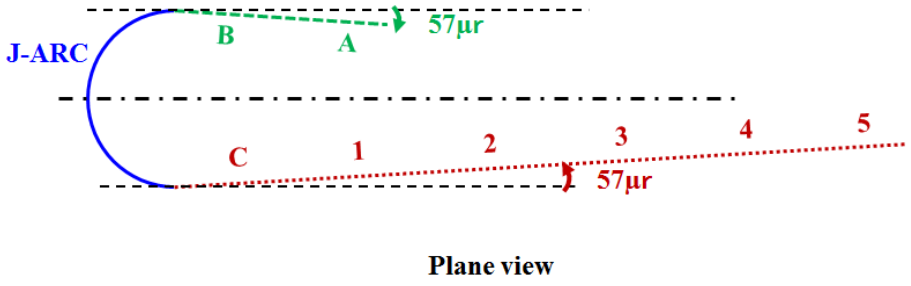

(b) Horizontal plane.

Figure 11.49: Relationship among straight lines and turn around. Figure (a) shows the vertical configuration, while (b) shows the horizontal configuration.

used for KEKB, sit on the independent girders which are aligned w.r.t. the adjacent accelerator unit girders by extending the arms and positioned by pin mechanism. The same new feature for the alignment of these magnets is that a precision base for setting the tracker reflector is mounted on each magnet yoke as shown in Fig. 11.51 (right). Then we can measure the magnet position directly by using the tracker w.r.t. any reference points nearby.

All the pulse magnets in sectors 3 to 5 are set on newly developed girders. The girder position can be measured by the laser tracker by using the reference points attached to the near-by girders. Another new feature on this girder is the integrated active alignment mechanism with the movers in horizontal, vertical and rotation along the beamline.

The hard wares in the new positron generation system are aligned by using the laser tracker. The hard wares in the electron generation area called AT for thermal electron gun system and A1 for RF gun system are all aligned with using a laser tracker. The reference line here is that defined with aligning unit girders in two sectors, A and B.

Relation	Value	Comment
Measured and set vertical inclining angle of J-ARC *	50 microrad	Angle w.r.t. the horizontal surface at J-ARC
Measured and set vertical inclining angle of A-B sector line *	50 microrad	Measured over B4-B8 unit w.r.t. the horizontal surface at J-ARC
Measured vertical inclining angle of C5 sector line *	69 microrad	Measured over C1-C6 unit w.r.t. the horizontal surface at J-ARC
Measured and set distance of ARC start and endpoints	15.015 m	from BM_01_U to BM_06_D
Measured and set opening angle of two straight lines, AB and C5	$2\pi - 114$ microrad	Two lines are symmetrically set w.r.t. J-ARC symmetry axis

* Values with respect to the level surface at J-ARC start/endpoints, measured as of October 2013 using laser tracker.

Table 11.16: Measurement/set results on reference-plane-related geometries.

The hard wares in the positron production area with target, flux concentrator and beam spoiler followed by solenoid magnet channel are also aligned with using the laser tracker with referring to the straight line defined by the unit girder alignment over a long distance.

11.7.5 Procedure for hardware alignment

The basic procedure of the alignment of the hard wares is in three steps. The first step, initial alignment of the girders, is performed by using the laser QPD system, where

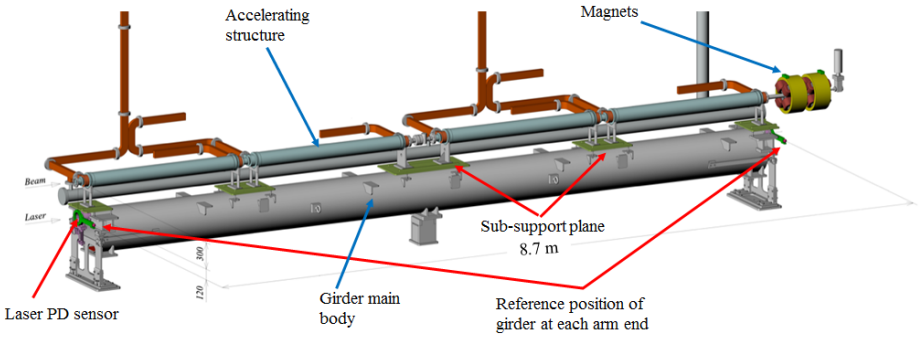

Figure 11.50: Unit girder equipped with laser QPD at each end with an arm for extending alignment fiducial to the place where the tracker laser beam can access.

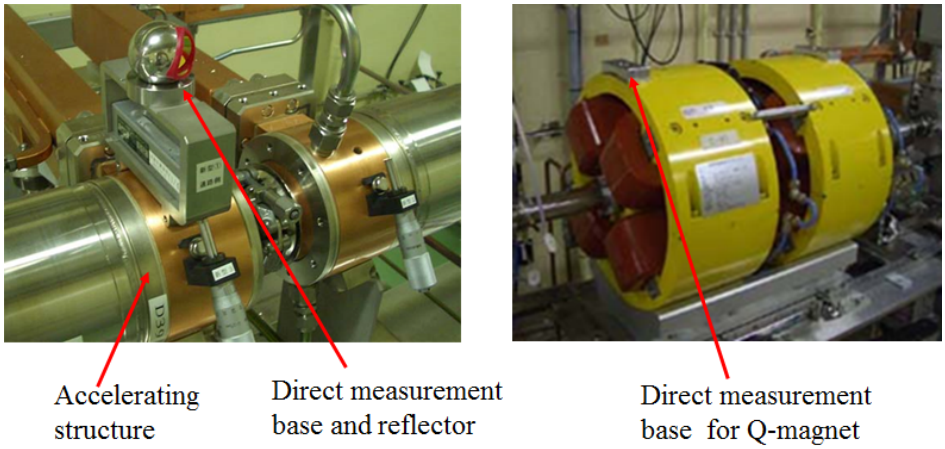

Figure 11.51: Direct position measurement point with laser tracker for all relevant hard wares.

the laser pass can define a straight line. The reading error is as small as 0.03 mm, but the systematic error is speculated to be an order of 0.1 mm or more. The girders for the quadrupole magnets from KEKB stage are aligned on a support structure resting on the adjacent accelerator unit girders with using mechanical pins or bars. On the contrary, the new pulse magnet (quadrupole magnets and steering ones) supports are independent on but aligned w.r.t. the adjacent accelerator girders by using a laser tracker.

In the second step, or frequently earlier than the girder alignment process, the beamline hard wares are set on the girder, mechanically referring to the reference bar and plate sitting precisely w.r.t. the girder reference points. This mechanical alignment error in this process is assumed ± 0.05 mm. The positions of the reference bar and reference plane are measured using laser tracker w.r.t. reference points attached to the girder as shown in Fig. 11.50. In addition, the hardware positions can directly be measured and confirmed and corrected if needed. We checked the stability of the hard wares on the girder. Most of the cases, the variation of the position w.r.t. the girder reference points is within 0.05mm. Therefore, we do not realign the hard wares unless noticing any suspect of movement on the girder.

In the third step, the hard wares are directly measured among each other, in addition to measure w.r.t. the reference points on the girder, with using the laser tracker. This is the process to estimate the hardware position information over a short distance in a most-precise manner, though not referred to the girder reference points.

11.7.6 New beam-line hard wares for SuperKEKB

In the alignment viewpoint, there are three most significant differences of SuperKEKB from KEKB. One is a double-deck electron source area with a thermionic gun and two photo-RF guns, the second a new positron generator at different position in linac than KEKB, and the third an introduction of positron DR.

The thermionic gun is elevated by 750 mm above the nominal beamline at 1200 mm above the floor. The two RF-guns are located at the nominal level, one in straight position along beamline and the other injected by 45 degrees from aside. These double-deck lines merge after acceleration by an angle of 24 degrees. The alignment of the hard wares in this area should be better than others especially due to the low beam energy. The alignment of this area can be measured by using the laser tracker so that we set the alignment tolerance of this area to be 0.1 mm, based on the capability of the measurement accuracy at a distance of 10 m spreading over 20 m scale.

For the positron production, heavy positron production hard wares were moved towards upstream by 40 m from the old (KEKB) location at the unit #2–1 to the new location (SuperKEKB) downstream of the 13 unit. By the end of January 2016, the radiation shield for this new positron production system, one the heaviest hard wares (40 tons) in the linac was completed and set at unit 15, spreading over 5 meters. In the same area, heavy hard wares, solenoid magnets with the weight of the order of 30 tons in total, spread over 15m from the unit 15 to 16, sitting on the aluminum girders.

Two new beam transport lines, to (LTR) and back (RTL) from DR, were created connected to the linac at a space between sectors 2 and 3. The old positron production area, unit 21, was now converted to the standard acceleration unit, but the weight did not change much because the radiation shield was integrated to the tunnel ceiling and was kept. Therefore, we do not expect any big change in this area due to the heavy load change on the floor. In turn, many heavy large-bore quadrupole magnets were densely located from unit 17 to 21. Due to the construction of LTR and RTL, the area between the units 28 and 32 was used for placing bending magnets and chicanes.

11.7.7 Refining alignment

The basic alignment information is obtained during any maintenance period by the laser QPD system. One of the typical recent measurement results is shown in Fig. 11.52. The calibration factors for each QPD sensor are assumed to be the same as those obtained one year ago. We should admit that the calibration factors are subject to the beam radiation and others and may vary. We assume from various evidence and experiences that the error is well below 1 mm but not as small as 0.1 mm level.

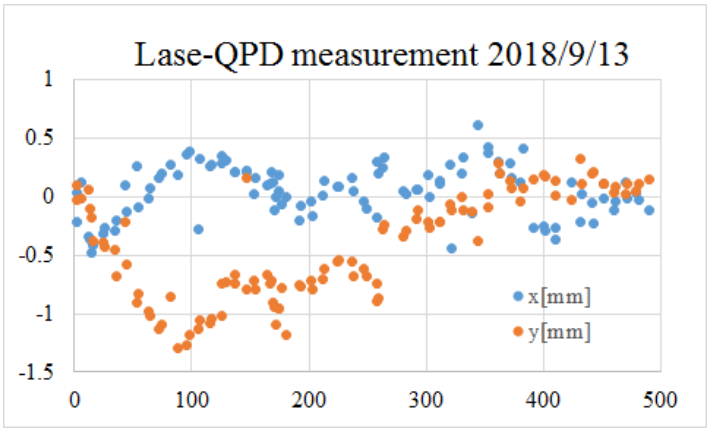

Figure 11.52: Recent laser QPD measurement result along C5 line.

The above is the result of the initial alignment and we do not adjust each girder alignment to zero the values. As the next stage, the girder alignment over a medium range is measured by a laser tracker. An example of the measurement in summer 2018 is shown in Fig. 11.53. Here each measurement spans over several tens to 100 m range and the overlapped regions are used for connection to estimate the whole feature. If we subtract smooth sinusoidal variation with the wavelength longer than 200m, much larger than the betatron wavelength at any place, the residual deviation is 0.5mm in sigma. Taking this residual information into account, we can improve the smoothness of the girders within much less than 1 mm over 100 m range by adjusting such area as those shown in the figure indicated by unit numbers. This local misalignment correction on the girder position is proceeded by the laser tracker measurement with a precision of ± 0.1 mm over 20 30 m range.

On top of this improvement of the girder alignment, we can use the direct measurement of the hardware positions among each other to further improve the smoothness in a short distance over 10-20 meter range with a precision of ± 0.1 mm, limited by the specification of the laser tracker device.

The beam based position measurement of quadrupole magnets can be applied for almost all of them. Assuming the mechanical precision of the magnet w.r.t. the magnetic center, we deduce the alignment information of the magnet. It will give us more precise alignment information among quadrupole magnets and the result can be used for improvement of the magnet alignment. We can also deduce the reference point position attached to the girder with respect to the quadrupole magnet measurement. In principle, it will serve to improve the girder alignment.

Such information of the direct alignment information and the indirect one based on the beam should be integrated and used in an optimized manner until reaching the

goal.

11.7.8 Floor movement and compensation

Once any golden alignment is obtained, the rest of the work is to keep it. The underneath base blocks, where all of the linac hard wares sit, extend over 80 m or so in beam direction and are supported with many piles of longer than 30m reaching to the firm soil. However, the very surface of the floor on which most hardware girders sit has only 150 mm thick concrete plate which is paved on the underneath base. Due to this feature, we suspect the very surface plate to move rather easily. Moreover, the underneath blocks are loosely connected for stress release purpose at the expansion joints and we know such joint areas are subject to the big mutual movement of a fraction of a millimeter. Considering this situation, we should design the way how to keep the alignment of the hard wares sitting on such a moving floor.

We measured the floor movement by using the laser QPD system for long period [30]. Figure 11.54 shows the overlay plot of all of the measurements in vertical direction over two years from May 2016 to June 2018. The vertical lines show the position of the expansion joints. The range of the vertical movement near the expansion joint is more than those of the area away from the joints. This feature in the vertical direction shown in Fig. 11.54 is more evident than that of the horizontal direction. From this measurement, we see the big motions of a fraction of a mm near the expansion joints which show a yearly cyclic feature, in contrast to the relatively quiet area away from the expansion joints by more than 10 m, as shown in Fig. 11.55. Since the daily movement is about 50 microns and the evolution speed over a week or month is at most of the order of 0.1 mm per week, a slow feedback, such as once a day, is enough to compensate the motion.

Thus, we obtained a gross feature of the floor movement. Then the most critical issue is the practical definition of the reference for the position feedback but we should admit that any practical method to define such feedback point is yet to be realized. What we have in mind now is the following. We can use online monitoring information, such as the laser QPD system with active insertion mechanism, the beam position monitor and the stretched wire/water leveling system. For the first two we have already the prototype hard wares but we need to develop the practical feedback protocol. For the last one, wire/water, the technology should be robust at least in a medium long range, 100 m or so, but we need some time to implement into the linac system. Assuming that we obtain such information well, we can feed back the girder positions toward the golden position found at some earlier time.

11.7.9 Active mover

Once we define the reference position as mentioned in the preceding section, we move the girders. We have developed the mover for the pulse magnet girder and installed in the sectors 3 to 5. The specification of the mover resolution is 0.01 mm and the actual positioning capability was found better than a micron level. We are also developing unit accelerating structure girder.

11.7.10 Resistivity against earthquake

Most of the injector linac for SuperKEKB suffered from the big Earthquake in March 2011. Linac is aligned in north-south direction and the long-lasted vibration made the accelerator structure girders swing in a large amplitude. Since the relation between the spring constant of the girder support and the weight load on the girder differs in many places, the resonantly excited swing frequency differs from a girder to the next. It resulted in a pi-mode oscillation between some girders and many of the hard wares in between suffer from damage and falling. Taking this problem in mind, we have installed the mechanism of fixing or limiting big movement on the unit girders. Actually, the girder center position is grabbed by a mechanism firmly fixed on the floor. The movers mentioned above should be stiff enough to replace this mechanism when actively controlled.

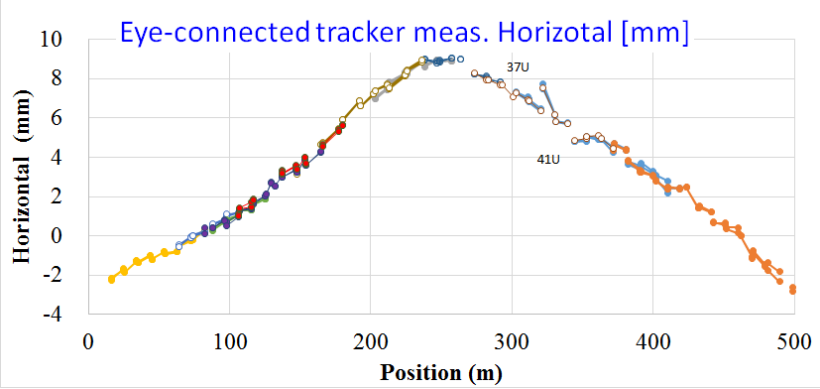

(a) Horizontal direction.

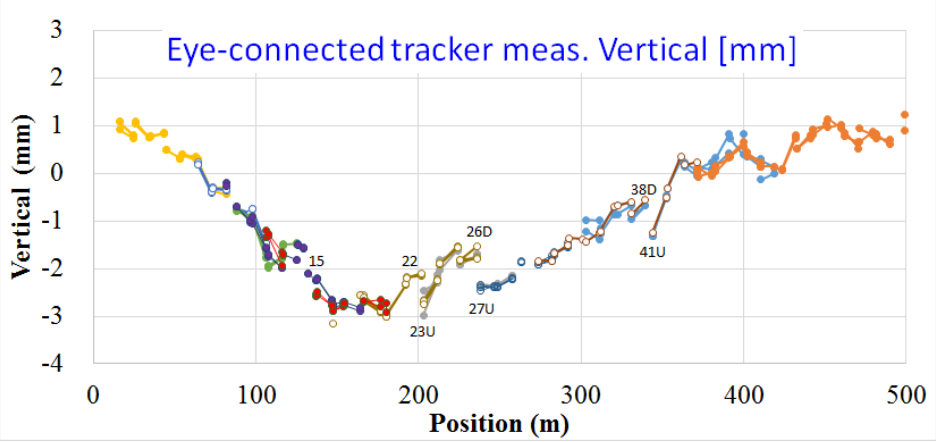

(b) Vertical direction.

Figure 11.53: Eye-connected ensemble of long-span laser-tracker measurements in (a) horizontal direction and (b) vertical direction. It is to be noted that in these plots the long-range bending feature over 100 m or more should not be understood as actual because it may come from the systematic error in measurement, due to the device and in the environment, etc

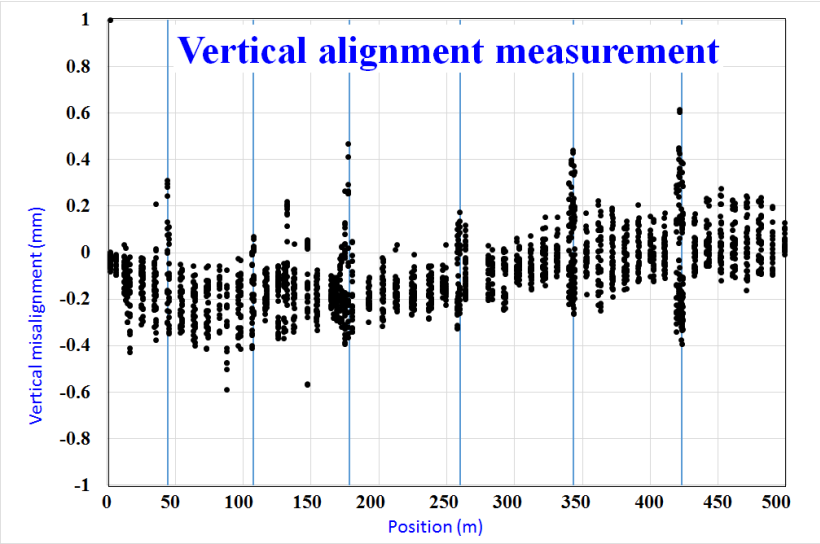

Figure 11.54: Ensemble of twenty data sets taken during two years, between May 2016 and June2018, measured by the laser QPD system.

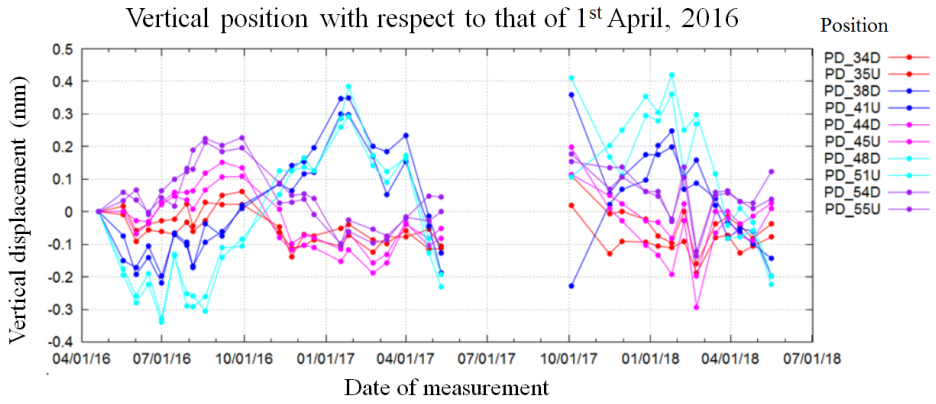

Figure 11.55: Vertical position over two years measured by laser QPD system. More movement with yearly-cyclic feature is seen in bluish points near expansion joints (a joint between unit 38 and 41 and another between 48 and 51) comparing to the reddish points in calm area away from joints.

11.8 Electron source

In order to realize different injection demands, one thermionic gun and two RF guns are used from SuperKEKB phase I, as listed in Table 11.17 [31]. The thermionic gun (AT-Gun) is adopted for generated electron beams for Photon Factory ring (PF), Photon Factory Advanced Ring (PF-AR), as well as for positron beam generation. Meanwhile, because the SuperKEKB project requires the electron beam for High Energy Ring (HER) with high charge and low emittance, the RF gun (A1-Gun) is adopted as the electron source for generating high-quality electron beam. To allow for smooth operation of SuperKEKB, a secondary RF gun (AS-Gun) is installed in 2017 as a backup for the main RF gun. All of these three guns are installed in the A sector of linac, as shown in Fig. 11.56.

Beam injection	Electron beam source	Electron charge at gun (nC)	Beam energy (GeV)
HER	RF gun	5 [b)]	7
LER [a)]	Thermionic gun	10	4
PF	Thermionic gun	0.3	2.5
PF-AR	Thermionic gun	0.3	6.5

a) For positron beam generation.

b) Phase III requirement for electron beam generated by RF gun.

Table 11.17: Electron beam generation source for different injection mode.

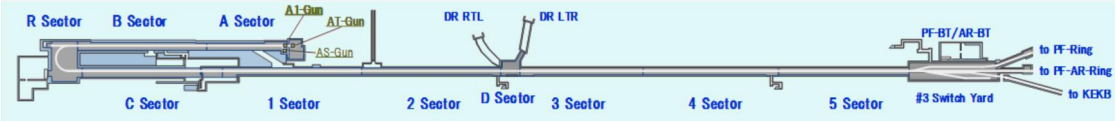

Figure 11.56: Linac schematic from electron beam source to beam transport (BT) part.

For the purpose of reserving the low emittance of the electron beam which is generated by the RF gun, the RF gun is installed in the main beamline. Accordingly, the thermionic gun, sub-harmonic buncher (SHB), pre-buncher (PB), buncher and accelerator structures are raised to the second floor (750 mm higher than the central beamline of the first floor). As shown in Fig. 11.57 a 24° line with 3 quadrupole magnets and two bending magnets are used for combining the electron beam, which is generated by the thermionic gun, into the main beamline at the first floor.

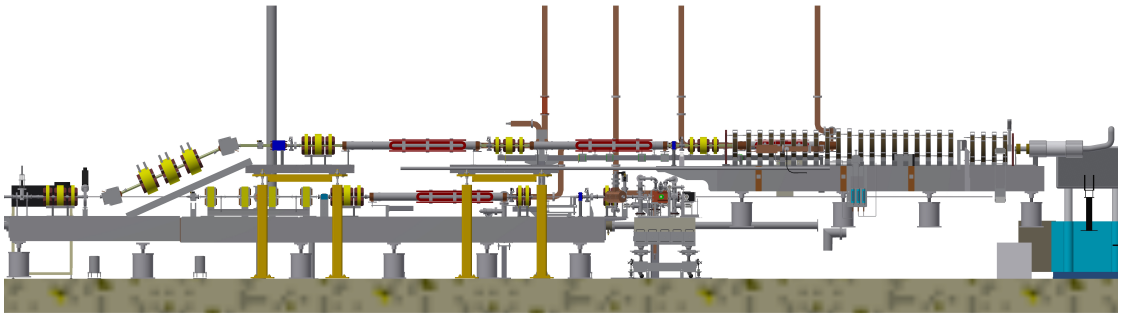

Figure 11.57: Layout of the thermionic gun, RF gun and the combination part at linac.

The layout of two the RF guns is illustrated in Fig. 11.58. The main RF gun (A1-Gun), quasi-traveling wave structure gun (QTW), is selected as main RF gun for SuperKEKB commissioning. It is installed in main beamline for generating 5 nC electron beam with low emittance. Laser impinges into the QTW RF gun with an angle of 60°. The secondary RF gun (AS-Gun), cut disk structure RF gun (CDS), is installed with a 90° angle with the beamline. Two bending magnets are applied to converge the electron into the beamline for acceleration. Due to the 90° angle, the laser beam injects into the CDS RF gun normally. A deflector, operated in HEM_{11} mode, will be added to measure the slice emittance of the electron beam in the pre-injector part between the two bending magnets [32]. Both of these two RF guns have the ability to generate more than 5 nC electron beam with less than 20 μm emittance [33].

For reducing the injection time into SuperKEKB rings, especially for the LER it is being inevitable to increase positron intensity as the stored beam increases, 50 Hz two bunch beams are required for both thermionic gun and RF gun.

11.8.1 Thermionic Gun (AT-Gun)

As to SuperKEKB commissioning, the main mission of thermionic gun is to generated 10 nC electron beam for the generation of positron beam (about 7 nC electron charge at positron target positon). The schematic layout of thermionic gun and pre-injector part is shown in Fig. 11.59, and the parameters are listed in Table 11.18 and Table 11.19.

The triode-type thermionic gun is under operation at 200 kV accelerating voltage. It is connected by a 300 mm long ceramic insulator with ICF-253 flanges. The cathode is a commercial EIMAC Y-796 product of 2 cm^2. 20 nC maximum charge can be generated with a pulse width of less than 1 ns. A high speed grid pulser is employed for such a high current which has a superb pulse feature of small time jitters ($\sigma = 4$ ps) as well as short pulse lengths. An electric analogue time delay module is also used that

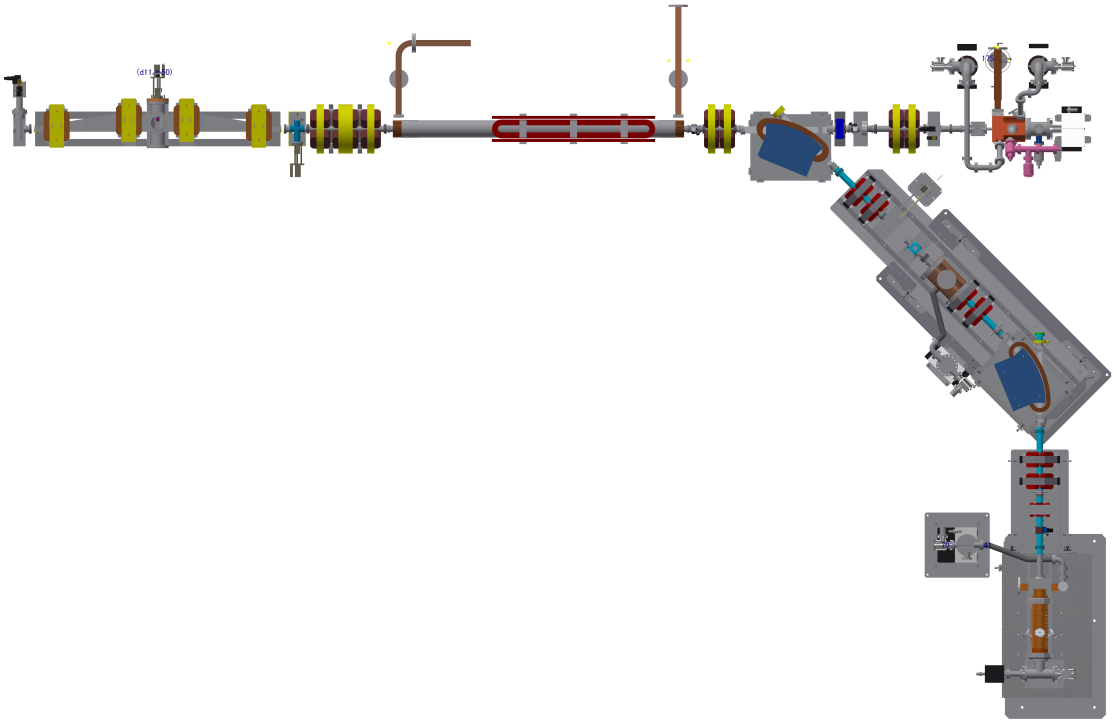

Figure 11.58: Layout of two RF guns at linac A1 unit.

continuously varies the gun trigger timing over a 3 ns range. This function is adopted for a digit feedback system to stabilize the beam timing. The grid pulser also controls the beam repetition rate with external trigger signals, as well as the beam intensity by changing the output voltage [1].

As listed in Table 11.19, The SHB frequencies are chosen from subharmonics near 100 and 500 MHz with the condition that each frequency should be a multiple of the linac/ring common frequency of 10.385 MHz which is a $5 \times 5 \times 11th$ sub-harmonic of 2856 MHz, resulting in the 25th and 5th subharmonics. The first SHB operating at 114.24 MHz (25th subharmonic) and the second SHB at 571.2 MHz (5th subharmonic) are both a standing-wave type re-entrant cavity with a tuning knob. The dimensions are given in Fig. 11.60 (a) and (b). The rfs are fed by corresponding 10-kW solid-state amplifiers through coaxial cables.

As shown in Fig. 11.61, the prebuncher and the main buncher are both traveling-wave type disk-loaded waveguides in which the phase shift is $2\pi/3$ per cell. Since the gun beam is to be velocity-modulated at around $\beta = 0.7$, all of the cell lengths are $\beta\lambda/3$ in the prebuncher, where β is the velocity in units of the light velocity, and λ is the free-space wavelength of the accelerating RF (10.5 cm). In the main buncher, however, the cell length varies from $\beta\lambda/3$ to $\lambda/3$ during the first 6 cells, because the gun

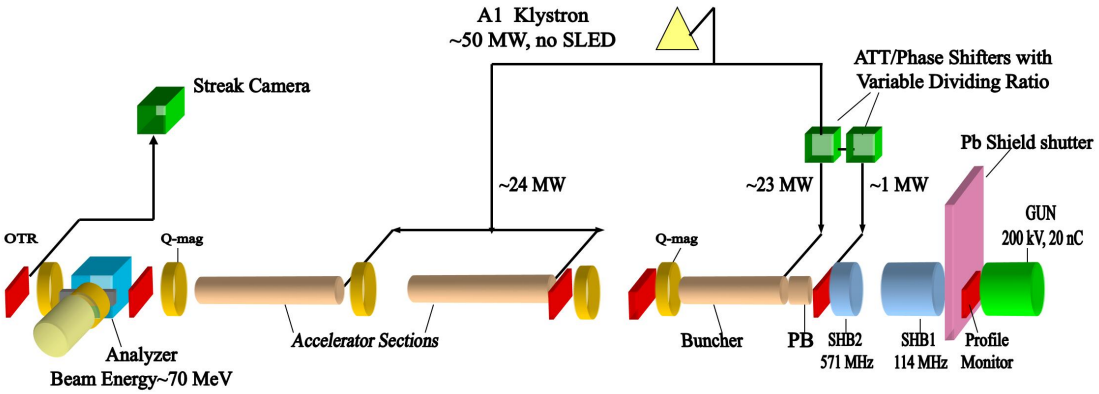

Figure 11.59: Schematic layout of pre-injector part at linac A1 unit.

Element	Repetition or frequency	Period	Voltage or power
Grid pulser	1-50 Hz	-	450-800 V
Gun	50 Hz	-	200 kV
25th SHB1 (standing wave)	114 MHz	8.75 ns	11 kW
5th SHB2 (standing wave)	571 MHz	1.75 ns	7 kW
Pre-buncher (traveling wave)	2856 MHz	350 ns	1 MW
Buncher (traveling wave)	2856 MHz	350 ns	23 MW
Accelerating sections (traveling wave)	2856 MHz	350 ns	$12MW \times 2$
Common frequency of SuperKEKB	10.385 MHz	96.289 ns	-

Table 11.18: Parameters for pre-injector part.

beam has to be accelerated to form a tight bunch as well as be modulated in velocity. As shown in the figure, the KEK prebuncher and the main buncher are assembled into one united body in order to reduce the distance between them and to suppress the divergence due to a strong space-charge force. The number of cells is four in the prebuncher; although that in the buncher is 33, bunching occurs through only the first few cells and the β of the beam reaches almost unity.

For stable operation, the bunch timing or phase with respect to the accelerating RF wave must be fixed as well as the bunch shape. If the status of the gun and the bunching section would become unstable, the bunch timing and shape would be changed. The tolerances for the devices are severe in the case of a high-intensity beam of 10 nC, as are shown in Table 11.20. The stability in the operation meets the requirements owing

Beam current	0 15 A
Grid pulse	-300 -700 V
Bias voltage	+300 +700 V
Grid/cathode distance	180 μm
Heater power	40 W
Cathode temperature	950°C
Acceleration voltage	200 kV
Gun pulse duration	4 μs
Beam duration	1 ns
Beam time jitter	8 ps
Residual gas pressure	1×10^{-7} Pa
ML magnetic field	900 G

Table 11.19: Parameters for thermionic gun.

to digital feedback loops. The tolerances on the devices came from the goal of keeping the beam transmission rate above 90% at the target.

Beam timing	$\pm 45ps$
Gun high voltage	$\pm 0.38\%$
SHB1 phase	$\pm 1.1°$
SHB2 phase	$\pm 1.3°$
Buncher phase	$\pm 1.7°$

Table 11.20: Tolerance to stabilize a high current electron beam.

11.8.2 RF Gun (A1-Gun and AS-Gun)

The main mission of RF gun is to generate required 5 nC electron beam with lower than $20\mu m$ normalized emittance for SuperKEKB HER. As shown in Fig. 11.58, two RF guns are employed. The main RF gun (A1-Gun) is installed on the beamline for generating high charge electron beam with low emittance. The secondary RF gun (AS-Gun) is perpendicular to the beamline. It acts as a backup for smooth commissioning of SuperKEKB.

As shown in Fig. 11.62, the main RF gun is a quasi-traveling wave structure (QTW). Two side coupled cavities are staggered for achieving two standing wave fields. As

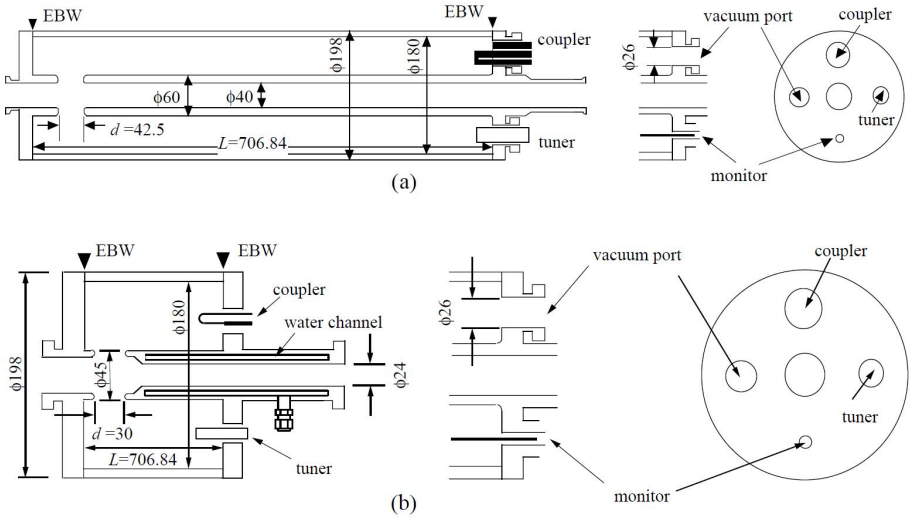

Figure 11.60: Configuration of SHB1 and SHB2.

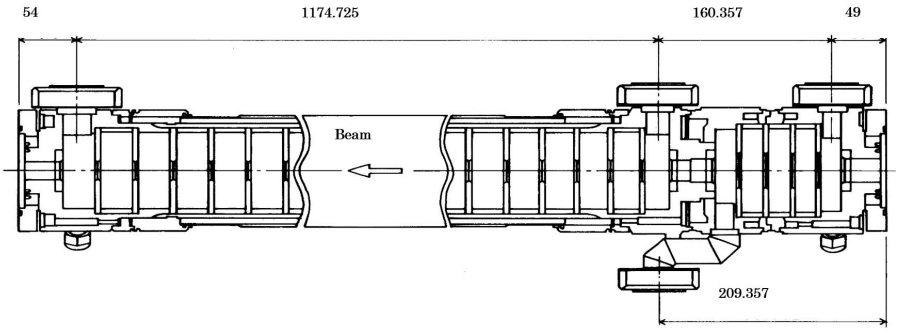

Figure 11.61: Configuration of prebuncher and buncher.

shown in Fig. 11.63, these two standing wave side coupled cavities are independent electromagnetically. By feeding RF power with $\pi/2$ phase difference, the acceleration field inside the RF gun is similar to a traveling wave for electron beam acceleration. Because it is possible to design the two side coupled cavities coaxially, a quasi-traveling wave is available. The quasi-traveling wave can realize beam acceleration efficiently and strong focusing [34].

The QTW RF gun has seven acceleration cavities. These are divided into two standing wave structure of 3 and 4 side coupled cavities respectively. There is no coupling between two adjacent cavities on the main axis of RF gun. Figure 11.64 shows the simulated electric filed in the RF gun. The maximum electric filed strength in the first cavity (cathode cell) and regular cells are 120 MV/m and 100 MV/m separately. The strong focus filed in the first cell is very helpful to realize low emittance because

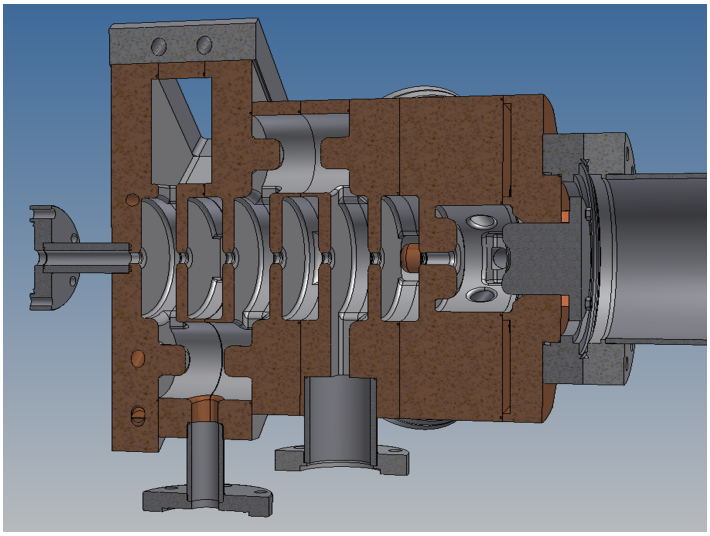

Figure 11.62: Configuration of QTW RF gun.

the beam size and emittance with low energy in cathode cell initially is affected by space charge easily. Meanwhile, the beam tracking simulation for 5 nC result is shown in Fig. 11.65. At the exit position of QTW RF gun (z = 250 mm), the beam emittance is 5.5 mm-mrad with a beam size of 0.4 mm. It is also obvious that the beam size becomes smaller gradually inside RF to the strong focusing electric field. The beam energy will achieve 11.5 MeV under 20 MW RF input. And the energy spread is 0.6%. In addition, the QTW RF gun has the ability to generate 10 nC electron beam with1.2 mm beam size, 10 mm-mrad emittance and 1.0% energy spread. All of these parameters fulfill the requirements for linac of SuperKEKB.

The secondary RF gun (AS-Gun) is simple a cut disk structure (CDS) with large coupling value for improving RF conditioning efficiency, as shown in Fig. 11.66. Low RF power (7 MW) is enough for acceleration with low risk of discharge. In addition, the choke configuration is helpful to solve the breakdown problem for the photocathode rod. As shown in Fig. 11.67, the electric filed and magnetic field are weak around the photocathode rod thanks to the choke configuration, it is good for keeping high vacuum level inside the RF gun.

The beam tracking simulation for 5 nC electron beam results are shown in Fig. 11.68. All the results show the CDS gun can generate qualified electron beam for SuperKEKB. In addition, different from the QTW RF gun, the CDS gun has bigger aperture (8 mm), and the laser beam can impinges into the photocathode with an angle of 0° or 60°.

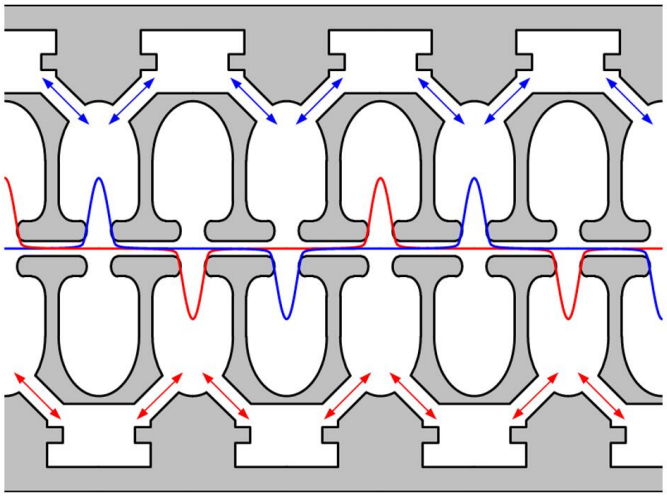

Figure 11.63: Quasi-traveling wave generated by the side coupled cavities.

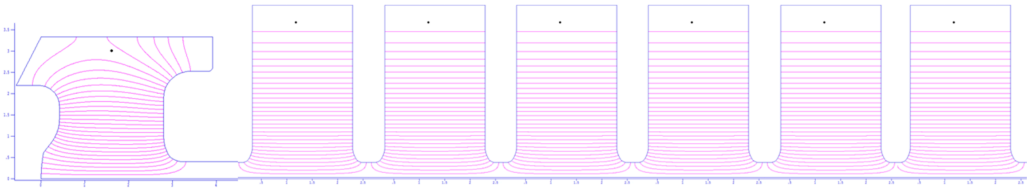

Figure 11.64: Designed RF gun cavities.

11.8.3 Photocathode

For SuperKEKB smooth operation with long term, the RF gun photocathode is critical. It must possess high quantum efficiency to generate high electron charge to fulfill the 5 nC charge requirement. Meanwhile, the lifetime must longer than 1 year under 10-6 vacuum environment. Therefore, iridium cerium metallic compound is selected as the photocathode for RF gun. Iridium cerium has a low work function of 2.57 eV at 1300 K and a high melting point (1900 °C 2500 °C). Moreover, the iridium cerium compound possesses long life time thanks to its good resistance to poisoning and ion bombardment. The iridium cerium photocathode with a diameter of 8 mm is shown in Fig. 11.69, as well the quantum efficiency map of the Ir_7Ce_2 photocathode which is used in SuperKEKB RF gun. The highest quantum efficiency is about 1.49×10^{-4} [35].

In order to enhance the quantum efficiency during the SuperKEKB operation time, an electron beam heating type photocathode plug is design, as shown in Fig. 11.70. The photocathode is bombarded by an accelerated electron beam as a thermal source

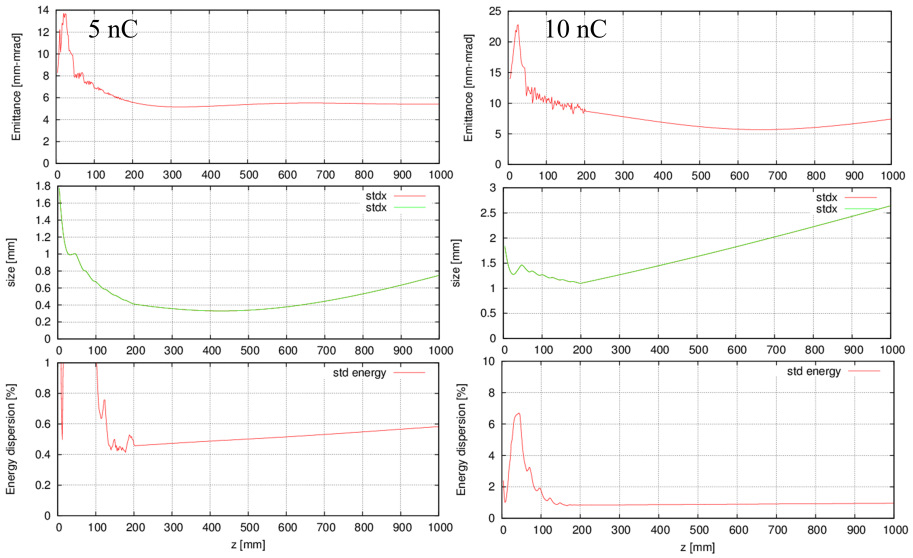

Figure 11.65: Beam tracking simulation result of emittance, beam size and energy spread for 5 nC and 10 nC electron beam.

which is emitted behind the photocathode. This heating method can be used for a longer term than the other heating methods without any maintenance since it is not necessary to heat the filament with a high temperature. 1000 $^{\circ}C$ heating temperature can be realized during SuperKEKB commissioning. In addition, the new photocathode plug is designed with a choke structure for RF shielding, as shown in Fig. 11.71.

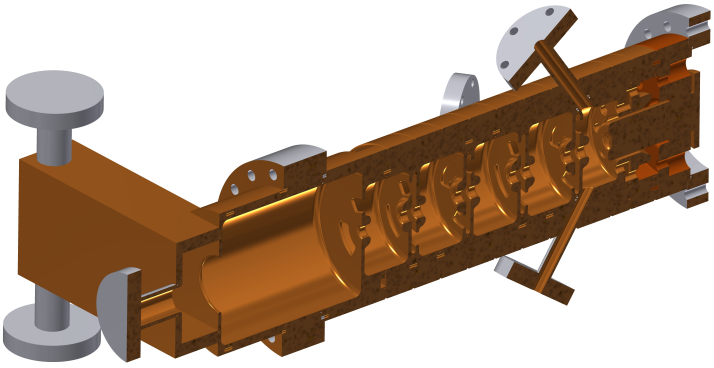

Figure 11.66: Configuration of CDS RF gun.

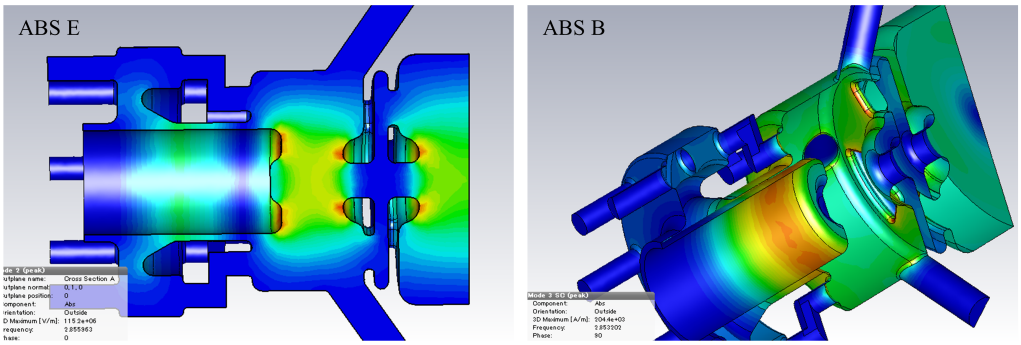

Figure 11.67: Distribution of the electric field and magnetic field near photocathode rod.

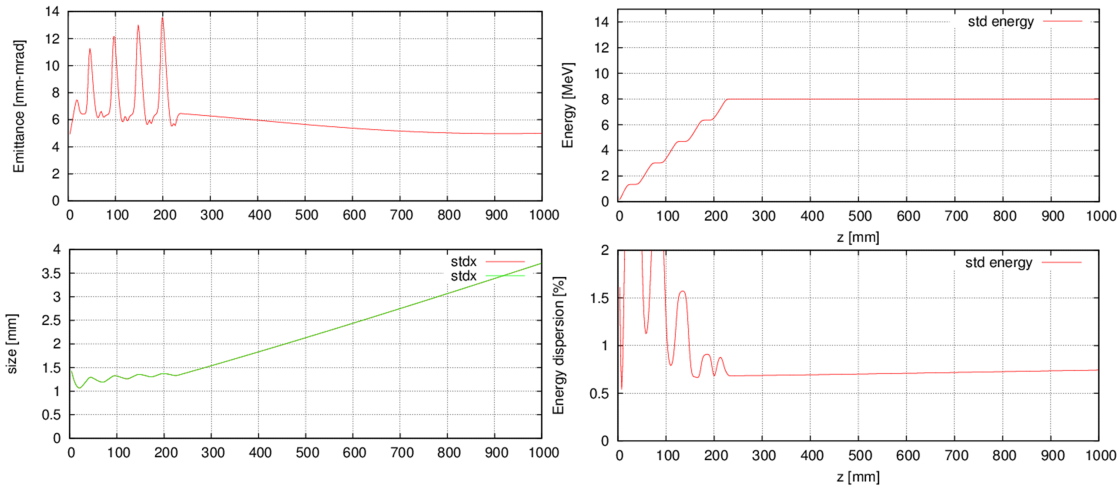

Figure 11.68: Beam tracking simulation result of emittance, beam energy, beam size and energy spread for 5 nC electron beam.

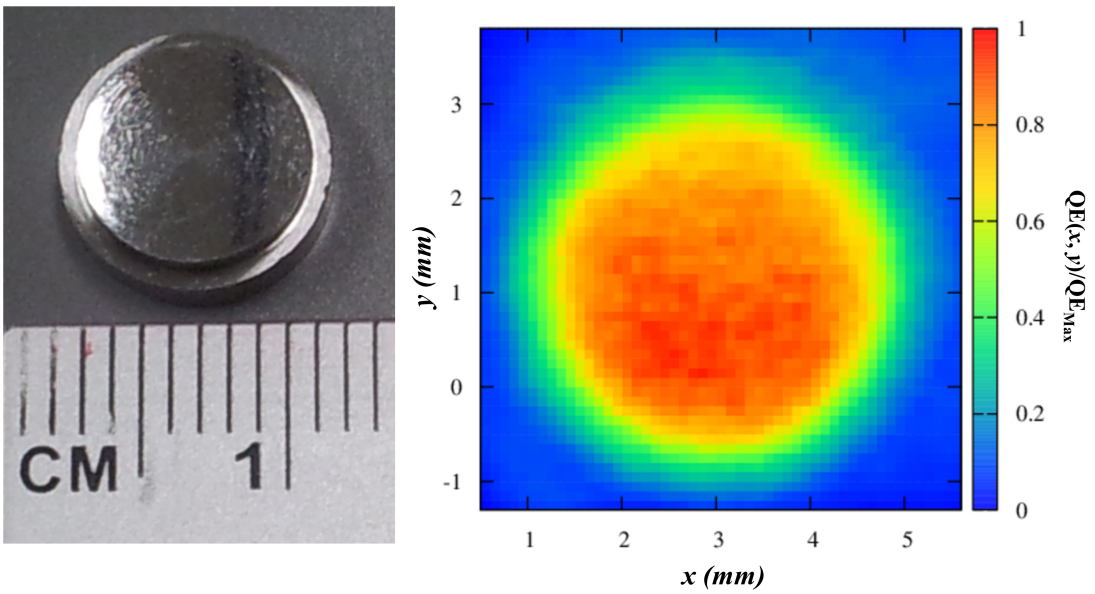

Figure 11.69: Ir_7Ce_2 photocathode and the measured quantum efficiency map.

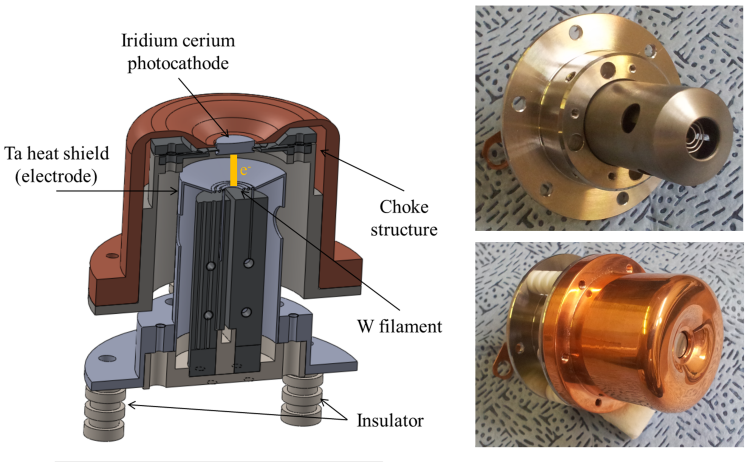

Figure 11.70: Electron beam heating type photocathode plug for SuperKEKB RF gun.

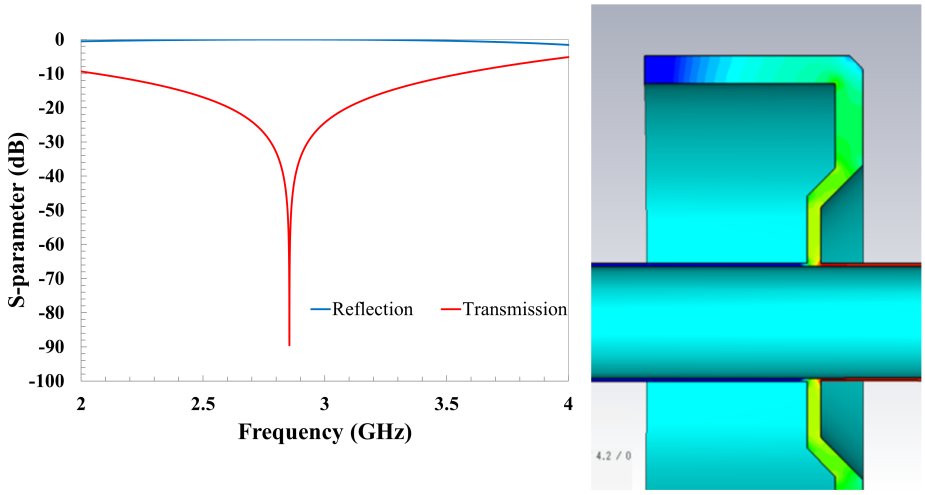

Figure 11.71: RF shielding simulation result for electron beam heating type photocathode plug choke structure.

11.8.4 Laser source

The electron beams with a charge of several nC and a normalized emittance of less than 10 μm are expected to be generated in the photocathode RF gun for injector linac of SuperKEKB accelerator project. To high-current, low-emittance beams generation, the laser source with mJ pulse energy, center wavelength of 259 nm and a pulse width of 20 ps are needed at the A-1 unit (Fig. 11.4). Especially, the pulse shape should be reshaped to rectangle structure. Also, the high reliability and remote control system is required for long-term operation.

11.8.5 Laser type

For high peak power ultra-short UV pulse generation, the most common approach is to employ the nonlinear processes of solid-state Ti:Sapphire lasers. A Ti:sapphire laser is usually pumped with another laser with 532 nm, for which frequency-doubled Nd:YAG lasers are used. However, the low energy-extraction efficiency and heavy maintain limit the application for long-term running.

In contrast, laser diodes (LD) pump laser structure offers high efficiency for reduction of the laser price and maintenance costs. Especially, the Yb-doped fiber laser fiber laser has attracted attention as one of the promising practical alternatives to usual solid-state lasers. The stability of the fiber laser is evidently higher than the other solid lasers with simple cooling conditions because of high energy-extraction efficiency of fiber. But, because of the core diameter size limitation, the fiber structure is difficult realized the mJ level amplification. Then from μJ to mJ energy amplification, the Yb:YAG or Nd:YAG solid states amplifier with LD pump should be employed.

Yb:YAG crystal has large absorption bandwidth to reduce thermal management requirements for diode lasers, a longer upper-state lifetime, three to four times lower thermal loading per unit pump power, which is more suitable for diode-pumping for high power diode-pumped lasers. Compared with the Yb:YAG crystal, commonly used Nd:YAG rods with high optical homogeneity, high damage threshold, consistent performance and high processing accuracy. Although the pulse shaping of Nd:YAG is difficult to be adjusted because of the narrow spectrum gain, the structure of the Nd:YAG is simple, that means reliable convenience and less maintenance. The Emission wavelength of Yb:YAG and Nd:YAG are around 1030 nm and 1064 nm with the bandwidth of 3.0 ns and 0.5 ns, which contained in the spectrum of Yb-doped fiber oscillator.

11.8.6 Optical design for ground laser (Yb fiber + Nd:YAG)

The on the ground laser system consists Yb-doped fiber oscillator, Yb-doped fiber amplifiers and Nd:YAG rod laser amplifiers. The detail of laser part that shows in Fig. 11.72.

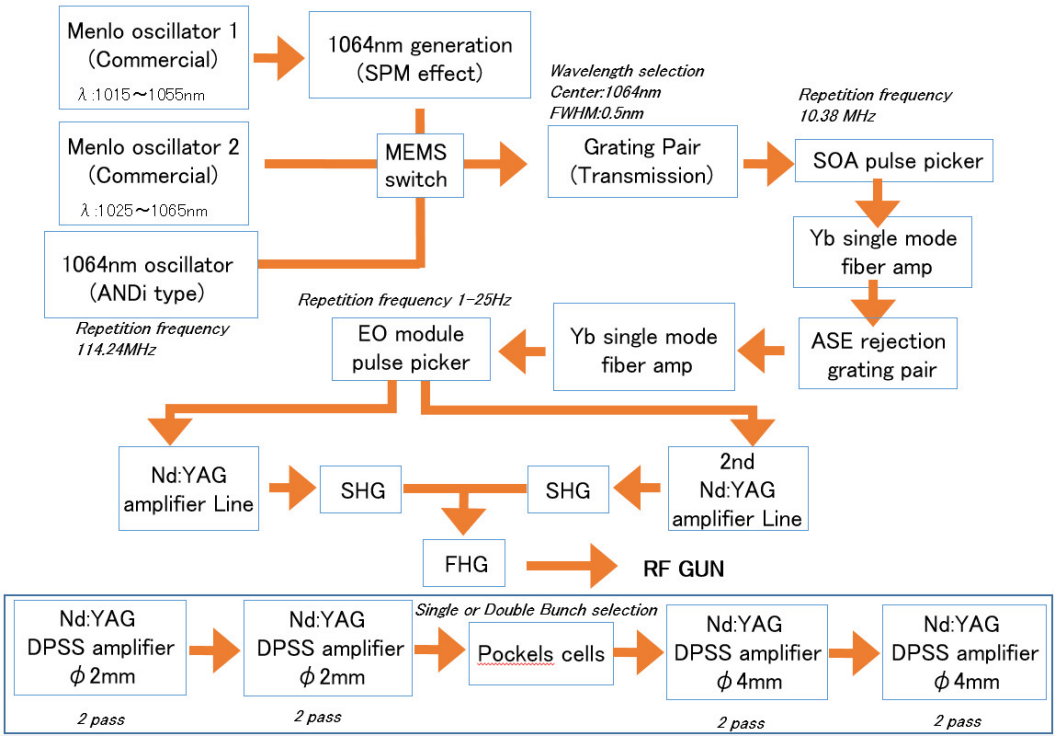

Figure 11.72: Layout of on the ground laser system.

Fiber oscillator

The laser system starts with 114 MHz mode lock Yb-doped fiber oscillators [36]. Three different structure Yb-doped fiber oscillators are employed, two of them are commercial products (Menlo system), and the other one is homemade cavity with the all normal dispersion (ANDi) structure.

As the Fig. 11.73, the ANDi type oscillator is developed with a spectral filter inside the ring fiber cavity. By increasing the nonlinear phase shift accumulated by the pulse and inserting a spectral filter in the cavity, self-amplitude modulation via spectral filtering is enhanced. The pulse duration and chirp decrease in the spectral filter.

One MEMS optics switch is adopted to select oscillator for the following amplifier stages (Fig. 11.74).

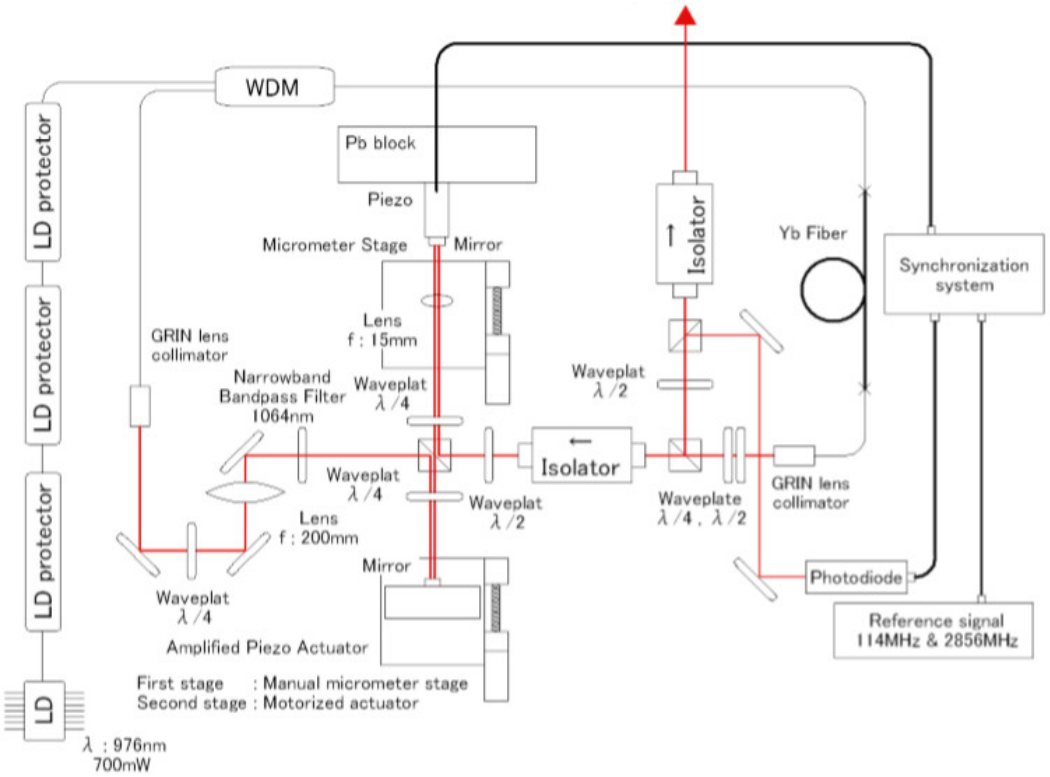

Figure 11.73: ANDi type Oscillator.

Yb-doped fiber amplifier

The nJ level seed pulse with center wavelength of 1064 nm is selected by MEMS optical switch. A transmission grating pair stretcher was employed to expend pulse to 10 ps and select the spectrum width of 0.5 nm with the centre wavelength of 1064 nm. The weak pulses reduced repetition rate to 10.38 MHz by a semiconductor optical amplifier (SOA) pulse picker, which was driven by a 5 ns 100 mV electrical pulse at 10.38 MHz amplified through a high power RF amplifier. To compensate the energy loss of the gratings and SOA, two stages Yb-doped single mode fiber amplifier was employed [36] (Fig. 11.75). Because the amplified spontaneous emission (ASE) easy to be amplified with the weak seed pulse by strong pump power, an additional transmission grating was used to separate and cut the noise by a slit. After fiber amplifier, an Electro-optic module (E.O.) adopted as a pulse picker is used to pick out the 1-25 Hz signal from a sequence of pulses of 10.38 MHz.

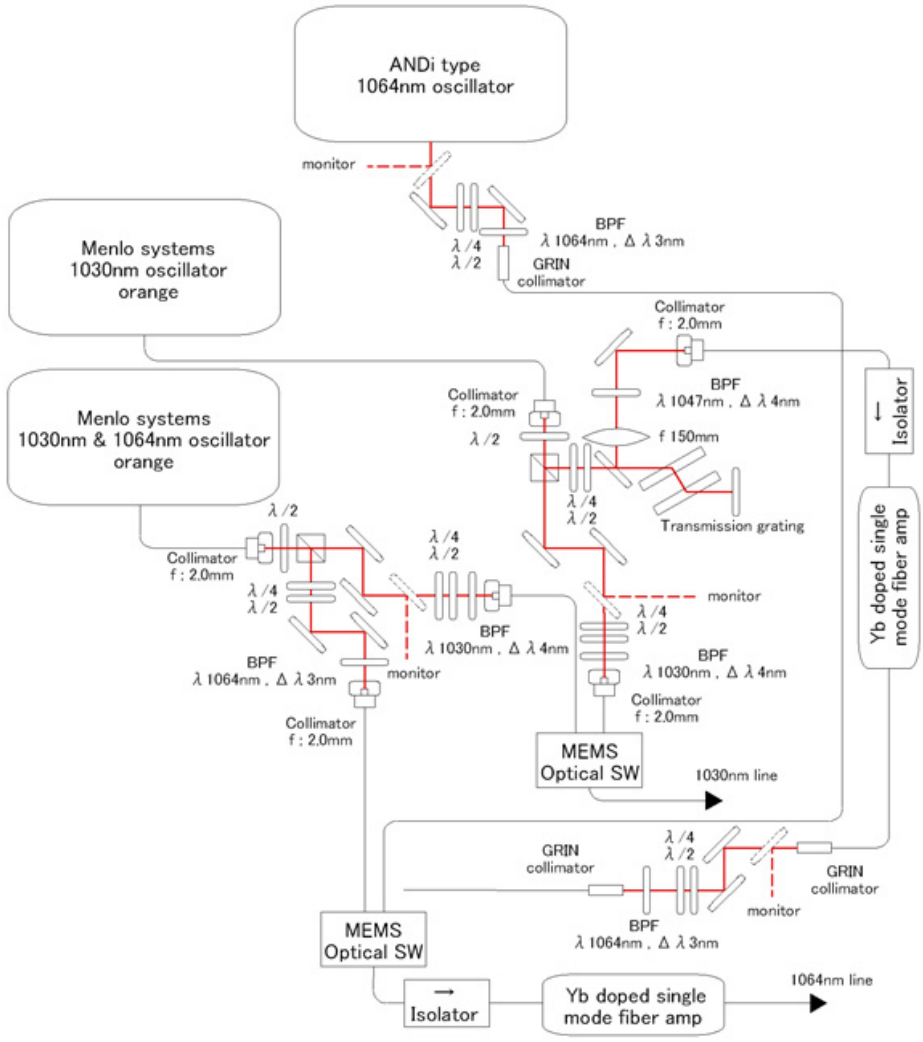

Figure 11.74: MEMS optics switch.

Nd:YAG amplifier part

In order to guarantee the injection and commissioning reliably, two beam lines were prepared. At the end of the fiber part, the signal was separate to two equal parts (first beam line and second beam line) by a polarizer (Fig. 11.72).

The Nd:YAG lines which has 5 stages Nd:YAG rod amplifiers is proposed to provide the stable laser pulses with high quality. 2×79 mm Nd:YAG rod crystal are used in the first and second stages for high amplification efficiency [37, 38]. A Pockels cell pulse picker is insert to switch the single/double bunch mode. After the Pockels cell, the third and fourth stages amplify the pulse energy up to the 4.0 mJ by using of 4×93 mm Nd:YAG rod crystal. The firth stage (Φ6 mm) is built to pursue higher pulse energy. The final pulse energy is up to 8.0 mJ by five Nd:YAG amplifier stages. A beta barium

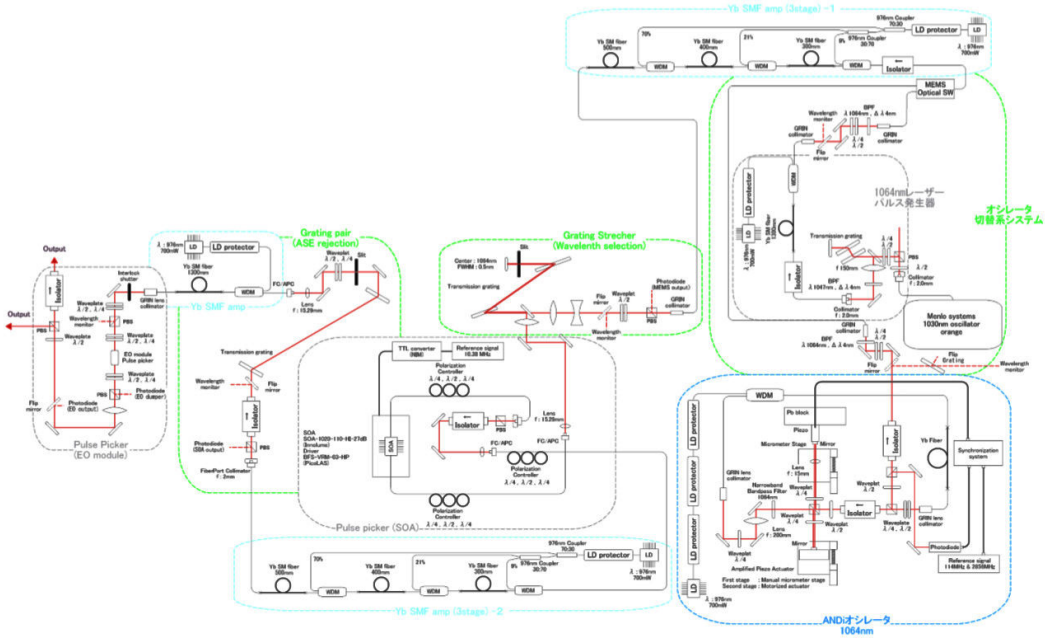

Figure 11.75: Fiber amplifier system.

borate (BBO) crystal is used to second harmonic generation (SHG) stage. The pulse energy of SHG beam is more than 3.8 mJ in both sides.

Transporting line

There is about 12 m distance from the laser clean room to the underground RF gun. The transport line is focus to reduce the energy loss and jitter in the air. Therefore, vacuum tube was built to isolate the air turbulence between the laser room and RF box [38]. Two laser beams are converged by a thin film polarizer and transported to RF gun box by one transporting line. Inside the RF gun box, the laser beams are separated again by another polarizer. The transport rate can be up to 80%. UV pulses were generated by BBO frequency-doubling stages. 500 μJ are achieved by the two laser lines to RF gun. The optics system is shown in Fig. 11.76.

The QTWSC RF gun could be irradiated by each laser sources with 60 degree, and another laser source works with the backup line. Furthermore, it is optional to select two laser injection with both sides. A delay line is inserted into the second laser line to adjust the optical path for realizing two laser synchronous injection into RF gun. Also, a flip mirror is placed in the first laser line for changing the transmission direction to the 90 degree CDS RF gun.

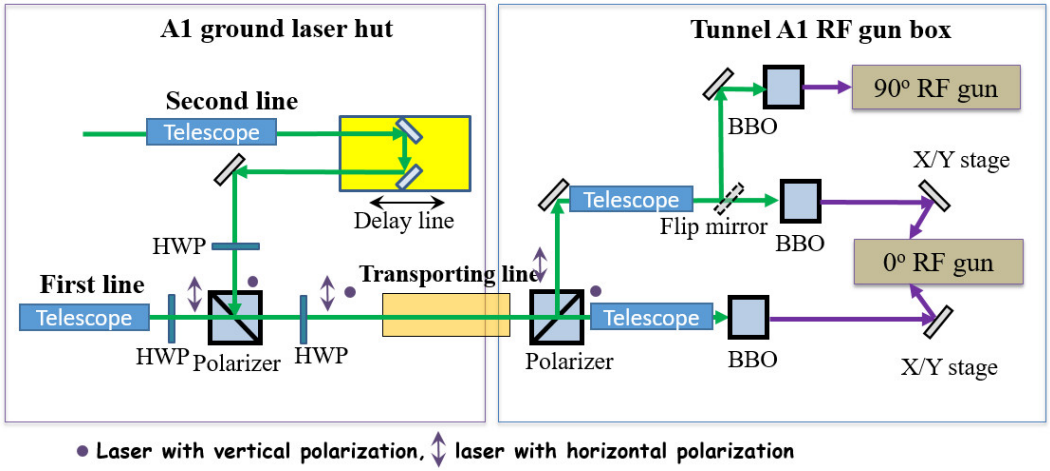

Figure 11.76: Transporting line.

11.8.7 Optical design for Underground laser (Yb fiber + Yb:YAG)

For Yb:YAG crystal amplifier, the broadband gain spectrum is expect. To avoid the nonlinear effect, the chirped pulse amplification (CPA) method has emerged as a useful technique for the generation of high energy pulses. Therefore, the signal pulses should be firstly stretched to longer pulse width, and compressed to 20 ps after amplification.

As the Fig. 11.77, the pulse that generated by Yb-doped fiber amplifier is separated to two parts. One part of the signal is transport to underground laser room by a 15m long PM fiber. Pulse width is adjusted to 1 ns in a chirped volume Bragg grating (CVBG) stretcher. After several fiber amplifier stages and Yb:YAG thin disk amplifier stage, the mJ pulses is reshaped to 20 ps in a CVBG compressor.

CVBG

In CPA systems where stretching is provided by a CVBG, the same device with reverse incidence can also be used for compression (Fig. 11.78).

The reflection band of the compressor CVBG (OptiGrate) is centered at 1030 nm and exposes a width of 3 nm. The antireflection (AR)-coated, rectangular shaped CVBG (aperture: $10 \times 8mm^2$) with a length of 60 mm exposes a stretching factor of 600 ps/nm. Signal pulses are stretched to 820 ps and the measured reflectivity amounts to 90%.

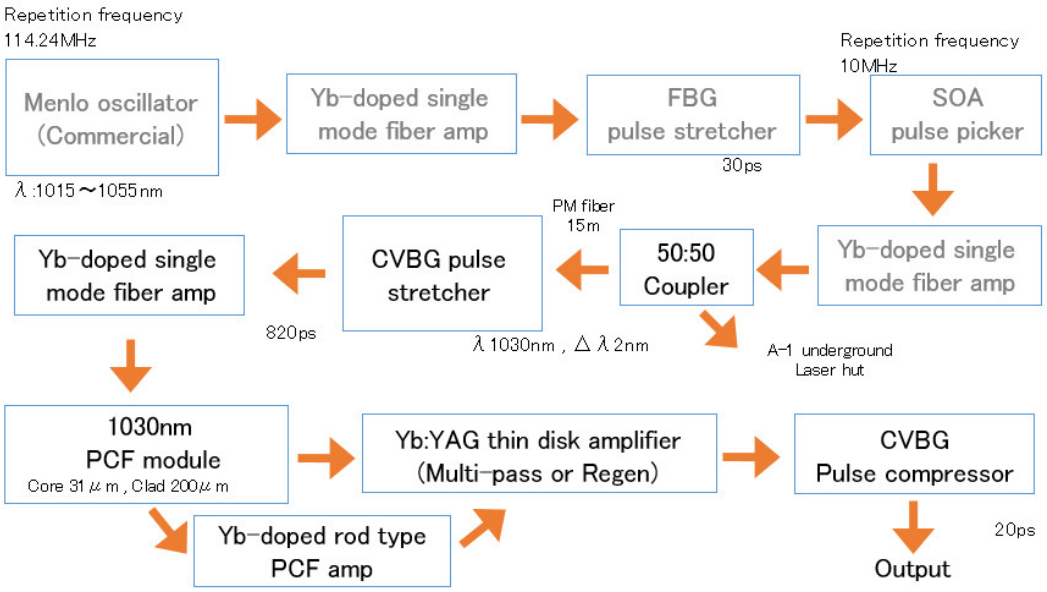

Figure 11.77: Layout of Underground laser system.

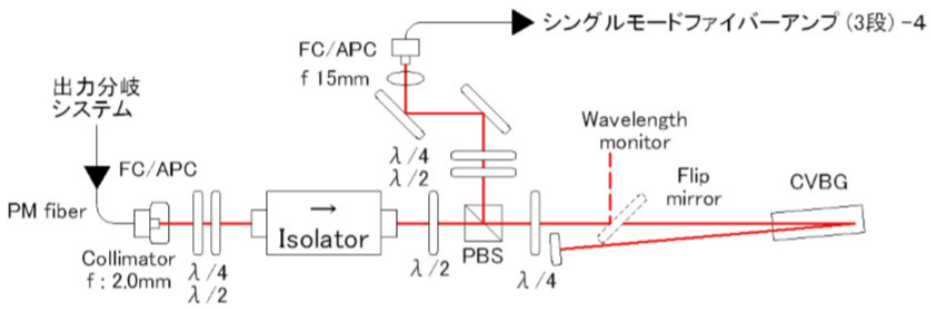

Figure 11.78: Layout of CVBG stretcher.

The Yb:YAG thin-disk amplifier

For high energy amplification, the thin-disk laser optimizes heat removal, which makes possible the high energy pulse amplifier [39]. Because the thickness of the gain crystal is only 1 mm, to increase the gain, multi-pass or regenerative amplify structure is needed to added the round trips. As the Fig. 11.79, a multi-pass amplifier inset into a cavity was designed. The inject signal beam amplified 10-15 times pass through the Yb:YAG thin-disk crystal with single loop. After the two loops, the amplified pulse went out the cavity by the reflection of polarizer.

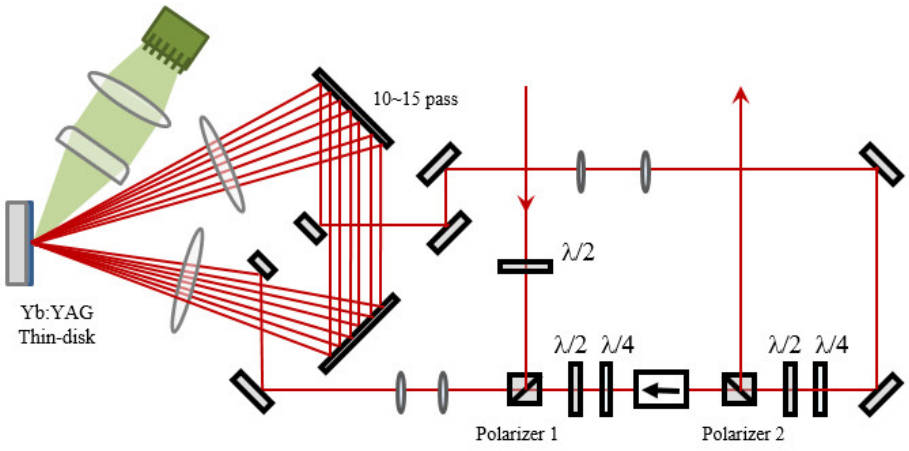

Figure 11.79: Multipass amplifier.

11.8.8 Synchronization system

The frequency of the seed pulse signal that generated by fiber oscillator is locked to 114.24 MHz with the cavity length control. Firstly, the phase shifter controller system is performed to synchronize the laser pulses with both 114.24 and 2856 MHz RF frequency. Then, frequency of the laser signal is reduce to 10.38 MHz by the SOA section, which is also synchronized with 10.38 MHz of RF frequency.

After fiber amplifier system, two E.O. pulse picker are employed to pick the laser signal to low frequency (1-25 Hz, double bunch). And a Pockels cell is employed to switch the single/double bunch signal. Both of the sections are synchronized with the Event generator (EVG) signal that produced by the event timing system.

For final amplification, 10 pump modules are used in the Nd:YAG amplifier section. All the modules is also synchronized with the EVG signal. For the thermal stability, the frequency of pump is fix to 25 Hz. The detail is shown in Fig. 11.80.

11.8.9 Monitoring and remote control system

Since the electron beam with high stability and quality are required in commissioning, the status of laser system and RF cavity are monitored and recoded.

In oscillator, the stepping motor and piezo that adjust the frequency in the cavity is controlled to synchronize RF frequency signal. Status monitors and I/Q monitor are employed for detect the mode-lock and synchronization. When the RF frequency is drift, the laser frequency can be auto-adjusted immediately.

The temperature of the laser room and RF gun cavity and all the current of the power supply are monitored and recorded. Furthermore, the pulse output power of the

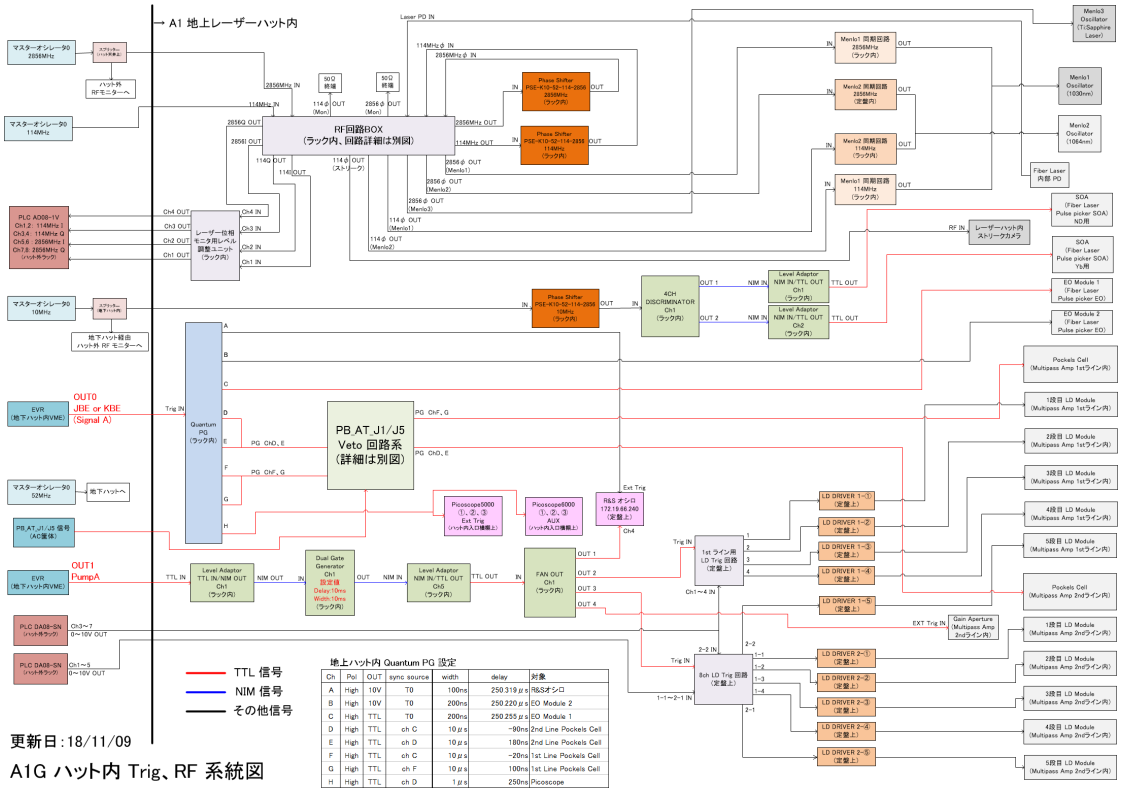

Figure 11.80: Layout of trigger system.

every stages and the pulse shaping of the every pulse pickers are also monitored by photo diode detectors. The long term reliability of laser are recorded, and any unusual changes will be alarmed by monitoring system.

The optics system inside RF gun box is set near the electron gun. A beam profile monitor and laser energy meter are set in the two laser lines to oversee the laser status. The real-time data can be confirmed on internet anytime. For optimize the laser source in the commissioning study, lots of adjustment unit were insert, such as telescope lenses distance, BBO crystal angle, X/Y stage and rotation stage. All of these units are adjusted by fully remote control. Thus, we can get the best condition to generate highest electron charge during beam study. Figure 11.81 shows the monitoring and remote control system panel by Windows-PC.

11.8.10 Pulse shaping in time domain

In order to get low energy spread in a strong space charge effect, laser pulse with rectangular temporal shape is required. Temporal shaping scheme by pulse stacking technology is developed for Nd laser system. The pulse is directly stacked up using

Figure 11.81: Monitoring and remote control panel by windows.

birefringent effect of a crystal array (Fig. 11.82). Output laser pulse with temporal rectangular shape is restricted from the input Gaussian shape pulse.

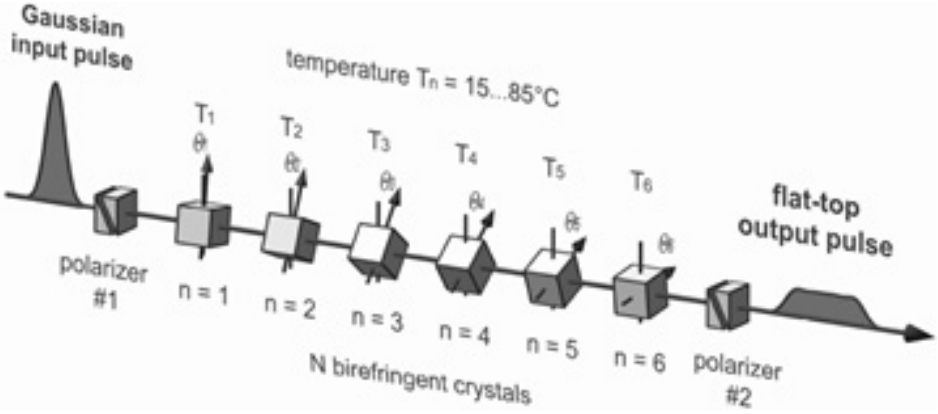

Figure 11.82: Pulse stacking technology.

11.9 Postron Source

11.9.1 Layout of positron source in KEK linac

The positron source of the KEK electron/positron injector linac experienced two major upgrades, at first in the upgrade from Photon Factory/TRISTAN injector to KEKB injector and recently in the upgrade to SuperKEKB injector. At the time of TRISTAN injector, it had a 400-m long 2.5-GeV main linac and a 70-m long 0.25-GeV linac dedicated to positron production. The main linac had five sectors of accelerator each having eight accelerator-units and the positron production linac had six accelerator-units. The first three units in the positron linac accelerated a primary electron beam up to 0.25 GeV to irradiate a positron production target, the fourth unit was used for positron capture and the remaining two units accelerated positrons up to 0.25 GeV. The positron beam was deflected 30 degrees toward the main linac and merged in the middle of the Sector-1 (at the unit #1-5).

In the first upgrade to KEKB [14], the positron beam intensity was required to increase by 20 times (0.032 $\rightarrow$ 0.64 nC/pulse) to achieve high luminosity. The positron source (the positron production target, the pulsed solenoid coil and the DC solenoids in the positron capture section) were relocated to the Sector-2 of the main linac (at the unit #2-1) to increase primary electron beam energy from 0.25 GeV to 4.0 GeV. It is because the produced positron intensity is proportional to the primary beam energy. The position #2-1 was selected because it has heavy concrete in the ceiling between the beam line tunnel and the klystron gallery. It was advantageous in view of shielding against radiations from the target. For the injection to the KEKB electron storage ring (HER) at 8.0 GeV and to the positron ring (LER) at 3.5 GeV, the injector linac was reformed in J-shape by reusing the facilities in the positron linac and by extending the building. Three new sectors (called as Sector-A, B, C) were added. The 8.0 GeV electron beam energy was achieved with the 55 accelerator units which have typical 0.16 GeV energy gain for HER injection with sufficient energy margin. With the position of the positron source at #2-1, the 26 accelerator units were allocated for an acceleration of the primary electron beam up to 4.0 GeV and the remaining 29 units were used for positron acceleration up to 3.5 GeV with sufficient energy margin for LER injection.

In the recent upgrade to SuperKEKB, the beam injection energy was changed to 7.0 GeV for HER and 4.0 GeV for LER. Since the positron beam emittance for LER injection is required to be two orders of magnitude smaller compared with the KEKB, a positron damping ring (DR) is introduced beside the linac building. The position of the extraction and re-injection of the positrons is determined to the region between the Sector-2 and the Sector-3 because it has a beam switch-yard (SY2) convenient

for construction of the beam transport line to the DR. The beam energy of the DR was determined to 1.1 GeV in balance of the radiation damping time and the ring compactness. Details of the DR is described elsewhere. The position of the return from DR at #3-2 was chosen since the 22 accelerator units are secured for accelerating positrons up to 4.0 GeV. However, if the positron source is remained at #2-1, we have only six units for positron acceleration except for the capture section before the DR and it is not sufficient for 1.1 GeV injection. Thus, the relocation of the positron source became necessary. We decided to relocate the positron source to #1-5 where we have an available wide area for the equipments around the target, originally used for the beam merging from the positron linac in the TRISTAN period [40]. The primary beam energy is 3.3 GeV there with the beam energy 1.5 GeV at the J-arc section. If definitely needed, the J-arc beam energy can be increased up to 1.7 GeV, so some design parameters were optimized at 3.5 GeV primary electron beam energy. We have ten units for the positron acceleration up to 1.1 GeV before the DR with sufficient energy margin. However due to the selection of this location, it is required to build a heavy radiation shield structure inside the tunnel. Details of the shield is described in section 11.9.6.

11.9.2 Positron intensity upgrade for SuperKEKB

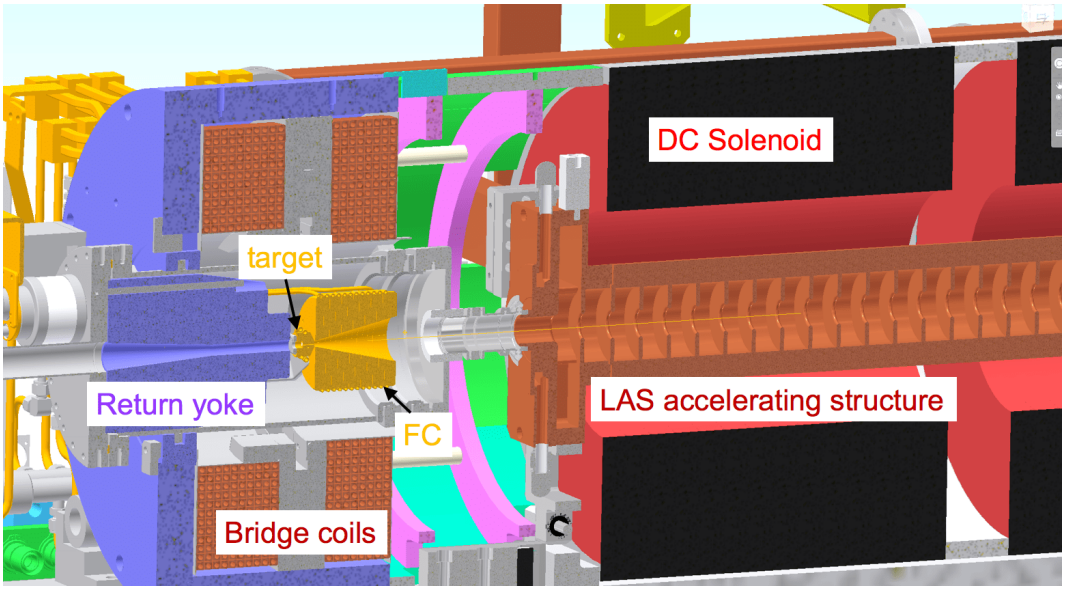

Figure 11.83: SuperKEKB positron source

In the upgrade from KEKB to SuperKEKB, the positron beam intensity was required to increase by four times (1 nC/bunch $\rightarrow$ 4 nC/bunch). Because it was difficult

to increase primary beam energy or intensity from a viewpoint of the cost, we took a course for increasing the capture efficiency of positrons produced at the target. At the KEKB positron source, a air-core pulsed solenoid coil (peak field 2.3 T, field length 65 mm FWHM) was used for transverse phase-space matching for positrons emerging from the target. This short high-peak field worked as a Quarter-Wave Transformer whose positron-energy acceptance is narrow. For SuperKEKB, we introduce a flux concentrator (FC) type of pulsed solenoid (3.5 T) and DC bridge coils (1.0 T) which generate a slowly varying field from a 4.5 T peak field to a long solenoid field (0.4 $\sim$ 0.5 T) generated by DC solenoids as shown in Fig. 11.84. Details of the FC are described in section 11.9.4.

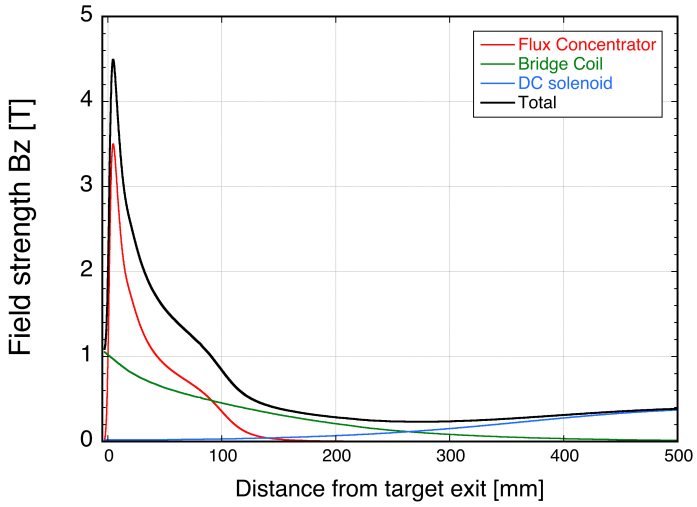

Figure 11.84: Field distribution by FC, bridge coils and DC solenoid

Focusing with this kind of field profile called as "Adiabatic Matching" has the broad positron-energy acceptance. It results in the larger longitudinal phase-space acceptance for positrons.

The positron capture section is a pre-accelerator to capture positrons from the FC by the solenoidal field and accelerate them before passing to regular accelerator units. Transverse phase-space acceptance of the capture section is determined by the solenoidal field strength and the aperture of the accelerating structures inside the solenoids ($U \propto Ba^2$; U:acceptance, B: field stregnth, a:aperture radius). For the SuperKEKB capture section, large-aperture S-band accelerating structures (called as LAS-type structures) are introduced. They have the aperture diameters (30 mm), larger than those (typically $\sim$20 mm) of the regular S-band structures. Details of the LAS structures are described in Section 11.3. While the KEKB capture section used four accelerating structures (two 1m-long and two 2m-long structures) whose total ac-

celeration length is 6 m, the SuperKEKB capture section uses six LAS structures (2m in each length) whose total acceleration length is 12 m. The positron beam energy from the capture section is raised from 70 MeV to 120 MeV. It improves the positron energy-spread and the beam transmission efficiency to the subsequent accelerator unit (#1-7). The field distribution of the solenoids covering the capture section is shown in Fig. 11.86. The field dips are caused by solenoid gaps for the waveguides of the accelerating structures. The capture section is composed of two accelerator units. In the first unit (#1-5), the klystron feeds an RF power of flat pulse shape directly into the two accelerating structures in the capture section. In the second unit (#1-6), the RF power from the klystron is compressed by a SLED cavity and is fed into the four structures. The unit #1-5 also has a SLED cavity, but it is detuned and not used because RF breakdowns happened in the structures.

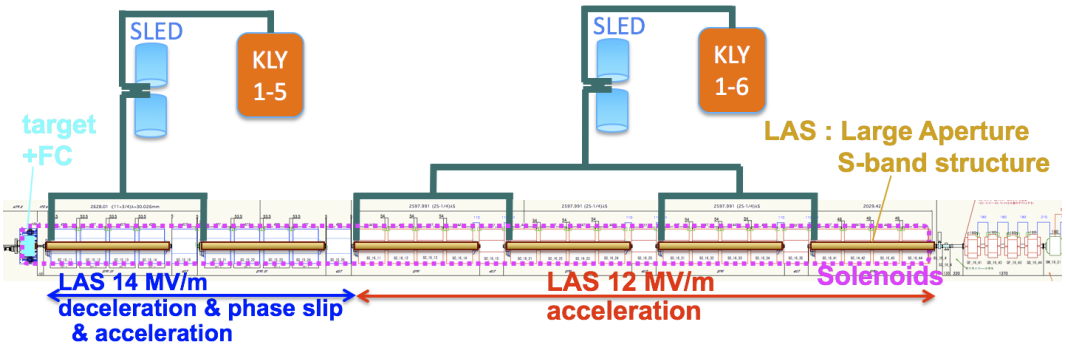

Figure 11.85: SuperKEKB positron capture section layout

The RF phases of the accelerating structures in the capture section are set so as to decelerate positrons from the FC. The simulation study reveals that the positrons captured by the decelerating phase contains smaller numbers of particles in the energy distribution tail, which results in less beam background at the DR injection [41]. In the case of acceleration capture, the longitudinal distribution of the positrons in a bunch does not change and the particles in the energy tail remains the same. On the other hand in the deceleration capture, since the positrons are decelerated, their longitudinal velocity becomes slow and starts to slip from the velocity of the microwave in the structure. As the phase slip continues, the positrons finally reaches to the accelerating phase and the phase slip stops. In this phase slipping process, compression in the longitudinal phase space occurs and the positrons contains less energy tail particles.

Particle tracking simulation studies were performed to evaluate the expected positron yield, that is the ratio between the positron beam intensity and the primary electron beam intensity. Positron production in the target was simulated with the GEANT4 [42], magnetic field distribution by the FC, the bridge coils and the DC solenoids were

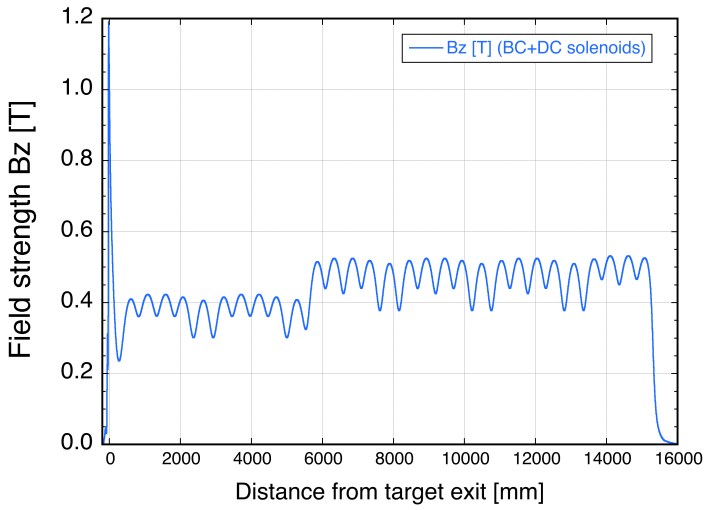

Figure 11.86: Field distribution by Bridge coils and DC solenoids (FC field not included)

evaluated with the CST EM STUDIO [43], the particle motion in the capture section was simulated with the GPT code [44] and the beam transmission was evaluated with the SAD code [45]. Figure 11.87 shows the expected beam size and the positron yield from the exit of the capture section till the end of the Sector-2 for the case of the parameters satisfying the specification (the primary electron beam energy 3.5 GeV, the FC current 12 kA, the bridge coil current 600 A, the DC solenoid current 650 A, the acceleration field in the unit #1-5 14 MV/m, that in the unit #1-6 12 MV/m, the deceleration capture and the offset positions of the target and the FC taken into account). The positron yield at the end of Sector-2 (that is the entrance of the transport line to the DR) is 0.39, which corresponds to a positron beam intensity 3.9 nC/bunch for a primary electron intensity 10 nC/bunch. The positron yield dependences upon the parameters of the capture section were also estimated with the simulations. The positron yield at the exit of the capture section was evaluated with the GPT code in various cases of the FC and the bridge coil currents as shown in Fig. 11.88.

11.9.3 Positron production target and beam passage hole

The positron production target is made of tungsten because of its large cross section of the electron-positron pair creation and its high melting temperature. The length of the target is 14 mm (4.0 X_0 radiation lengths). The tungsten is attached in a copper support by hot isostatic pressing. A cooling pipe is wound around the copper support with a radius of 20 mm as shown in Fig. 11.89.

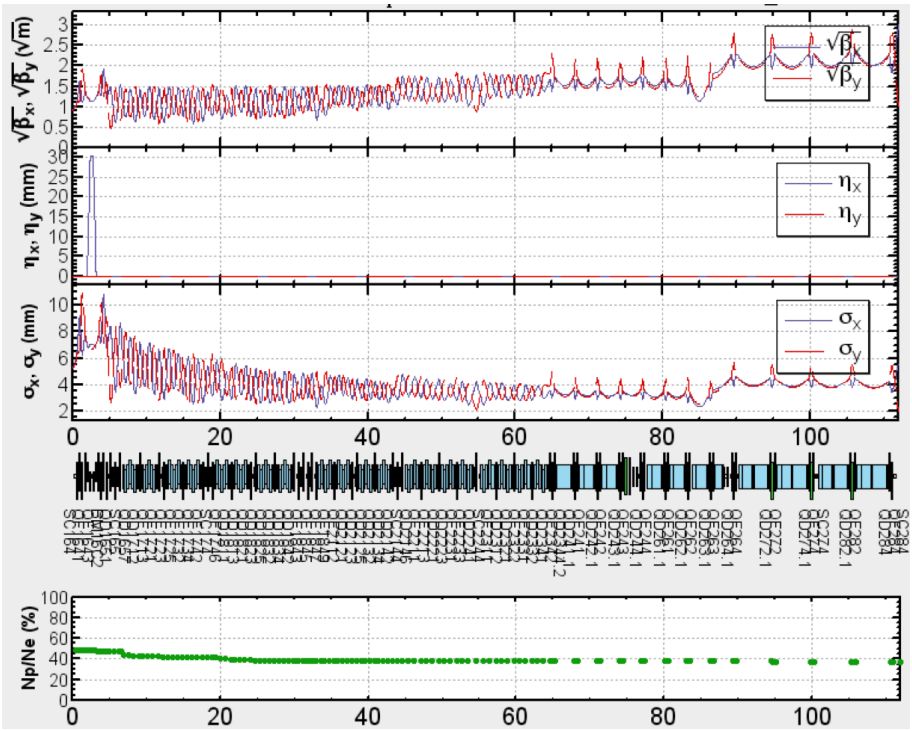

Figure 11.87: Beta-functions, dispersions and beam size of positrons in design optics and positron yield

Even the stationary heat is removed by the cooling water, due to repetitive energy deposition in the target by the intense primary electron beam, the target could be potentially damaged by fatigue breakdown. To avoid the target destruction, the peak energy deposition density (PEDD) should be well below the critical limit (35 J/g) based on the SLC operation experience [46]. For the case of 3.5-GeV primary electron beam with a charge of 20 nC/pulse (10 nC/bunch $\times$ 2 bunches), a spot size (σ_x, σ_y) of primary electron on the target entrance should be larger than 0.7 mm with a factor two of the safety margin. To avoid the spot size to become too small, a beam spoiler made of an aluminum-oxide screen (0.14 mm, 0.002 X_0) and aluminum foil (0.25 mm, 0.028 X_0) is installed three meters upstream from the target to enlarge the spot size by multiple scattering [47]. The spoiler is removable and is used in the situation where the PEDD approaches to the critical limit.

In the KEKB period, pulse-by-pulse switching of electron injection to HER and positron injection to LER has begun. To achieve the switching, a small hole was made in the copper support beside the tungsten target. Electron beam orbit is switched by pulse steering magnets making an electron beam for HER to pass through the hole, while the primary electron beam for positron production strikes on the target. In the KEKB positron source, the tungsten target was placed on the central axis of the beam

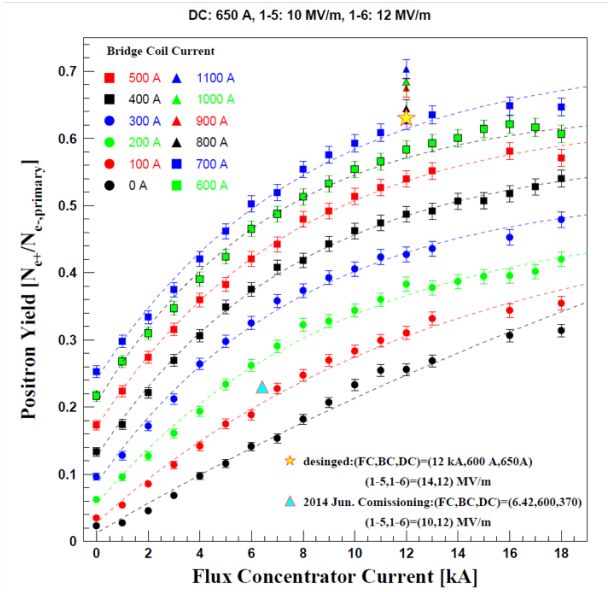

Figure 11.88: Positron Yield dependence on Capture section Parameters

line, while the hole had a few mm offset from the axis. For SuperKEKB, the injection electron beam generated with a photo-cathode RF-gun has low emittance and the hole is required to be on the axis to avoid an emittance growth by the orbit excursion in the accelerating structures. This makes a strict constraint on the layout of the target, the hole and the FC. Because the aperture of the FC at the entrance is only seven mm in diameter, the target and the hole should be contained within the aperture. At first the diameter of the hole is determined to be 2.0 mm assuming an rms radius of the spot size of the injection electron beam is 0.5 mm. Then, the diameter of the tungsten is determined to be 4.0 mm keeping a 0.5 mm thickness copper layer between the tungsten and the hole, to avoid direct exposure of the target surface to the hole. As a result, the center of the target has 3.5 mm offset and the axis of the FC aperture has 2.0 mm offset from the central axis of the beam line as shown in Fig. 11.90.

11.9.4 Flux Concentrator

FC has been used for positron focusing at BINP [48], SLAC [49], IHEP [50] and other facilities. The design of the FC for SuperKEKB is basically the same as those of SLAC and IHEP. They have a slight difference. While the FC of the SLAC operated at a pulse repetition of 60 Hz, the FC of the IHEP operated at 50 Hz has slight different dimension of the central conductor copper block to make the resonant vibration frequency to be away from 50 Hz. The pulse repetition of the SuperKEKB linac is 50 Hz and the dimension of the FC is the same as that of IHEP.

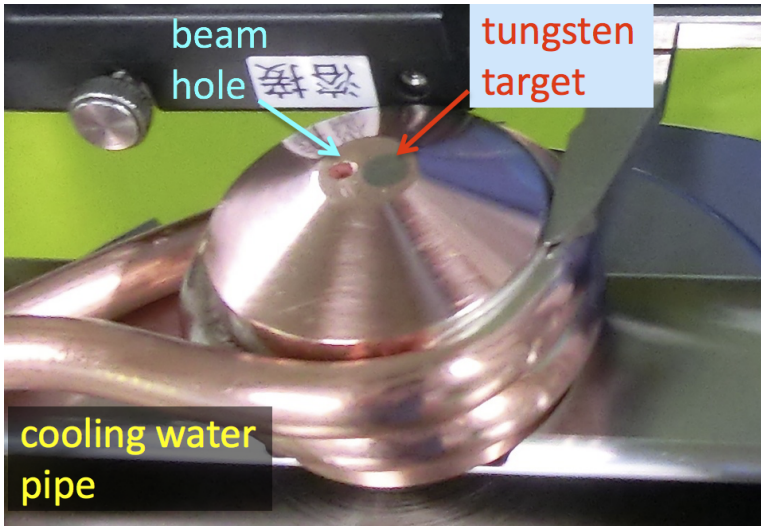

Figure 11.89: Target of SuperKEKB positron source

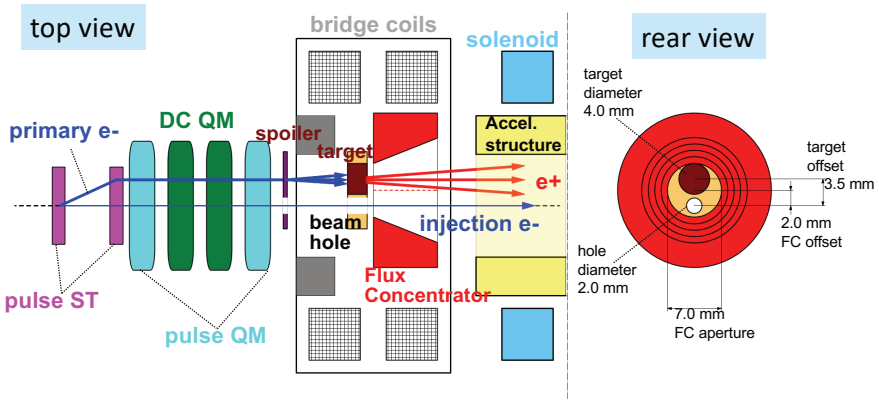

Figure 11.90: Target, FC offset layout

The FC is made of a copper cylinder block of 108 mm in diameter and 100 mm in length and it has a conical hole inside along the axis whose hole diameter are 7 mm at the entrance and 52 mm at the exit as shown in Fig. 11.91. The cylinder has a spiral slit processed by discharging wire-cut at KEK and formed as spiral coil of 12 turns as described in reference [51].

A copper pipe is brazed around the cylinder along the spiral and serves as a pipe feeding a pulsed current and as a water cooling pipe. When a pulsed current of 12 kA at peak in half-sine shape of 8 μs is introduced to the conducting pipe, an eddy current flows in the inner surface of the FC. The magnetic flux is concentrated inside the conical hole and forms a strong solenoidal field (3.5 T at peak). The positrons emerged from the target are focused by this solenoidal field.

Each turn of the copper spiral is isolated by 0.2 mm gap of the slit. At both ends

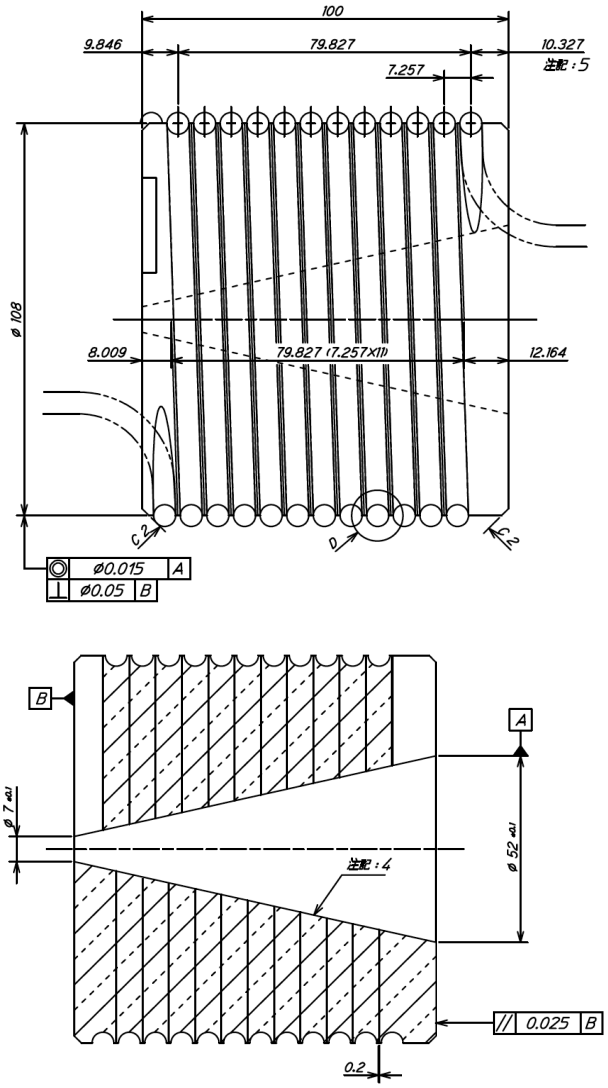

Figure 11.91: SuperKEKB FC dimension

of the spiral slit, it runs in radial direction. Because of the radial slit, the magnetic field has transverse component and axially non-symmetric. This transverse magnetic field component gives a 'transverse kick to the positrons.

As described in section 11.9.3, the target has 3.5 mm offset and the FC has 2.0 mm offset from the beam line axis. These offsets degrade the positron yield, however it can be mitigated by utilizing the transverse kick. With a simulation study, the orientation of the radial slit was determined to optimize the yield [52].

The front surface of the FC is placed 2 mm apart from the exit of the target to avoid discharging between them. Due to an eddy current in the copper part of target support induced by a time-varying magnetic flux from the FC, magnetic field by the

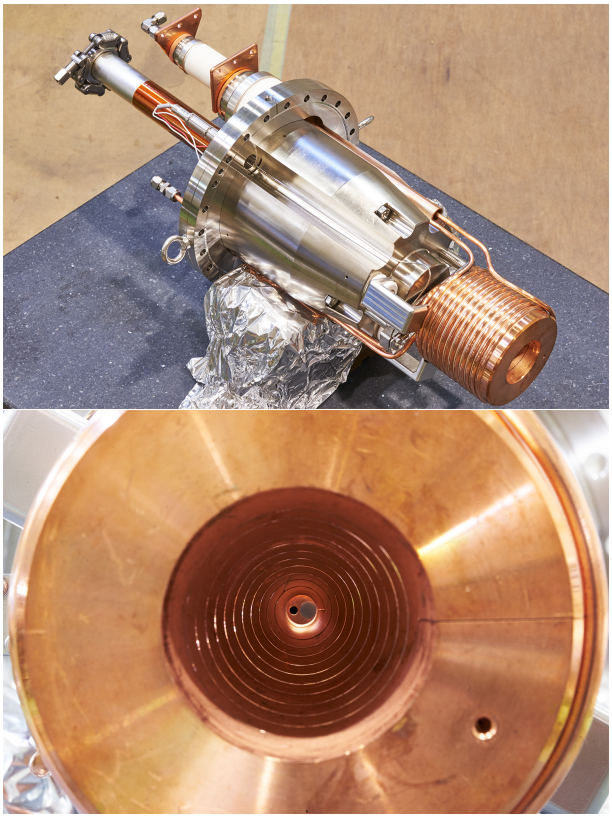

Figure 11.92: SuperKEKB FC photo

FC is almost zero at the target. The positrons feel only DC field by the bridge coils at the target and they feel strong field after entering in the FC as shown in Fig. 11.84.

The design of the pulse modulator for the FC is based on the klystron modulator of the KEK linac, except that the pulse-forming-network for flat output pulse is replaced with a capacitor bank for a single half-sine pulse and two sets of the thyratron switch and the capacitor bank are used [53, 54]. The specification of the modulator is described in table 11.22. The inductance of the modulator and the power transmission line could be comparable to that of the FC (1 μH) and should be minimized to reduce induced high-voltage. The ten parallel coaxial cables (18 m long) are used in the transmission line from the modulator to the linac tunnel [55]. In the tunnel the cables are connected to copper three-layer parallel plates (2 m long, 250 mm width, 35 mm plates distance). The plates are connected to copper two-layer parallel plates (0.54 m long, 75 mm width, 35 mm plates distance). At the connection to the FC, the copper plates with fork plugs are used for quick disconnection.

The copper plate transmission line is used to make the terminal of the coaxial cables distant from the high-radiation area because a non-radiation-resistant material is used in the terminal. A CR snubber circuit (2.5 Ω, 100 nF) is connected in the middle of the

Length	100 mm
Outer diameter	108 mm
Inner diameter (min.)	7 mm
Inner diameter (max.)	52 mm
Peak current	12 kA
Peak field	3.5 T
Inductance	1.0 μH

Table 11.21: Specifications of SuperKEKB FC

copper plate line to compensate for the pulse wave form deformation by a reflection due to mismatching to the load.

Peak current	12 kA
Pulse width (half-sine)	8 μs
Load (FC) inductance	1 μH
Total inductance	$\sim$ 3.35 μH
Capacitance	1.4 μF
Charging voltage	17 kV
Pulse Repetition rate	50 Hz

Table 11.22: Specifications of FC modulator

11.9.5 Quick exchange system of FC and target

The residual radiation dose from the target will be much increased because the time-integrated target irradiation beam power is higher at SuperKEKB operation than those for KEKB. An excessive exposure dose of workers in the exchange of the target, the FC and the accelerating structure in the capture section is a serious problem. The FC assembly and the exchange mechanism are designed to minimize the exposure dose. The assembly is composed of the FC, the target, the vacuum chamber, the bridge coils and the return yokes. The assembly can be exchanged in short time without dismantling the component. It is advantageous because the the bridge coils and the return yokes surrounding the target works as a shield and the radiation dose outside the assembly is relatively low. In the connecting part of the power cables of the bridge coils, the water cooling pipe of them, the signal cables for interlocks and the signal cables of thermal sensor to the assembly, the multi-coupling plates of Staubli company is adopted. They can connect and disconnect these cable and pipe connections in a

single action. The power feed line to the FC is connected by copper plates with fork plugs. These plates can be disconnected in a short time. The FC assembly has wheels and mounted on rails. It is easy to move the assembly to the position for lifting up by a crane as shown in Fig. 11.93 (left)

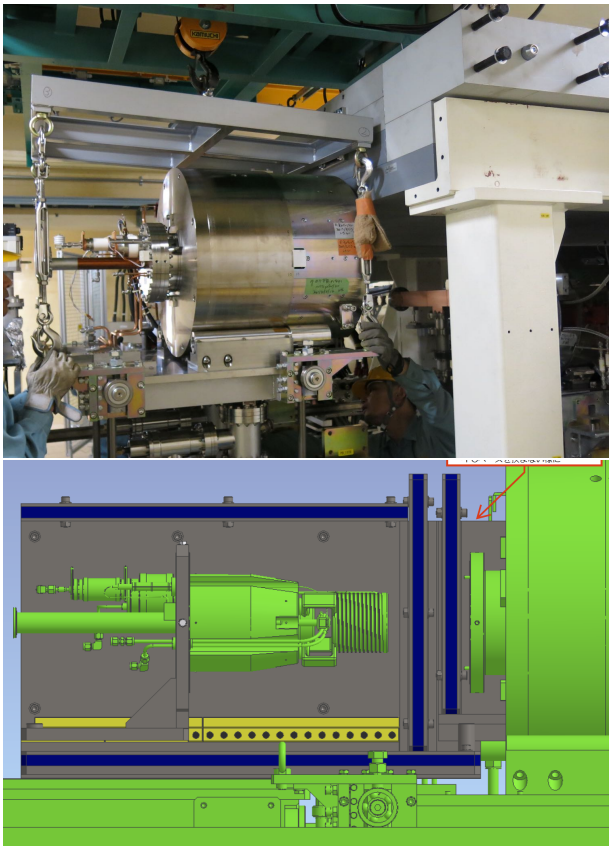

Figure 11.93: Quick exchange mechanism of FC and target

For the quick exchange work and minimizing the exposure dose, jigs for the exchange and a trailer with a radiation shield are prepared. For a case of exchange of the FC base which contains only the endplate, the return-yoke head, the target and the FC, jigs with shield walls are also prepared as shown in Fig. 11.93 (right). The entrance part of the first accelerating structure in the capture section is also highly radioactive after the beam operation. Jigs with a radiation shield for exchanging the structure is also prepared.

11.9.6 Radiation shield structure

As describe in section 11.9.1, the ceiling (2.5 m thickness) between the klystron gallery and the tunnel at #1-5 where the SuperKEKB positron source is installed, is made of normal concrete unlike the heavy concrete at #2-1 for the KEKB positron source.

Simulation studies using the MARS code [56] showed that an additional shield iron 1.25 m width, 500 mm thickness, 6.0 m length was required to keep the radiation dose at the klystron gallery below the limit 20 μSv/h of the radiation controlled area for the 1250 nA full-specification primary beam intensity. A support structure by 11 iron pipe pillars sufficient for this weight and additional supports for suppressing vibrations were designed and installed in the tunnel [57, 58]. In the first stage, shield irons were installed in 2.0 m width, 100 mm thickness, 6.0 m length in the first layer, in 1.25 m width, 100 mm thickness, 6.0 m length in the second layer. The shield was composed of pieces whose weights are less than the load limit of a crane, 1000 kg.

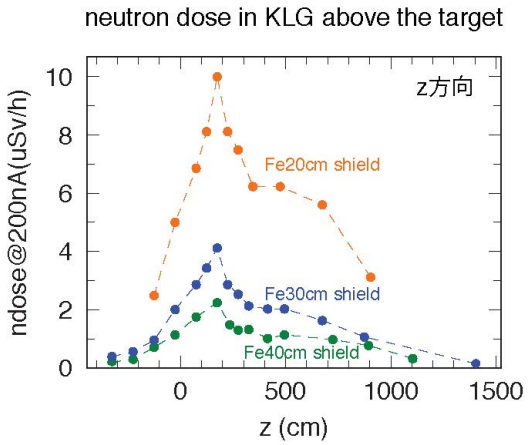

Figure 11.94: Improvement of Radiation dose by increasing shield thickness

The shield thickness was increased step by step in 4.0 m length region and the radiation doses were measured in each step as shown in Fig. 11.94. It was shown that the dose with 400 mm thickness at 200 nA beam intensity was 2.2 μSv/h. which corresponds to 14 μSv/h at 1250 nA. The thickness 400 mm is sufficient for the region straight above the target. However, to make the radiation dose outside the linac building to be below the limit 0.2 μSv/h, an additional shield of 2.0 m width, 400 mm thickness, 4.0 m length (including the first-stage layers) and a side wall (0.8 m height, 100 mm thickness, 4.0 m length) were installed as shown in Fig. 11.95. The resonant vibration frequencies of the shield structure were calculated to be sufficiently above the frequency of earthquake vibration by simulation studies and confirmed by measurements.

11.9.7 Beam separator and secondary-electron stopper

A beam from the capture section contains not only the positrons but comparable amount of secondary-electrons produced in the target. These electrons prevent mea-

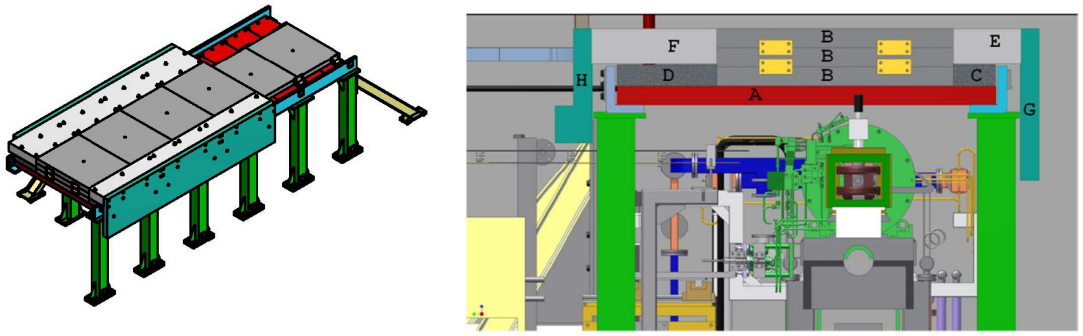

Figure 11.95: Radiation shield structure

surements of the positron beam position and charge due to cancellation of the signals in the beam position monitors. They are accelerated up to 1.1 GeV, and lost at the entrance of the beam transport line to the DR and make beam line components radioactive unnecessarily. To eliminate the secondary electrons, a beam separating chicane with four bending magnets and a beam stopper were installed after the exit of the capture section as shown in Fig. 11.96. The orbits of the positrons and the secondary electron ($\sim$ 120 MeV) are separated approximately 70 mm in the chicane. On the path of the secondary electrons, a beam stopper block made of tungsten-copper alloy (tungsten 70%, copper 30%) of 76 mm thickness ($\sim$ 15.0 X_0) is inserted. The block is retractable using a pulsed motor which is radiation tolerant (Empire Magnetics company). The position of the block is adjusted not to prevent the electron beams for HER injection.

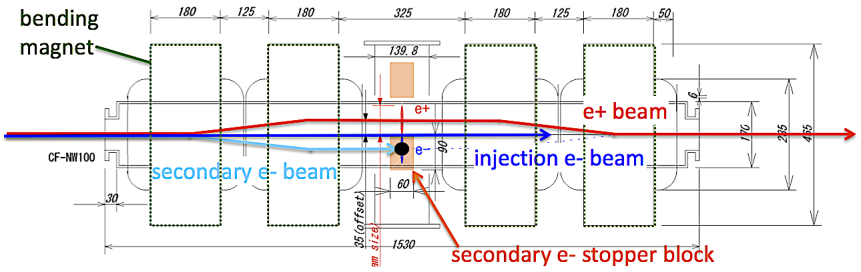

Figure 11.96: Beam separator and Secondary-electron stopper

11.10 Machine operation and safety

11.10.1 Overview

The basic function of the linac safety system is to ensure that the injector linac is operated only when a pre-determined set of personnel and machine safety conditions are met [59, 60]. The required safety conditions are symbolically summarized in Fig. 11.97.

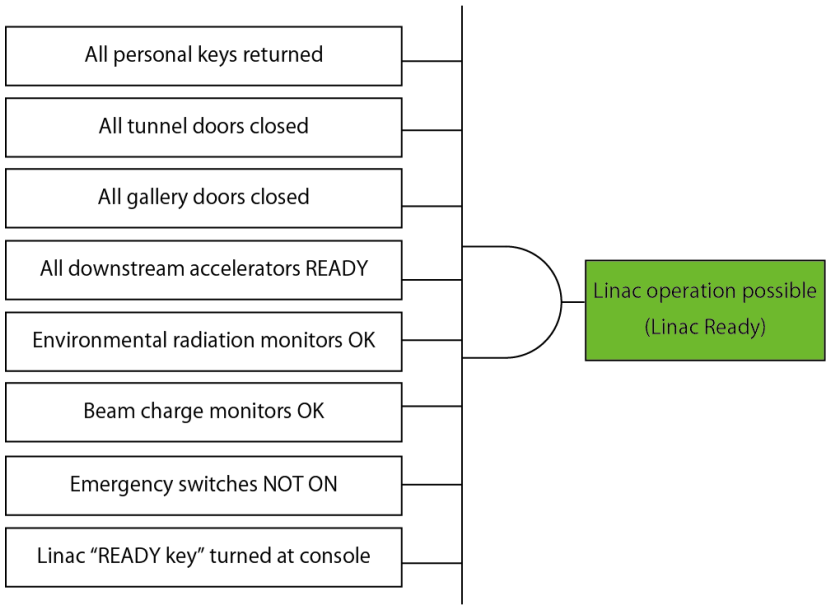

Figure 11.97: Safety conditions to be met before beam operation of the injector linac is allowed.

The whole set of beam generating equipment for the linac is housed in an underground tunnel which is designated as radiation controlled area. The tunnel is built with shielding capability and containment measures to keep the radiation in non-controlled areas below the levels specified by the KEK radiation safety regulation. Beam operation is allowed only when no personnel is present there ("All personal keys returned") and all the entry and exit doors for the underground tunnel are closed ("All tunnel doors closed").

High power klystrons which produce the microwave power required for operating the linac are installed at the surface level (called, "klystron gallery") of the linac building. Since the klystrons also produce a certain amount of X-rays during operation, all the entry points to the klystron gallery are closed during operation, so that only the registered radiation workers, if any, can be present in the klystron gallery ("All gallery doors closed").

Since the linac situates at the upstream end of other electron/positron accelerators at the Tsukuba campus of KEK, all the downstream accelerators have to positively give their beam permission (called "downstream READY") signals to the injector linac ("All downstream accelerators READY"), before the linac starts beam operation. It may mean that the downstream accelerator actually intends to accept the beam from the linac and it is ready for that. It may also mean that the downstream accelerator intends to allow personnel into their accelerator tunnels for maintenance and other activities and it has completed a prescribed set of preparatory arrangement, such as beam stoppers being "in" and a designated set of major beam bending magnets being "off" in the beam transport line etc, so that it knows that it can guarantee that the linac beam does not affect the safety of any personnel and equipment there.

The linac safety system is also linked with environmental radiation monitors at the ground level in the perimeter of the linac system. Reports of radiation levels from these monitors have to stay below the limits set forth by the internal rule of KEK and national regulation ("Environmental radiation monitors OK"). Signals from a selected set of beam current monitors along the linac beam lines are also fed to the safety system. The beam currents (product of beam charge and repetition rate) have to stay within the range ("Beam charge monitors OK"), as authorized by Nuclear Regulation Authority. If the accumulated beam current approaches the authorized limit, the linac safety system issues a warning and stops beam operation before exceeding the limit. Additionally, the linac safety system is linked with certain status signals from the linac beamline equipment, such as those from vacuum gate valves and large bending magnets, so that the beams do not inadvertently hit vacuum system components to produce unintended radiation or radio-activation.

With all other conditions met, the safety system requires that an operator uses a special key called "beam key" on the console and physically turns it to activate the Linac READY status ("Linac READY key turned at console"). Incorporation of this active human action eliminates the possibility of accidental automatic start-up of beam operation.

The linac safety system ensures that if any of the conditions above are violated, the beam operation of the linac immediately stops. If for any reason one of the emergency stop buttons are pressed by an operator in the operation room or by personnel accidentally trapped in the tunnel, the linac beam operation also immediately stops. In the following, some key points in implementation of this linac safety system are described.

11.10.2 System layout

Figure 11.98 shows a sketch of the linac safety system.

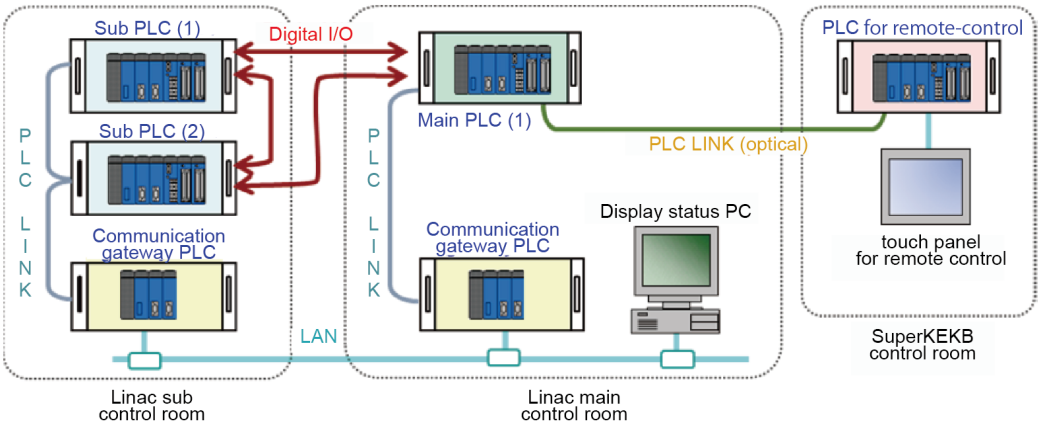

Figure 11.98: Schematic layout of the linac safety system.

A programmable logic controller (PLC) manufactured by Yokogawa Co. serves as the main CPU for managing the safety logic (main safety PLC). The main PLC communicates with two sub PLCs, and these three safety PLCs are responsible for collecting the safety-related signals directly from the linac equipment via metal cables and for performing logical evaluations of the combined status of the injector linac.

The communications among these PLCs are made through dedicated digital I/O lines, without relying on the local area network which are used by the rest of the control system of the injector linac.

Table 11.23 shows the destinations and numbers of linac interlock signals.

The linac safety system communicates with downstream accelerators and receives downstream READY status signals from them, too. For instance, the SuperKEKB has its own safety PLC, and its status information is fed to the linac main safety PLC as listed, among others, in Table 11.23.

The status information of the linac safety system is made available to the linac control system through additional PLCs (two communication gateway PLCs). The communication gateway PLCs are connected to the main or sub safety PLCs via PLC links, and are also connected to the local area network (LAN) of the linac control system. This arrangement allows to display the status of the safety system at operators' terminals along with the rest of hardware status of the linac in a unified graphics user interface, as shown in Fig. 11.99. Yet the use of dedicated safety PLC links ensures continued availability and operation of the safety system, even during possible failures of the control system LAN.

At this moment the injector linac can be operated either from the linac control

Destination of signal	Number of I/Os	Personnel protection	Machine protection
Doors	20 / 0	✓	
Emergency switches	8 / 0	✓	
Beam trigger system	0 / 10	✓	
High power RF PS	50 / 17	✓	
Electron guns	2 / 1	✓	
Operation console	17 / 36	✓	✓
Charge monitors	10 / 0	✓	✓
Vacuum gate valves	36 / 0	✓	✓
Vacuum gauges	15 / 0		✓
PF-AR	4 / 2	✓	
PF-ring	4 / 5	✓	
Damping Ring	6 / 5	✓	
SuperKEKB	4 / 6	✓	
Radiation monitors	1 / 0	✓	
Focus coil and e+ target interlock	1 / 0		✓
Bending magnet status	1 / 0		✓
Sector B beam dump water flow	1 / 0		✓
Tunnel clear	1 / 0		✓
Maintenance mode	1 / 0		✓

Table 11.23: Destination and number of linac interlock signals at the central CPU.

room located near Sector 1 of the linac, or from the SuperKEKB control room. For this reason another PLC is prepared for remote-controlling the linac safety system from the SuperKEKB control room, and it is linked with the linac main PLC (see Fig. 11.98).

11.10.3 Operator console

As described in the discussion on Fig. 11.97, an operator must turn the "beam key" on the console to bring the linac safety system into the Linac READY status when other requirements are met. As shown in Fig. 11.100 this console is prepared as a physical panel, separated from the graphical user interface of the computer control system of the linac. It can be manipulated only by hand in the linac control room.

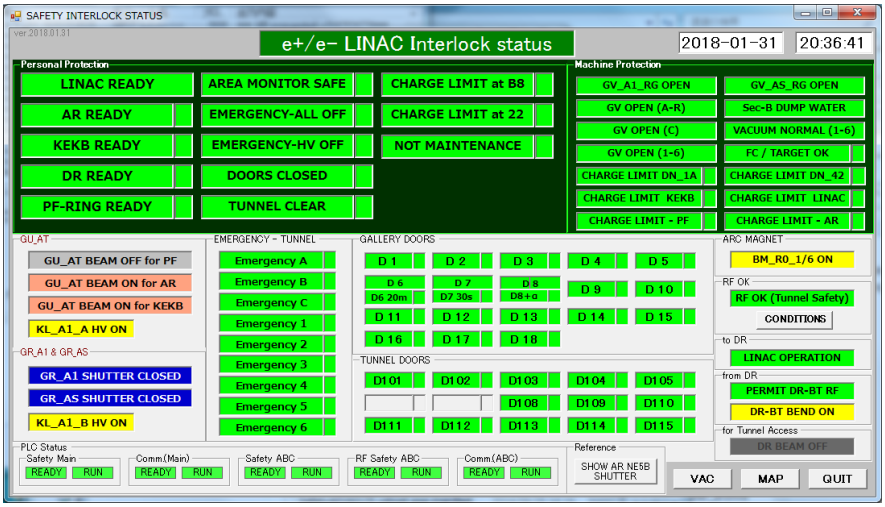

Figure 11.99: Typical display of the status window for the linac safety system.

Figure 11.100: Image of the latest control panel. The beam key is used to switch the safety status from OFF, RF OK and Linac READY.

11.10.4 Personnel safety management

To account for personnel who enter the underground linac tunnel, personal keys (Fig. 11.101) are used at the injector linac. When a radiation worker wishes to enter the linac tunnel while the injector linac is not in beam operation, each individual worker must first use her registered card key on the key bank to pull out a personal key. This action is automatically logged by the safety system. The access door to the underground tunnel can be opened with this personal key. After completing the work in the tunnel, the worker must return the personal key to the key bank. Otherwise, the system assumes that the worker still could be in the tunnel, and "All personnel keys returned" status

is not made up. The “All personnel keys returned” status is realized only when all the personal keys are physically returned to the key bank, and only then, with all other required condition met, the Linac READY status can be realized.

Figure 11.101: Personal keys used for entrance to the linac tunnel and the key bank.

11.10.5 Transitionary period during linac upgrade

In the course of preparation toward SuperKEKB, the injector linac had to go through immense renovation work both in the underground tunnel and in the klystron gallery while electron beams had to be kept available for operation of PF and PF-AR. To cope with this situation in the period between September 2010 and May 2017, the linac tunnel was treated as two distinct radiation generating equipment rooms, upstream and downstream sections, partitioned by a shield wall introduced at the downstream end of sector 2. The upstream section included sectors A through 2, while the downstream section consisted of sectors 3 through 5 and the beam switchyard.

In the downstream section a temporary thermionic electron gun was installed at the upstream end of the sector 3, and electron beams generated there were accelerated up to 4 GeV by using klystrons within the downstream section. The beam energy of 4

GeV was sufficient for the PF which operates at 2.5GeV and acceptable to the PF-AR which could accelerate the injected 4GeV beam up to 6.5GeV for user operation. The shield wall separating the upstream and downstream section was built thick enough so as to allow presence of personnel in the upstream section while the downstream section was in beam operation for PF and PF-AR. This arrangement allowed construction of new RF gun at the upstream end of sector A, excavation of additional new tunnels for beam transport lines to/from the damping ring, and other work while the PF and PF-AR operation is supported.

During this transitionary period the door at the shield wall between the upstream and downstream sections incorporated interlock sensors which communicate their status with the safety system. Also, two sets of key banks were used so as to deal with human access control to upstream and downstream sections of the injector linac separately. However, in the summer maintenance period of 2017, when beam transport lines with the new damping ring were mostly completed near the end of sector 2, the partitioning of upstream and downstream sections was abolished. The partitioning shield wall and the temporary thermionic gun at sector 3 were removed then, and since the Fall of 2017 the entire linac tunnel has been treated, again, as a single radiation generating equipment room in terms of radiation safety.

11.10.6 Operation of electron guns

As described earlier in this design report, the present electron source for the injector linac includes a thermionic gun and RF guns. In case of the thermionic gun, the "DC high voltage (DC-HV) applied to the gun electrodes" can be reasonably equated to the "beam on" status in the language of the safety system. Thus, the thermionic gun DC-HV-on was allowed only after the linac safety status turns to "Linac READY".

In case of the RF gun, since it has no DC-HV, per se, "RF power applied to the gun assembly" is equated to the "beam on" status in terms of the safety system (see Fig. 11.102).

In addition, a "Laser shutter" is incorporated in the laser beam path and a gate valve is introduced on the beamline as shown in Fig. 11.103. The gate valve has to be closed during human access to the tunnel during maintenance so as to guarantee human safety. The safety system incorporates a logic where it demands both "Linac READY" and "gate valve open" before the RF source for the RF gun can be applied.

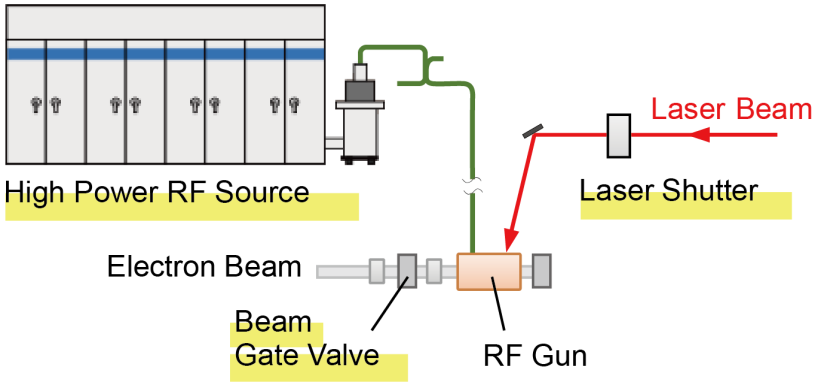

Figure 11.102: A sketch of RF source and laser beam used to generate beams with an RF gun.

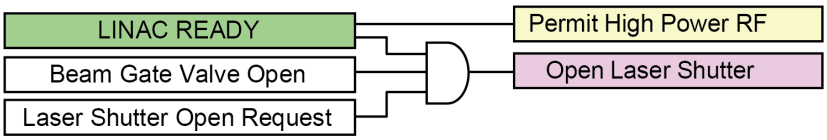

Figure 11.103: Requirements for operating the RF gun.

11.10.7 Latest status

The linac safety system, compatible with operation of SuperKEKB together with the damping ring, PF and PF-AR has been in active service since Fall, 2017. It has been reliably functioning to ensure the safe operation of the linac and to control access human entries to the linac tunnels for maintenance activities.

Bibliography

[1] I. Abe *et al.*, "The KEKB Injector Linac", Nucl. Instrum. Meth. **A 499**, 2003, p.167, doi:10.1016/S0168-9002(02)01787-4 11.1, 11.4.1, 11.8.1

[2] M. Akemoto *et al.*, "The KEKB Injector Linac", Prog. Theor. Exp. Phys. **2013**, 2013, 03A002, doi:10.1093/ptep/ptt011 11.1, 11.6

[3] Y. Ohnishi *et al.*, "Accelerator Design at SuperKEKB", Prog. Theor. Exp. Phys. **2013**, 2013, 03A011, doi:10.1093/ptep/pts083 11.1, 11.6

[4] M. Satoh *et al.*, "Commissioning Status of SuperKEKB Injector Linac" in *Proceedings of IPAC2016, Busan, Korea*, 2016, THPOY027, p.4152, doi:10.18429/JACoW-IPAC2016-THPOY027 11.1

[5] M. Yoshida, N. Iida, S. Kazama, T. Natsui, Y. Ogawa, S. Ohsawa, H. Sugimoto, L. Zang, X. Zhou, D. Sato, "Generation and Acceleration of Low-emittance, High-current Electron Beams for SuperKEKB", in *Proceedings of LINAC2014, Geneva, Switzerland*, 2014, MOIOB03, p.21, https://jacow.org/LINAC2014/papers/moiob03.pdf 11.1

[6] T. Kamitani *et al.*, "SuperKEKB Positron Source Construction Status", in *Proceedings of IPAC2014, Dresden, Germany*, 2014, MOPRI004, p.579, doi:10.18429/JACoW-IPAC2014-MOPRI004 11.1

[7] Y. Seimiya, Y. Enomoto, K. Furukawa, T. Higo, T. Kamitani, F. Miyahara, Y. Ohnishi, M. Satoh, T. Suwada, M. Tanaka, "Emittance Growth by Misalignments and Jitters in SuperKEKB Injector Linac", in *Proceedings of IPAC2016, Busan, Korea*, 2016, THPOR040, p.3871, doi:10.18429/JACoW-IPAC2016-THPOR040 11.1

[8] F. Miyahara, K. Furukawa, M. Satoh, T. Suwada, R. Ichimiya, H. Saotome, "High position resolution BPM readout system with calibration pulse generators for KEK e+/e− linac", in *Proceedings of IBIC2015, Melbourne, Australia*, 2015, TUPB023, p.369, doi:10.18429/JACoW-IBIC2015-TUPB023 11.1

[9] K. Furukawa, M. Satoh, T. Suwada, T.T. Nakamura, "Pulse-to-pulse Beam Modulation and Event-based Beam Feedback Systems at KEKB Linac", in *Proceedings of*

IPAC2010, Kyoto, Japan, 2010, TUOCMH01, p.1271, https://jacow.org/ipac10/papers/tuocmh01.pdf 11.1

[10] K. Furukawa *et al.*, "Upgrade of KEK Electron/positron Linac Control System for the Both SuperKEKB and Light Sources", in *Proceedings of ICALEPCS2017, Barcelona, Spain*, 2017, THMPL02, p.1257, doi:10.18429/JACoW-ICALEPCS2017-THMPL02 11.1

[11] N. Higashi *et al.*, "Construction and Commissioning of Direct Beam Transport Line for PF-AR", in *Proceedings of IPAC2017, Copenhagen, Denmark*, 2017, WEPAB044, p.2678, doi:10.18429/JACoW-IPAC2017-WEPAB044 11.1

[12] H. Sugimoto, M. Satoh, M. Yoshida, "Design study on KEK injector linac upgrade for high-current and low-emittance beams", in *Proceedings of IPAC2012, New Orleans, USA*, 2012, TUPPC021, p.1206, https://jacow.org/IPAC2013/papers/tupfi004.pdf 11.2.1

[13] M. Yoshida, N. Iida, T. Natsui, Y. Ogawa, S. Ohsawa, H. Sugimoto, L. Zang, X. Zhou, "Longitudinal manipulation to obtain and keep the low emittance and high charge electron beam for SuperKEKB injector", in *Proceedings of IPAC2013, Shanghai, China*, 2013, WEPME061, p.1337, https://jacow.org/IPAC2013/papers/tupfi004.pdf 11.2.2

[14] I. Sato *et al.*, "Design Report on PF Injector Linac Upgrade for KEKB", KEK Report 95–18, 1996, https://lib-extopc.kek.jp/preprints/PDF/1995/9524/9524018.pdf 11.3, 11.3.1, 11.3.4, 11.9.1

[15] S. Matsumoto, T. Higo, K. Kakihara, T. Kamitani, M. Tanaka, "Large-Aperture Travelling-wave Accelerator Structure for Positron Capture of SuperKEKB Injector Linac", in *Proceedings of IPAC2014, Dresden, Germany*, 2014, THPRI047, p.3872, doi:10.18429/JACoW-IPAC2014-THPRI047 11.3.1

[16] S. Yamaguchi, Y. Igarashi, K. Kakihara, A. Enomoto, "High power test of the S-band Accelerator Guide for the KEKB Injector Linac", in *Proceedings of APAC98, Tsukuba, Japan*, 1998, 4D023, p.136, https://jacow.org/a98/APAC98/4D023.PDF 11.3.4

[17] T. Higo, Y. Enomoto, H. Ego, S. Ushimoto, "Inspection of inner surface of S-band accelerating structures of KEK electron-positron injector linac used for more than 30 years", in *Proceedings of PASJ2018, Nagaoka, Japan*, 2018, WEP055, p.445, https://www.pasj.jp/web_publish/pasj2018/proceedings/PDF/WEP0/WEP055.pdf 11.3.5

[18] A. Saji *et al.*, "Manufacturing of S-band Accelerating Structure", in *Proceedings of PASJ2018, Nagaoka, Japan*, 2018, THP048, p.918, https://www.pasj.jp/web_publish/pasj2018/proceedings/PDF/THP0/THP048.pdf 11.3.7

[19] M. Akemoto, S. Fukuda, H. Honma, M. Kawamura, H. Nakajima, T. Natsui, T. Shidara, "Present Status of the Klystron Modulator for the KEK Electron-Positron Injector Linac", in *Proceedings of PASJ2018, Nagaoka, Japan*, 2018, WEP060, p.476, https://www.pasj.jp/web_publish/pasj2018/proceedings/PDF/WEP0/WEP060.pdf 11.4.1

[20] M. Kawamura *et al.*, "Present Status of Capacitor-Charging Power Supplies for the Klystron Modulators in SuperKEKB Injector Linac", in *Proceedings of LINAC2018, Beijing, China*, 2018, THPO095, p.898, https://jacow.org/linac2018/papers/thpo095.pdf 11.4.1

[21] T. Matsumoto *et al.*, "Low-Level RF System for the SuperKEKB Injector Linac", in *Proceedings of IPAC2018, Vancouver, Canada*, 2018, WEPAK017, p.2131, doi:10.18429/JACoW-IPAC2018-WEPAK017 11.4.2

[22] T. Miura, M. Akemoto, D. Arakawa, H. Katagiri, T. Matsumoto, F. Qiu, Y. Yano, N. Liu, "LLRF Control Unit for SuperKEKB Injector Linac", in *Proceedings of the IPAC2018, Vancouver, Canada*, 2018, WEPAK018, p.2134, doi:10.18429/JACoW-IPAC2018-WEPAK018 11.4.3

[23] H. Katagiri, M. Akemoto, D. Arakawa, T. Matsumoto, T. Miura, F. Qiu, Y. Yano, "RF Monitor System for SuperKEKB Injector Linac", in *Proceedings of the IPAC2018, Vancouver, Canada*, 2018, WEPAK016. p.2128, doi:10.18429/JACoW-IPAC2018-WEPAK016 11.4.3

[24] K. Kakihara *et al.*, "Experimental study of stainless steel chamber for a pulsed bending magnet of the KEK e−/e+ injector linac", in *Proceedings of the PASJ2018, Nagaoka, Japan*, 2018, THP118, p.1185, https://www.pasj.jp/web_publish/pasj2018/proceedings/PDF/THP1/THP118.pdf 11.5.1

[25] A. Akiyama, K. Furukawa, E. Kadokura, M. Kurashina, K. Mikawa, T. Nakamura, J. Odagiri, M. Satoh, T. Suwada, "Accelerator Control System at KEKB and the Linac", Prog. Theor. Exp. Phys., **2013**, 2013, 03A008, doi:10.1093/ptep/pts081 11.6.2

[26] Y. Enomoto, K. Furukawa, T. Natsui, M. Satoh, H. Saotome, "A New Pulse Magnet Control System in the KEK Electron Positron LINAC", in *Proceedings of IPAC2018, Vancouver, Canada*, 2018, WEPAK014, p.2121, doi:10.18429/JACoW-IPAC2018-WEPAK014 11.6.2

[27] Apex Microtechnology, https://www.apexanalog.com/products/pa12.html 11.6.2

[28] S. Kazama, M. Satoh, H. Sugimoto, M. Yoshida, Y. Ogawa, "Emittance Preservation in SuperKEKB Injector", in *Proceedings of IPAC2015, Richmond, USA*, 2015, MOPWA053, p.239, doi:10.18429/JACoW-IPAC2015-MOPWA053 11.7.1

[29] T. Suwada, "High Stabilization of 500-m-Long Laser-Based Fiducial Line for High-Precision Laser-Based Alignment", J. the Particle Accelerator Society of Japan, **10**(4), 2013, p.226, https://www.pasj.jp/kaishi/cgi-bin/kasokuki.cgi?articles/10/p226-237.pdf 11.7.2

[30] M. Tanaka *et al.*, "Measurement of Long-Period Floor Movement in the KEK Injector Linac Tunnel", in *Proceedings of PASJ2018, Nagaoka, Japan*, 2018, WEP136, p.740, https://www.pasj.jp/web_publish/pasj2018/proceedings/PDF/WEP1/WEP136.pdf 11.7.8

[31] M. Yoshida, N.Iida, T. Natsui, M.Satoh, Y. Ogawa, L. Zang, "SuperKEKB injector upgrade for high charge and low emittance electron beam", in *Proceedings of IPAC2012, New Orleans, USA*, 2012, TUPPD035, p.1482, https://jacow.org/IPAC2012/papers/tuppd035.pdf 11.8

[32] A. Inoue, T. Natsui, M. Yoshida, "Cut disk structure type RF-deflector for slice emittance measurement for RF-gun at SuperKEKB", Energy Procedia, **131**, 2017, p.334, doi:10.1016/j.egypro.2017.09.431 11.8

[33] R. Zhang, X. Zhou, T. Natsui, D. Satoh, M. Yoshida, "Study on stable and high output energy laser system for RF-gun at SuperKEKB injector", in *Proceedings of PASJ2017, Sapporo, Japan*, 2017, WEP117, p.1201, https://www.pasj.jp/web_publish/pasj2017/proceedings/PDF/WEP1/WEP117.pdf 11.8

[34] T. Natsui, M. Yoshida, X. Zhou, R. Zhang, Y. Ogawa, "Commissioning of RF gun for SuperKEKB", in *Proceedings of PASJ2015, Tsuruga, Japan*, 2015, WEP006, p.405, https://www.pasj.jp/web_publish/pasj2015/proceedings/PDF/WEP0/WEP006.pdf 11.8.2

[35] D. Satoh, R. Zhang, X. Zhou, M. Nishida, T. Natsui, M. Yoshida, K. Furukawa, H. Sugawara, "Improvement of photoemission properties of iridium cerium compound for SuperKEKB injector linac," in *Proceedings of PASJ2017, Sapporo, Japan*, 2017, WEP106, p.1165, https://www.pasj.jp/web_publish/pasj2017/proceedings/PDF/WEP1/WEP106.pdf 11.8.3

[36] X. Zhou, T. Natsui, M. Yoshida, R. Zhang, Y. Ogawa, T. Shibuya, "Neodymium and Ytterbium Hybrid Solid Laser of RF Gun for SuperKEKB", in *Proceedings of IPAC2016, Busan, Korea*, 2016, THPMY041, p.3748, doi:10.18429/JACoW-IPAC2016-THPMY041 11.8.6, 11.8.6

[37] X. Zhou, T. Natsui, M. Yoshida, R. Zhang, Y. Ogawa, "Developing an Yb/Nd Doped Hybrid Solid Laser of RF Gun for SuperKEKB Phase II Commissioning", in *Proceedings of IPAC2017, Copenhagen, Denmark*, 2017, THPVA047, p.4540, doi:10.18429/JACoW-IPAC2017-THPVA047 11.8.6

[38] X. Zhou, M. Yoshida, R. Zhang, Y. Ogawa, "The Developing of the Beam Injection Section with Laser Source and S-Band Electron RF Gun for SuperkEKB Project", in *Proceedings of LINAC2018, Beijing, China*, 2018, MOPO007, p.50, doi:10.18429/JACoW-LINAC2018-MOPO007 11.8.6, 11.8.6

[39] X. Zhou, T. Natsui, M. Yoshida, R. Zhang, Y. Ogawa, "25 Hz, Sub-mJ Ytterbium Laser Source of RF Gun for SuperKEKB Linac", in *Proceedings of IPAC2015, Richmond, USA*, 2015, WEPMA044, p.2862, doi:10.18429/JACoW-IPAC2015-WEPMA044 11.8.7

[40] T. Kamitani *et al.*, "Positron Injector Linac Upgrade for SuperKEKB", in *Proceedings of LINAC2012, Tel-Aviv, Israel.* 2012, MOPLB02, p.141, https://jacow.org/LINAC2012/papers/moplb02.pdf 11.9.1

[41] N. Iida, H. Ikeda, T. Kamitani, M. Kikuchi, K. Oide, D. Zhou, "Beam Dynamics in Positron Injector Systems for Next Generation B-Factories", in *Proceedings of IPAC2011, San Sebastian, Spain*, 2011, THYA01, p.2857, https://jacow.org/IPAC2011/papers/thya01.pdf 11.9.2

[42] S. Agostinelli *et al.*, "Geant4 – a simulation toolkit", Nucl. Instrum. Meth. **A 506**, 2003, p.250, doi:10.1016/S0168-9002(03)01368-8, http://geant4.web.cern.ch 11.9.2

[43] "CST EM STUDIO", Dassault Systems, https://www.cst.com/products/cstems 11.9.2

[44] "General Particle Tracer (GPT) code", Pulsar Physics, http://www.pulsar.nl/gpt/ M.J. de Loos *et al.*, "General Particle Tracer: A new 3D code for accelerator and beamline design", in *Proceedings of EPAC1996, Sitges, Spain*, 1996, THP001G, p.1241, https://jacow.org/e96/PAPERS/THPG/THP001G.PDF 11.9.2

[45] "SAD: Strategic Accelerator Design", http://acc-physics.kek.jp/SAD/references.html 11.9.2

[46] V.K. Bharadwaj, Y.K. Batygin, J.C. Sheppard *et al.*, "Analysis of Beam-Induced Damage to the SLC Positron Production Target", in *Proceedings of PAC2001, Chicago, USA*, 2001, WPAH019, p.2123, https://jacow.org/p01/PAPERS/WPAH019.PDF 11.9.3

[47] L. Zang, K. Kakihara, T. Kamitani, K. Mikawa, F. Miyahara, T. Suwada, "Design, Manufacture and Operation of the Beam Spoiler for Positron Target Protection", in *Proceedings of IPAC2014, Dresden, Germany*, 2014, MOPRI002, p.573, doi:10.18429/JACoW-IPAC2014-MOPRI002 11.9.3

[48] F.A. Emanov *et al.*, "Feeding BINP Colliders with the new VEPP-5 injection complex", in *Proceedings of RuPAC2016, St. Petersburg, Russia*, 2016, WEXMH01, p.56, doi:10.18429/JACoW-RuPAC2016-WEXMH01 11.9.4

[49] A.V. Kulikov, S.D. Ecklund, E.M. Reuter, "SLC Positron Source Pulsed Flux Concentrator", in *Proceedings of PAC1991, San Francisco, USA*, 1991, p.2005, doi:10.1109/PAC.1991.164851 11.9.4

[50] S.H. Wang *et al.*, "Injector Linac Upgrade for the BEPCII Project", in *Proceedings of LINAC2004, Luebeck, Germany*, 2004, MOP34, p.111, https://jacow.org/l04/PAPERS/MOP34.PDF 11.9.4

[51] Y. Enomoto *et al.*, "Development of Flux Concentrator for SuperKEKB", in *Proceedings of PASJ2016, Chiba, Japan*, 2016, MOP063, p.520, https://www.pasj.jp/web_publish/pasj2016/proceedings/PDF/MOP0/MOP063.pdf 11.9.4

[52] L. Zang *et al.*, "Positron Yield Optimization by Adjusting the Components Offset and Orientation", in *Proceedings of IPAC2014, Dresden, Germany*, 2014, MOPRI003 p.576, doi:10.18429/JACoW-IPAC2014-MOPRI003 11.9.4

[53] M. Akemoto, S. Fukuda, H. Honma, T. Kamitani, S. Michizono, H. Nakajima, T. Shidara, "Development of Flux Concentrator Modulator for SuperKEKB", in *Proceedings of PASJ2013, Nagoya, Japan*, 2013, SUP057, p.1015, https://www.pasj.jp/web_publish/pasj10/proceedings/PDF/SUP0/SUP057.pdf 11.9.4

[54] M. Akemoto, Y. Enomoto, T. Kamitani, M. Kawamura, H. Nakajima, S. Fukuda, K. Yokoyama, "Present Status of Flux Concentrator Modulator for SuperKEKB", in *Proceedings of PASJ2017, Sapporo, Japan*, 2017, TUP067, p.504, https://www.pasj.jp/web_publish/pasj2017/proceedings/PDF/TUP0/TUP067.pdf 11.9.4

[55] T. Kamitani *et al.*, "Present Status of the Positron Source Upgrade for SuperKEKB", in *Proceedings of PASJ2015, Tsuruga, Japan*, 2015, THP044, p.1064, https://www.pasj.jp/web_publish/pasj2015/proceedings/PDF/THP0/THP044.pdf 11.9.4

[56] N.V. Mokhov *et al.*, "Recent Enhancements to the MARS15 Code", FERMILAB-Conf-04/053-AD, 2004, http://lss.fnal.gov/archive/2004/conf/fermilab-conf-04-053-ad.pdf 11.9.6

[57] S. Matsumoto, H. Iwase, K. Kakihara, T. Kamitani, T. Sanami, T. Higo, H. Yamaoka, "Radiation Shield Structure for the Positron Target Region of KEKB Injector Linac", in *Proceedings of PASJ2015, Tsuruga, Japan*, 2015, THP135, p.1403, https://www.pasj.jp/web_publish/pasj2015/proceedings/PDF/THP1/THP135.pdf 11.9.6

[58] S. Matsumoto *et al.*, "Radiation Shield for the Positron Target of KEKB Injector Linac", in *Proceedings of PASJ2016, Chiba, Japan*, 2016, TUP133, p.1288, https://www.pasj.jp/web_publish/pasj2016/proceedings/PDF/TUP1/TUP133.pdf 11.9.6

[59] A. Shirakawa, H. Honma, Y. Ogawa, "Upgrade of Safety Interlock System of e^+/e^- Linac for SuperKEKB Project", in *Proceedings of IPAC2013, Shanghai, China*, 2013, THPEA007, p.3161, https://jacow.org/IPAC2013/papers/thpea007.pdf 11.10.1

[60] I. Satake, H. Honma, A. Shirakawa, N. Toge, "Improvement of Personnel and Machine Protection System in SuperKEKB Injector Linac", in *Proceedings of IPAC2018, Vancouver, Canada*, 2018, WEPAL002, p.2140, doi:10.18429/JACoW-IPAC2018-WEPAL002 11.10.1